

T. R.
VAN YUZUNCU YIL UNIVERSITY
INSTITUTE OF NATURAL AND APPLIED SCIENCES
DEPARTMENT OF MECHANICAL ENGINEERING

**PROCESSING OF TITANIUM NIOBIUM SHAPE MEMORY ALLOYS BY
HOT PRESSING**

MASTER'S THESIS

PREPARED BY: Nuaman Jasim Filamarz Al-ZANGANA
SUPERVISOR: Assoc. Prof. Dr. Tarık AYDOĞMUŞ

VAN 2018

T. R.
VAN YUZUNCU YIL UNIVERSITY
INSTITUTE OF NATURAL AND APPLIED SCIENCES
DEPARTMENT OF MECHANICAL ENGINEERING

**PROCESSING OF TITANIUM NIOBIUM SHAPE MEMORY ALLOYS BY
HOT PRESSING**



MASTER'S THESIS

PREPARED BY: Nuaman Jasim Filamarz Al-ZANGANA

VAN 2018

ACCEPTANCE AND APPROVAL PAGE

Master thesis is entitled "PROCESSING OF TITANIUM NIOBIUM SHAPE MEMORY ALLOYS BY HOT PRESSING" has been prepared by Nuaman Jasim Filamarz Al-ZANGANA under supervision of Assoc Prof. Dr. Tarık AYDOĞMUŞ in the department Mechanical Engineering Department has been accepted as M.Sc. Thesis according to the Rules of Graduate School of Higher Education on 22/01/2018 and certified by all the majority members, whose signature are given below.

President: Yrd. Doç. Dr. Hüseyin ŞEVİK

Signature:

Member: Asst. Prof. Dr. Serap KOÇ

Signature:

Member: Assoc. Prof. Dr. Tarık AYDOĞMUŞ

Signature:

This thesis has been approved by the committee of The Institute of Natural and Applied science on /.../..... with decision number.....

Signature
Prof. Dr. Suat SENSOY
Director of Institute

THESIS STATEMENT

All information presented in this thesis was obtained in the frame of ethical behavior and academic rules. In addition, all kinds of information that does not belong to me have been cited appropriately in the thesis prepared by the thesis writing rules.

Signature

Nuaman Jasim Filamarz Al-ZANGANA



ABSTRACT

PROCESSING OF TITANIUM NIOBIUM SHAPE MEMORY ALLOYS BY HOT PRESSING

AI-ZANGANA Nuaman Jasim Filamarz
M. Sc. Thesis, Mechanical Engineering Department
Supervisor: Assoc. Prof. Dr. Tarik AYDOĞMUŞ
January 2018, 101 pages

For the production of Ti-Nb alloys, generally the casting methods (vacuum induction melting or vacuum arc remelting) have been used up to now. Since the melting temperatures of pure Ti and Nb are extremely high (1668 and 2477°C, respectively), it is not economical to produce Ti-Nb alloys by casting. In the case of powder metallurgy, it is possible to produce these alloys economically at much lower temperatures (less than melting temperature of Ti) completely in solid state. In the present study, Ti₇₄Nb₂₆ alloys were produced using pure Ti and pure Nb powders by combination of hot pressing and high temperature sintering for the first time. The influence of processing temperature and time on density, microstructure, and mechanical behavior were investigated. Density measurements showed that hot pressing at 800 °C provides full density. XRD and SEM investigations revealed that amount of β phase formed increases with increasing sintering time. In addition to main phase β , little amount of α phase and a very small amount of pure Nb was observed in the microstructure. Mechanical properties were measured by means of uniaxial compression and Micro Vickers indentation tests. The results indicated that 4hr of sintering at 1200 °C exhibited the highest value of hardness (336 HV), elastic modulus (44 GPa), yield strength (894 MPa), and compression strength (1178 MPa).

Keywords: Hot pressing, Mechanical testing, Microstructure, Powder metallurgy, Sintering, Titanium-Niobium alloys.

ÖZET

SICAK PRES YÖNTEMİ İLE TİTANYUM NİYOBYUM ŞEKİL BELLEKLİ ALAŞIMLARIN ÜRETİMİ

Al-ZANGANA Nuaman Jasim Filamarz
Yüksek Lisans Tezi, Makine Mühendisliği Anabilim Dalı
Tez Danışmanı : Doç. Dr. Tarık AYDOĞMUŞ
Ocak 2018, 101 sayfa

Geçmişten günümüze Ti-Nb alaşımlarının üretimi için genellikle döküm yöntemleri (vakum indüksiyon ergitme veya vakum ark ergitme) kullanılmıştır. Saf Ti ve Nb'un erime sıcaklıkları son derece yüksek olduğundan (1668 ve 2477 °C sırasıyla), döküm yoluyla Ti-Nb alaşımlarını üretmek ekonomik değildir. Toz metalurjisi yöntemi ile bu alaşımları çok daha düşük sıcaklıklarda (Ti erime sıcaklığından daha az) ve tamamen katı halde ekonomik olarak üretmek mümkündür. Bu çalışmada Ti₇₄Nb₂₆ alaşımları, ilk kez sıcak presleme ve yüksek sıcaklık sinterlemesinin kombinasyonu ile saf Ti ve saf Nb tozları kullanılarak üretilmiştir. Üretim sürecinde uygulanan işlem sıcaklığı ve zamanının yoğunluk, mikroyapı ve mekanik davranış üzerindeki etkileri araştırılmıştır. Yoğunluk ölçümleri 800 °C'de yapılan sıcak presleme işleminin tam yoğunluğu sağladığını göstermiştir. XRD ve SEM incelemeleri, sinterleme süresinin artmasıyla birlikte β fazı oluşumunun arttığını ortaya koymuştur. Ana faz β'ya ilaveten, mikroyapıda az miktarda α fazı ve çok az miktarda saf Nb gözlenmiştir. Mekanik özellikler tek eksenli basma ve Mikro Vickers sertlik testleri ile belirlenmiştir. Mekanik test sonuçları 1200 °C'de 4 saatlik sinterlemenin en yüksek sertlik (336 HV), elastik modül (44 GPa), akma mukavemeti (894 MPa) ve basma mukavemeti (1178 MPa) değerlerini sağladığını göstermiştir.

Anahtar kelimeler: Mekanik test, Mikroyapı, Sıcak presleme, Sinterleme, Titanyum-Niyobyum alaşımları, Toz metalurjisi.



ACKNOWLEDGMENTS

Thanks a lot for God (ALLAH) I would never have been able to finish my dissertation without His help.

I would like to express my gratitude to my dear supervisor, Assoc. Prof. Dr. Tarik AYDOĞMUŞ, for his continuous guidance, patience and encouragement in this dissertation. He was always there to listen and give advice and valuable observations.

I would like to specially thank Mr. Fevzi KELEN, PhD candidate, for his helping during the preparation samples and mechanical tests

I would like to thank all my dear teachers at the Yuzuncu Yil University/ Institute Of Science/ Mechanical Engineering Department, for being always there to help and support throughout the course.

I would also like to show my gratitude to VAN Yuzuncu Yil University for providing the appropriate opportunity and atmosphere to study and work in laboratories to complete the research.

I would like to express special thanks to my family, especially my wife for their endless supports and encouragements along with the research.

2018

Nuaman Jasim Filamarz Al-ZANGANA



CONTENTS

	Pages
ABSTRACT.....	i
ACKNOWLEDGMENTS	v
CONTENTS.....	vii
LIST OF TABLES.....	ix
LIST OF FIGURES	xi
SYMBOLS AND ABBREVIATIONS.....	xvii
1. INTRODUCTION	1
2. LITERATURE REVIEWS	5
2.1. Titanium and Titanium Alloys.....	5
2.2. Ti Alloys: Structure and Properties.....	8
2.3. Ti-Nb Alloys	11
2.3.1 General	11
2.3.2 Ti-Nb phase diagram.....	11
2.3.3 Effects of Nb concentration on phase and microstructure	12
2.3.4 Mechanical properties	15
2.4. Fundamentals of Shape Memory Alloy (SMA).....	18
2.4.1 Shape memory effect.....	20
2.5. Production of Ti-Nb Alloys	21
2.5.1 Vacuum arc melting (VAM)	21
2.5.2 Vacuum induction melting (VIM)	23
2.6. Powder Metallurgy.....	23
2.6.1 General	23
2.7. Powder metallurgy of Ti Nb alloys.....	29
2.7.1 Hot pressing	29

2.7.2 Hot Isostatic Pressing (HIP).....	30
2.7.3 Spark plasma sintering (SPS).....	31
2.7.4 Metal injection molding (MIM).....	34
2.7.5 Conventional sintering (CS).....	38
3. MATERIALS AND METHODS.....	39
3.1. Powders Used.....	39
3.2. Sample Production.....	40
3.2.1 Hot-pressing.....	40
3.2.2 High Temperature Sintering.....	44
3.3. Density Measurements.....	48
3.4. Metallographic Sample Preparation.....	48
3.5. Microstructure.....	49
3.5.1 X-ray diffraction (XRD).....	49
3.5.2 Scanning Electron Microscopy (SEM).....	50
3.6. Mechanical Tests.....	51
3.6.1 Micro hardness testing.....	51
3.6.2 Uniaxial Compression Tests.....	52
4. RESULTS AND DISCUSSION.....	55
4.1. Density and Porosity.....	55
4.2. X-ray Diffraction.....	56
4.3. Scanning Electron Microscopy.....	56
4.4. Micro Hardness Tests.....	66
4.5. Uniaxial Compression Tests.....	67
5. CONCLUSIONS.....	75
APPENDIX: EXTENDED TURKISH SUMMARY (GENİŞLETİLMİŞ TÜRKÇE ÖZET).....	85
CURRICULUM VITAE.....	101

LIST OF TABLES

Tables	Pages
Table 2.1. Mechanical Properties of Different Ti-Nb alloys	18
Table 2.2. The porosity of Ti–Nb alloys fabricated by MIM and sintered at different temperatures	37
Table 4.1. Density and porosity of the samples produced in different condition.....	55
Table 4.2. EDS point analysis results obtained from α and β phases in the samples sintered at 1200 °C for different times	67
Table 4.3. Vickers micro hardness tests results.....	68
Table 4.4. Mechanical properties of $Ti_{74}Nb_{26}$ alloys sintered at 1200 °C for variable times.....	70
Table 4.5. Comparison of mechanical properties with the ones existing in the literature.....	73

LIST OF FIGURES

Figures	Pages
Figure 2.1. Density of selected metals.....	5
Figure 2.2. Effect of temperature on specific strength of selected materials compared with titanium alloys.	6
Figure 2.3. Adding Nb to Ti decrease elastic modulus.	7
Figure 2.4. Dental implant components.....	7
Figure 2.5. An example of an orthodontic mini-implant for anchorage.....	8
Figure 2.6. A zygomatic implant.....	8
Figure 2.7. Crystal structure of hcp α phase and bcc β phase	9
Figure 2.8. Influence of alloying elements on Ti alloys phase diagrams	9
Figure 2.9. Explanation of Ti alloys in three-dimensional phase diagram	10
Figure 2.10. Phase diagram of Ti-Nb system	12
Figure 2.11. Comparison of Ti-Nb alloys having various Nb contents which prepared using SEM device a) 14% Nb b) 18% Nb c) 22% Nb d) 26% Nb e) 30% Nb f) 34% Nb	13
Figure 2.12 X-ray diffraction configurations of the Ti-Nb alloy	14
Figure 2.13. X-ray diffraction profile of a) Ti at 26% Nb b) Ti-24Nb alloys after solution treatment (ST)	14
Figure 2.14. X-ray diffraction for Ti-35Nb alloy subjected to different processing step	15
Figure 2.15. Hardness of the Ti-Nb alloys.	16
Figure 2.16. Young's modulus of the Ti-Nb	16
Figure 2.17. Stress-strain curves of Ti-(20–28) at %Nb alloys obtained at room temperature after the solution treatment at 1173K for 1.8 ks.	17
Figure 2.18. Elastic modulus and Nb content curve.....	17

Figures	Pages
Figure 2.19. Diagram suggesting region of shape memory effect and transformation pseudo elasticity in temperature-stress coordinates	20
Figure 2.20. Graphic of stress-strain curve exemplifying the shape memory effect (OBCDO) and super elasticity (DEFGD).....	21
Figure 2.21. Right side view of Vacuum Arc Melting furnace with main parts	22
Figure 2.22. Characteristic graphic microstructures of water quenched quaternary Ti-Nb-Zr-Sn alloys: (a) Ti-24Nb-4Zr-7.5Sn, (b) Ti-24Nb-4Zr-3.5Sn and (c) Ti-20Nb-4Zr-7.5Sn alloys	22
Figure 2.23. Graphic explained three levels of the increasing homogeneity	24
Figure 2.24. Methods of die pressing a) single pressing and b) double pressing	24
Figure 2.25. density distribution in single and double action pressing	25
Figure 2.26. Pressure distributions in single-action pressing of three height to diameter ratios	25
Figure 2.27. Simple view of the stages of metal powder compaction	26
Figure 2.28. Options for processing metal powders to full density	27
Figure 2.29. A diagram of pore structure and grain boundaries between particles during sintering	28
Figure 2.30. Different developed techniques for material sintering.....	28
Figure 2.31. The hot pressing process: graphic of the device.	30
Figure 2.32 Main parts for SPS device.....	31
Figure 2.33. DC pulse current flow through the particles.	32
Figure 2.34. Four stages of spark plasma sintering.	33
Figure 2.35. Consolidation of CP-Ti powders by SPS.....	33
Figure 2.36. XRD diffraction pattern of sintered sample of Ti-23 at% Nb alloy.....	34
Figure 2.37. MIM processes process.	35
Figure 2.38. Effect of sintering temperature on the relative density of Ti-6Al-7Nb allo compacts for 3 types of mixed powders.	35

Figures	Pages
Figure 2.39. Effect of sintering temperature on the tensile properties of Ti-6Al-7Nb alloy compacts for 3 types of mixed powders.	36
Figure 2.40. XRD results for the Ti-16Nb alloys sintered at different temperatures.	37
Figure 2.41. Optical micrographs of Ti-16N at (a) 900°C; (b) 1100°C; (c) 1300°C and (d) 1500°C.	37
Figure 3.1. SEM micrographs of pure (a) Ti and (b) Nb powders.	39
Figure 3.2. XRD patterns of as-received (a) Ti powders and (b) Nb powders.....	40
Figure 3.3 The argon-filled glovebox used to store Ti and Nb powders.....	41
Figure 3.4 The electronic balance employed to measure weight of the raw powders.....	41
Figure 3.5. Graphite dies with the inner diameter of 15 mm and its accessories, top and bottom punches	42
Figure 3.6. Location of the graphite die filled with powder mixture inside the hot pressing chamber.	43
Figure 3.7. Grinding wheel rotating type machine.....	43
Figure 3.8. Hot pressed Ti-Nb specimen before and after grinding.....	44
Figure 3.9. Experimental set-up including vertical tube furnace used for high temperature sintering operations.....	45
Figure 3.10. Temperature-time curves of hot pressing (HP) for 1h and following sintering (HP+S) processes for different times.....	45
Figure 3.11. The macrograph of the sample sintered at 1200 °C for 1h without using Ti getters.	46
Figure 3.12. The sample sintered at 1200 °C for 2h without using Ti getters.....	46
Figure 3.13. Ti sponge getters used during sintering.	47
Figure 3.14. The sample sintered at 1200 °C for 2h using Ti getters.....	47
Figure 3.15. Oxidized Ti getters after high temperature (1200 °C) sintering process. ...	48
Figure 3.16. Precision balance and the density determination kit.	48
Figure 3.17. Processing of cutting samples with dimensions 5x5x10mm.....	49

Figures	Pages
Figure 3.18 Two electrical discharge machines used for cutting samples.	50
Figure 3.19. X-ray diffraction (XRD) device.	50
Figure 3.20. Scanning electron microscope (SEM).	51
Figure 3.21. Vickers hardness testing machine	52
Figure 3.22. Uniaxial compression testing machine equipped with a heating-cooling system.	53
Figure 4.1. XRD patterns of specimens hot pressed at 800 °C for 1h and then sintered at 1200 °C for different times	56
Figure 4.2. SEM images of hot pressed samples at a) 600, b) 650, c) 800 °C for 1h.	57
Figure 4.3. EDS point analysis showing Nb dissolution in Ti and β phase formation at 800 °C. (Nb: 23.7 wt. %).	58
Figure 4.4. EDS point analysis showing pure Ti region. (Nb: 0 wt. %).	59
Figure 4.5. SEM images of $Ti_{74}Nb_{26}$ alloy sintered for 1h at 1200 °C.	60
Figure 4.6. SEM image of $Ti_{74}Nb_{26}$ alloy sintered for 2h at 1200 °C.	60
Figure 4.7. SEM image of $Ti_{74}Nb_{26}$ alloy sintered for 3h at 1200 °C.	61
Figure 4.8. SEM images of $Ti_{74}Nb_{26}$ alloy sintered for 4h at 1200 °C.	61
Figure 4.9. BSE micrograph of bulk $Ti_{74}Nb_{26}$ alloy sintered at 1200 °C for 1h.	62
Figure 4.10. BSE micrograph of bulk $Ti_{74}Nb_{26}$ alloy sintered at 1200 °C for 2h.	62
Figure 4.11. BSE micrograph of bulk $Ti_{74}Nb_{26}$ sintered at 1200 °C for 3h.	63
Figure 4.12. BSE micrograph of bulk $Ti_{74}Nb_{26}$ sintered 1200 °C for 4h.	63
Figure 4.13. EDS point analysis result showing undissolved pure Nb.	64
Figure 4.14. EDS point analysis result for α phase (3h sintering), Ti% (atomic) = 95.7 and Nb% (atomic) = 4.3.	65
Figure 4.15. EDS point analysis result for β phase (3h sintering), Ti% (atomic) = 81.7 and Nb% (atomic) = 18.3.	66

Figures	Pages
Figure 4.16. Stress-strain curves of samples hot pressed at different temperatures for 1h.	69
Figure 4.17. Stress-strain curves of sintered samples at 1200 °C for different times (1, 2, 3 and 4h). The curve of hot pressed sample at 800 °C for 1h (HP) is also included for comparison.	70
Figure 4.18. Elastic modulus-sintering time relation.	71
Figure 4.19. Yield and compressive strength as a function of sintering time	71
Figure 4.20. Effect of Ti getter usage during sintering at 1200 °C for 2hr on stress-strain curves.	72



SYMBOLS AND ABBREVIATIONS

Some symbols and abbreviations used in this study are presented below, along with descriptions

Symbols	Explanation
Hcp	Hexagonal close packing
Bcc	Body centered cubic
Cp-T	Commercially pure titanium
HV	Vickers hardness
GPa	Gigapascal
°C	Degree Celsius
K	Kelven
min	Minute
MPa	Migapascal
h	Hour
KPa	Kilopascal
mm	Milimeter
g	Gram
cm	Centimeter
VAM	Vacuum arc melting
VIM	Vacuum indaction melting
CS	Conventional Sintering
HP	Hot pressing
HIP	Hot isostatic pressing
SPS	Spark plasma sintering
MIM	Metal Injection Molding
SEM	Scanning electron microscopy
XRD	X-ray diffraction
BSE	Backscattering electron
EDS	Energy dispersive spectroscopy



1. INTRODUCTION

Stainless steels, cobalt chromium alloys and titanium alloys are metallic biomaterials. Ti alloys show the highest biocompatibility, high mechanical strength, and corrosion resistance between these metallic biomaterials. Titanium and its alloys are used in many fields such as biomedical industry and aerospace because they have numerous favorable mechanical properties such as good fatigue strength, high wear resistance, excellent fracture toughness and high strength to weight ratio if compared with other materials or alloys (Elias et al., 2006; Kim et al., 2006; Afonso et al, 2007; Bolzoni et al., 2012; Niinomi et al., 2012; Cremasco et al, 2013; Zhuravleva et al., 2013; Yu et al., 2014; Han et al., 2015; Sharma et al., 2016).

Expensive machining operations and high cost of raw materials make acceptance of titanium and its alloys to use in aerospace field and medical application limited. Significant cost reductions can be achieved by using powder metallurgy (P/M) techniques and vacuum hot pressing (VHP) to get near net shapes while reducing machining time and material waste. To solve the toxicity problems of some additional elements, such as Ni, Al and V new Ti alloys were suggested. Recently, the new metastable β titanium alloys such as Ti-Nb, Ti-Ta and Ti-Zr show considerable promise due to their superior properties, lower elastic module, higher tensile strengths, good ductility and compositions absent of potentially cytotoxic elements (Chai et al., 2008; Bolzoni et al., 2012; Kent et al., 2013). Ti has α phase closed packed hexagonal crystal structure (HCP) at lower temperature, but for pure Ti according to equilibrium phase diagram when temperatures up more than 882 ± 2 °C it suffers an allotropic transformation to β phase body centered cubic structure (BCC). Commonly titanium alloys are categorized as α , $\alpha+\beta$ and β alloys (Ping et al., 2006; Elmay et al, 2014). Vanadium, Molybdenum, Tantalum and Niobium are examples of β -isomorphs elements and it is possible to decrease β -transition temperature more by increasing the rate of these elements to the alloy. These elements are fully dissolvable in the Ti β phase. Niobium is a biocompatible element acting as a β phase stabilizing element, and reduces the Young's modulus when added to Ti alloys; it is a non-toxi

element and is not reacted with any tissue in human body (Wang and Zheng, 2008; Zhao et al., 2013; Zhao et al., 2015) The adding of niobium to titanium improves its oxidation resistance while at the same time reducing the density (Sikka et al., 1993).

The concentration of Ti and Nb can effect of the physical and mechanical properties, as well as transformation characteristics. Hardness, strength, and the melting temperature are increased with increasing of concentration of niobium in the Ti-Nb alloys (Kikuchi et al., 2003).

Ti-Nb alloys are generally produced by casting and forging techniques. Porosity, rough microstructure, and composition segregation are the main defects normally present by casting and greatly worsen the mechanical properties. Also, melting point of Ti and Nb, 1668 and 2477°C, respectively are very high that special furnaces, too much energy and expensive equipment's such as vacuum are needed to produce Ti-Nb alloys with casting method. Forging gives better mechanical properties, but high costs and low use of raw materials sternly limit its range of application. Powder metallurgy processing techniques on the other hand are much more economical fabrication methods to improve the manufacturing efficiency, effective in creating small parts with complex shapes and suitable techniques for preparation of the Ti-Nb based alloys using elemental powders, since they require low temperature (1000-1400°C) for manufacturing (Štěpán et al, 2010; Andrade et al, 2015; Cai et al., 2016). Powder metallurgy techniques can be used to produce bulk Ti-Nb samples and allow a reduction in production costs when compared to other processing methods since there is the possibility to avoid or limit machining and 90% of the raw materials can be used and, when powder metallurgy used, net-shape or near-net-shape can be achieved.

According to production process, powder metallurgy techniques can be classified into two types as a function of the temperature at which the consolidation process is done:

- Cold consolidation processes: pressing powder at room temperature is followed by the sintering at high temperature.
- Hot consolidation processes: both compaction pressure and temperature are applied at the same time to the powder. Also, full density can be achieved by hot consolidation processes, if compared with conventional sintering.

The objective of this work is the preparation and characterization of bulk $\text{Ti}_{74}\text{Nb}_{26}$ alloys for use as metallic biomaterials. Density, final microstructure and desired mechanical properties can be controlled by adjusting hot pressing parameters such as pressure, temperature, and time. Mixed Ti and Nb powders were put into hollow cylindrical graphite dies with inner diameter of 15 mm and hot pressed at 600, 650 and 800°C for 1h under a constant pressure of 50 MPa and under flowing argon gas to produce nonporous samples with a height of 10 mm. After hot pressing at optimum temperature, 800°C, specimens were further sintered in a vertical furnace at 1200°C for 1, 2, 3 and 4 hours to provide Nb for dissolution in Ti and accordingly to get β phase. Effect of hot pressing temperature and time of sintering on the microstructure, density and mechanical behavior of the samples produced were investigated by Scanning Electron Microscopy (SEM), X-ray Diffraction (XRD), Archimedes' technique, uniaxial compression and micro Vickers indentation tests.



2. LITERATURE REVIEWS

2.1. Titanium and Titanium Alloys

William Gregor discovered the element metal titanium in England in 1790, but the name of titanium was given by Klproth in 1795 (Viteri and Fuentes, 2013). Titanium is a low density element. Its density is only 4.5 g/cm^3 about 60% of the density of steel (7.9 g/cm^3). It can be used with components which operate at elevated temperatures, especially where large strength to weight ratios are required (Hermawan et al., 2009). Ti alloys are used in medical applications, due to their excellent corrosion resistance, high specific strength, and superior biocompatibility (Silva et al., 2009; Zhao et al., 2013; Mohammed et al., 2014; Prashanth et al., 2016). Different types of metals which are varying in density were shown in Figure 2.1. The density of 5 g/cm^3 is separation point between light and heavy metals. The heaviest light metal among the light metals is titanium (Leyens and Peters, 2003).

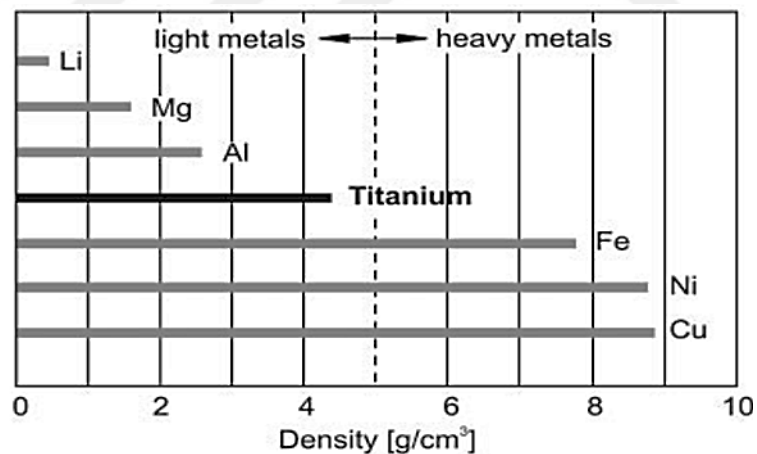


Figure 2.1. Density of selected metals (Leyens and Peters, 2003).

Figure 2.2 shows that only carbon fiber reinforced plastics at temperatures below 300°C have higher specific strength than titanium alloys. The specific strength of

titanium alloys is especially attractive at high temperatures (Leyens and Peters., 2003).

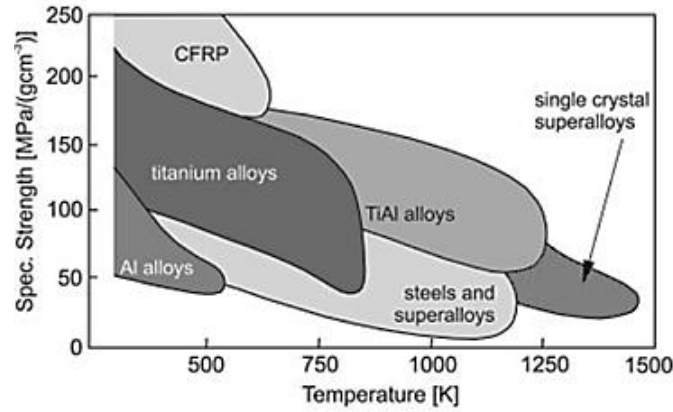


Figure 2.2. Effect of temperature on specific strength of selected materials compared with titanium alloys (Leyens and Peters, 2003).

Inadequate wear resistance, high oxidation at raised temperatures, low hardness and yield strength of titanium reduce the lifetime of parts and limit fields of its application (Shymanski et al., 2015). Titanium gives excellent flexibility since its modulus of elasticity is very low, about half that of steel, it resembles human bone flexibility (Holz et al., 2011). Temperature, oxygen partial pressure and water vapor content in the surrounding atmosphere are several factors which effect on oxidation behavior of pure titanium. Titanium reacts with oxygen from the air with increasing the temperature above 600°C and makes the TiO_2 . Nb or Ta alloying elements are used to increase the resistance of titanium to oxidation (Kunčická et al., 2014).

The main properties of Ti alloys are mechanical compatibility, biocompatibility, safety and good corrosion stability in human body, high fatigue resistance, superior toughness, and high specific strength, for these reasons it is widely used as biomaterials in metallic implants and prostheses for dental and orthopedic procedures (Elias et al., 2008; Bolzoni et al., 2012; Friak et al., 2012; Kuo et al., 2012; Mohammed et al., 2012; Elmay et al., 2014; Guo et al., 2015; Zhao et al., 2015; Cai et al., 2016; Konopatskii et al., 2016). Ti alloys will be widely used in industrial applications because its Young's modulus can be largely increased or decreased by alloy design. Fedotov and Belousov reported that after adding Nb to Ti elastic modulus decreases as shown in Figure 2.3 (Ozaki et al., 2004).

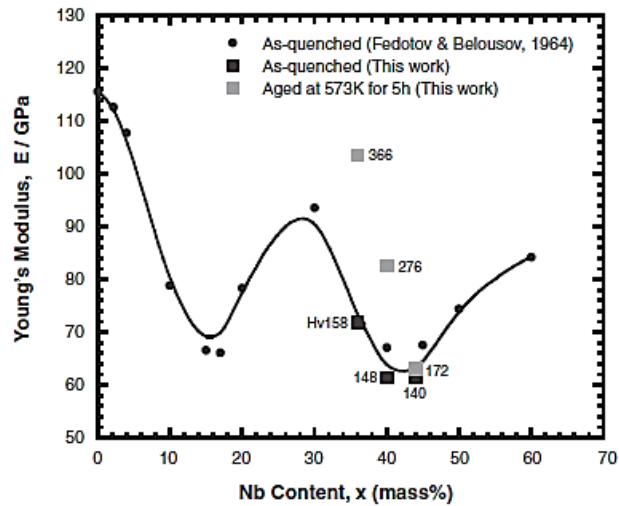


Figure 2.3. Adding Nb to Ti decrease elastic modulus (Ozaki et al., 2004).

Varies physical, chemical and mechanical properties of titanium alloys can be achieved by mixing the titanium powder with several metallic elements such as aluminum, vanadium, iron, tin, niobium, molybdenum, chromium and zirconium (Brunette et al., 2001). Many dentistry devices like bridges, screw and abutment teeth which are used in dental implant prosthesis components such as Osseo integrated, mini-implant for orthodontic anchorage as shown Figure 2.4 and Figure 2.5 and zygomatic fixture as shown Figure 2.6 can be made by using titanium and its alloys (Elias et al., 2008).

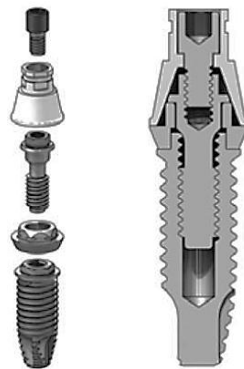


Figure 2.4. Dental implant components (Elias et al., 2008).



Figure 2.5. An example of an orthodontic mini-implant for anchorage.

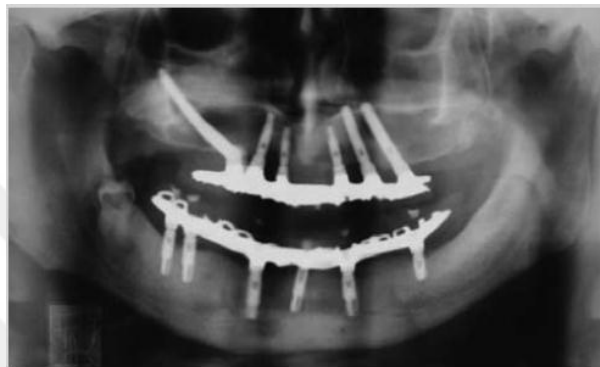


Figure 2.6. A zigomatic implant (Elias et a.l, 2008).

2.2. Ti Alloys: Structure and Properties

The body centered cubic β phase at higher temperature, and the hexagonal α phase at low temperature are the two stable phases of Ti-based alloys, orthorhombic α'' and hexagonal ω phases also are another two metastable phases which occurring by quenching. Ti afford an allotropic transformation at $882\pm 2^\circ\text{C}$, at this temperature and under pure Ti has α -phase closed packed hexagonal crystal structure (HCP), but above $882\pm 2^\circ\text{C}$ it has β phase body centered cubic structure (BCC) which remains stable to the melting temperature. The atomic unit cells of the (hcp) α phase and the (bcc) β phase are shown in Figure 2.7. The arrangement, volume fraction, and individual properties of the two phases α and β can mainly determine the properties of titanium alloys. The hexagonal α is more thickly crowded and has an anisotropic crystal structure if it is compared with the body-centered cubic β (Leyens and Peters, 2003; Kim et al., 2005; Ping et al., 2006; Mantani and Kudou, 2013; Elmay et al., 2014; Panigrahi, 2015).

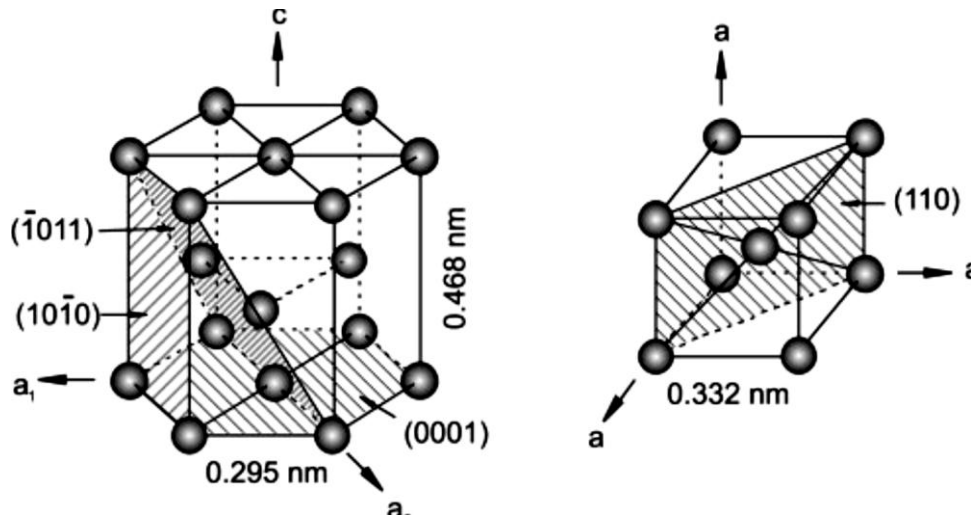


Figure 2.7. Crystal structure of hcp α phase and bcc β phase (Leyens and Peters, 2003).

A neutral, α -stabilizers, or β -stabilizers are the main classification of alloying elements of titanium. β -stabilizing elements shift the β phase field to lower temperatures. While α -stabilizing elements spread the α phase field to higher temperatures. Sn and Zr are neutral elements. Al, C, O and N are the example of α -stabilizing elements. β -stabilizing elements are classified as β -isomorphous and β -eutectoid. V, Ta, Mo, and Nb are examples of β -isomorphous elements that fully dissolvable in the β phase. Mn, Cr, Co, Cu, Si, Fe, Ni and H are examples of the β -eutectoid elements that solubility of these elements in Ti is limited, these elements form intermetallic phases by eutectoid decomposition of the β phase. Figure 2.8 shows the influence of alloying elements on Ti alloys phase diagrams (Leyens and Peters, 2003).

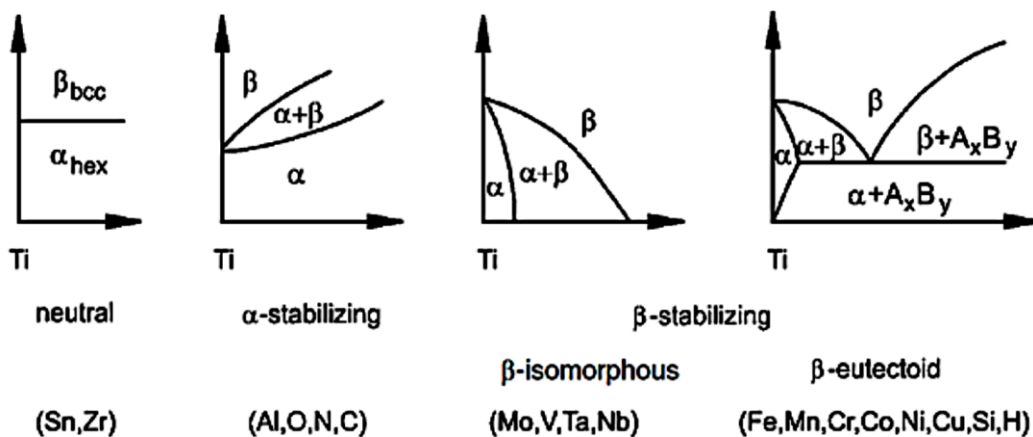


Figure 2.8. Influence of alloying elements on Ti alloys phase diagrams (Leyens and Peters, 2003).

Figure 2.9 shows a three dimensional phase diagram of titanium alloys. α , $\alpha + \beta$ and β alloys are the main classification of titanium alloys, commercially pure titanium alloyed with α -stabilizing and/or neutral elements. When adding a little amount of β -stabilizing elements, the α -stabilizing referred to as near- α alloy. Strength, ductility and toughness can be controlled for α , $\alpha + \beta$ and β alloys by controlling alloy composition, volume fraction of constituent phases and microstructure (Leyens and Peters, 2003; Ozaki et al., 2004). β alloys exhibit excellent formability and its strength is generally greater than that of $\alpha+\beta$ and α -alloys. Also, they have relatively high densities (Wood, 1972).

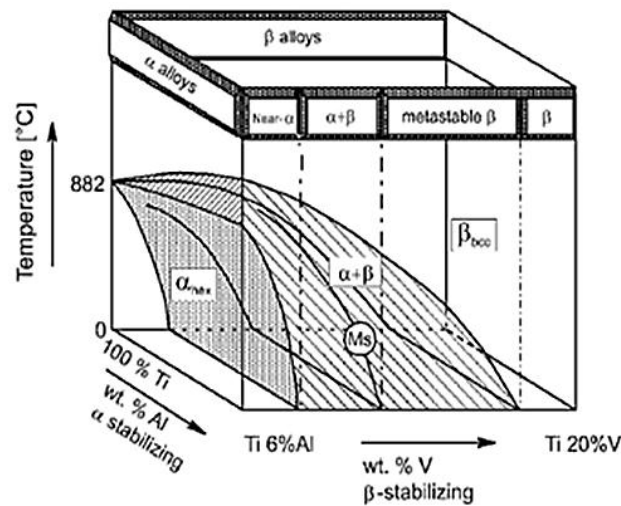


Figure 2.9. Explanation of Ti alloys in three-dimensional phase diagram (Leyens and Peters, 2003).

Nb, Ta, Mo and Zr and Sn are examples of elements used to offer β alloy and offer an active collection of high strength and low modulus which is necessary for biomedical titanium alloys. They do not cause sensitive reactions or inflammatory processes, mechanical properties of these alloys can be improved by heat treatment (Koike and Okabe, 2007; Cremasco, 2013; Kent et al., 2013).

Ti–V, Ti–Mo, Ti–Nb, Ti–Nb–Ta–Zr, Ti–Mo–Zr, are β type Ti-based alloys, between these alloys, Ti–Nb based alloys having the lowest elastic moduli and better shape memory effect, so they are suitable for medical applications (Ping et al., 2006; Niinomi., 2008). Niobium is a biocompatible element acting as a β -phase stabilizing element in Ti alloys, which makes Ti–Nb based alloys attractive for implant application,

the Young's modulus of Ti alloys can be reduced by adding niobium. Nb doesn't cause any tissue reaction because it is a non-toxic element (Wang and Zheng, 2008; Zhao, et al., 2013; Zhao et al., 2015). Using alloying elements, such as Ta or Nb increase the resistance of titanium to oxidation and contributes to decrease of oxygen solubility and further oxygen diffusion into the alloy (Kunčická et al., 2014).

2.3. Ti-Nb Alloys

2.3.1. General

Titanium–niobium alloys have no cytotoxicity, exhibits corrosion resistance similar or superior to Ti, very good biocompatibility and elastic modulus significantly lower than other titanium alloys for implants, these properties make it faithful and possible candidate biomedical materials for replacing TiNi alloys (Wang and Zheng., 2009; Farooq et al., 2014; Andrade et al., 2015; Bönisch et al., 2015; Bönisch et al., 2016; Prokoshkin et al., 2016). The concentration of Ti and Nb can affect the physical and mechanical properties, as well as transformation characteristics (Štěpán et a.,n.d). If the concentration of niobium increased in the Ti-Nb alloys, hardness, strength, and the melting temperature increase (Kikuchi et al., 2003).

2.3.2. Ti-Nb phase diagram

A homogeneous portion of a system that has identical physical and chemical characteristics is called a phase. Every pure material is considered to be a phase, solid, liquid, and gaseous. All kinds of phase transformations can be understood; also the microstructure and physical properties of an alloy are controlled and enhanced by the phase diagram (Otsuka and Ren, 1999). A variation of thermodynamic information can be delivered by phase diagrams through equilibrium among multiple phases and measurable data on phase distribution in a specific system (Seetharaman., 2005).

Phase diagram is very valuable to characterize the most stable relationship between phases in alloy system. Melting, casting and crystallization information can be found by phase diagram (Callister and Rethwisch, 2009). Equilibrium and non-equilibrium phases are two phase transformations in titanium alloys depended on the

content of alloying elements. The equilibrium α and β phases are usually produced through appropriate heat treatments in suitable phase fields of the alloys and then slow cooling to room temperature (Pathak et al., 2014).

The equilibrium phases of the Ti-Nb system contain liquid and solid solution which is body-centered cubic β with a complete range of solubility above 882°C and the close-packed hexagonal α solid solution restricted to temperatures below 882°C as shown in Figure 2.10 (Murray, 1981).

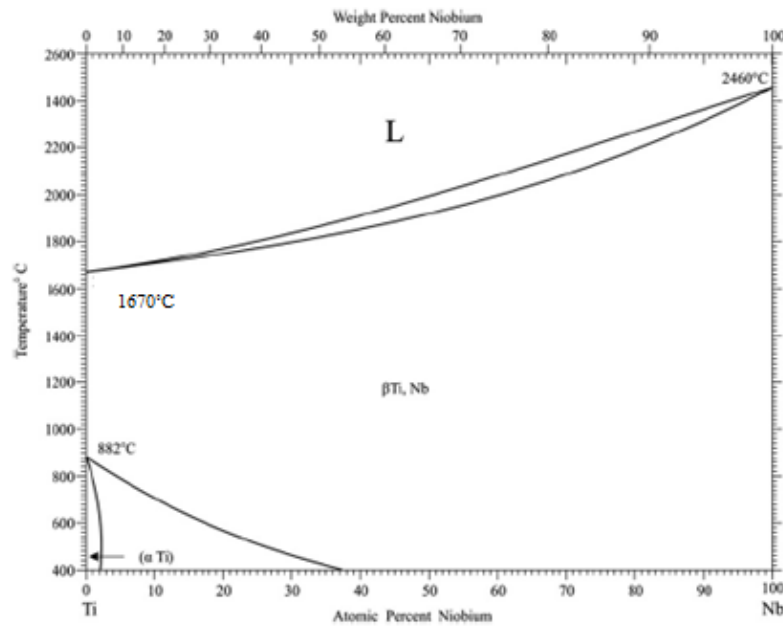


Figure 2.10. Phase diagram of Ti-Nb system (Aleksanyan et al., 2012).

According to the equilibrium Ti-Nb phase diagram as shown in Figure 2.10, pure Ti shows that the alloy with a niobium concentration up to 3% is located within the α region at 400°C. When Nb content increased ($\alpha + \beta$) mixture becomes stable. With increasing the Nb content to about 40% the β phase is stable. The two melting points that require to converting solid bcc β phase to liquid phase for pure Ti and Nb are 1670°C and 2469°C respectively (Aleksanyan et al., 2012; Bahador et al., 2017).

2.3.3. Effects of Nb concentration on phase and microstructure

In the Ti-Nb system various metastable phases can occur due to non-equilibrium conditions after quenching. The product from non-equilibrium depends on both the

cooling rate and the amount of Nb in the composition. With the increasing of Nb content in Ti–Nb binary alloys, many metastable phases appear such as β body-centered cubic, hexagonal α' martensite, orthorhombic α'' martensite, and the supplementary hexagonal ω phase (Moffat and Kattner, 1988; Tobe et al., 2013; Wu et al., 2013).

(Hon et al., 2003) investigated that the microstructures of Ti-Nb alloys consist of α and β phases when the ranging of the Nb content is from 14 to 34 mass%, With increasing of Nb content, the portion of the α phase decreases and β phase increases as shown in Figure 2.11 (a) to (f), the black (dark) regions perform α phase and the gray (light) regions perform β phase.

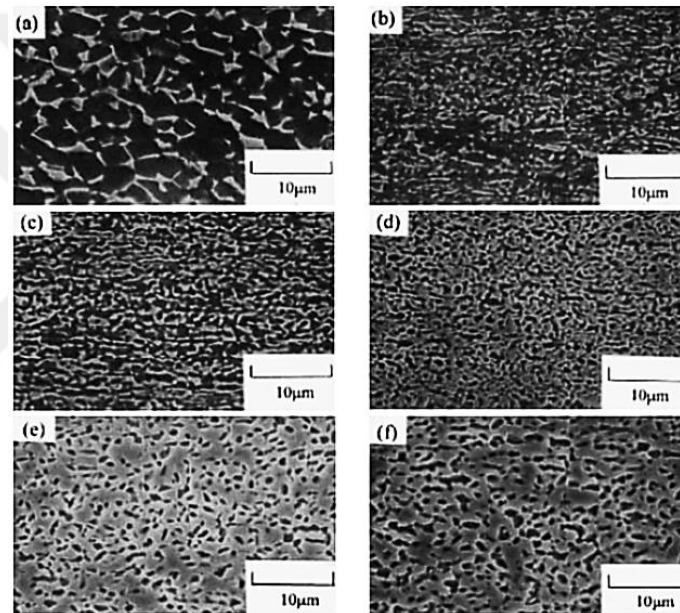


Figure 2.11. Comparison of Ti-Nb alloys having various Nb contents which prepared using SEM device a) 14% Nb b) 18% Nb c) 22% Nb d) 26% Nb e) 30% Nb f) 34% Nb (Hon et al., 2003).

X-ray diffraction (XRD) can be used to analyze the phases in Ti-Nb alloys. Figure 2.12 shows the XRD patterns of the titanium and the Ti-Nb alloys. With a niobium concentration up to 10% peaks matching to α and/or metastable α' phase were found. A small peak presumably corresponding to the metastable α'' phase (orthorhombic) appeared in the Ti-15%Nb. The metastable α'' phase that is broad peaks found in the Ti-20%Nb and Ti-25%Nb, peaks matching to the ω phase (hexagonal) and the metastable β (bcc) phase were institute in the Ti-30%Nb (Kikuchi et al., 2003).

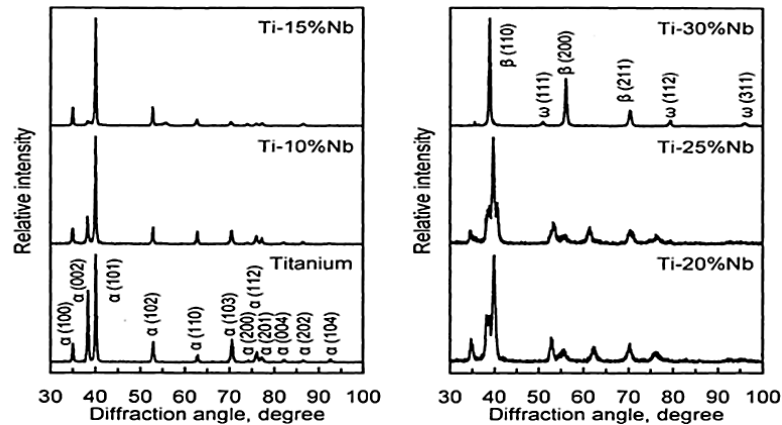


Figure 2.12. X-ray diffraction configurations of the Ti-Nb alloy (Kikuchi et al., 2003).

(Elmay et al, 2014) investigated that a single β phase can be identified for Ti at 26% Nb alloy, and XRD peaks corresponding to the α'' orthorhombic martensite can be clearly seen for Ti-24Nb alloy as shown in Figure 2.13.

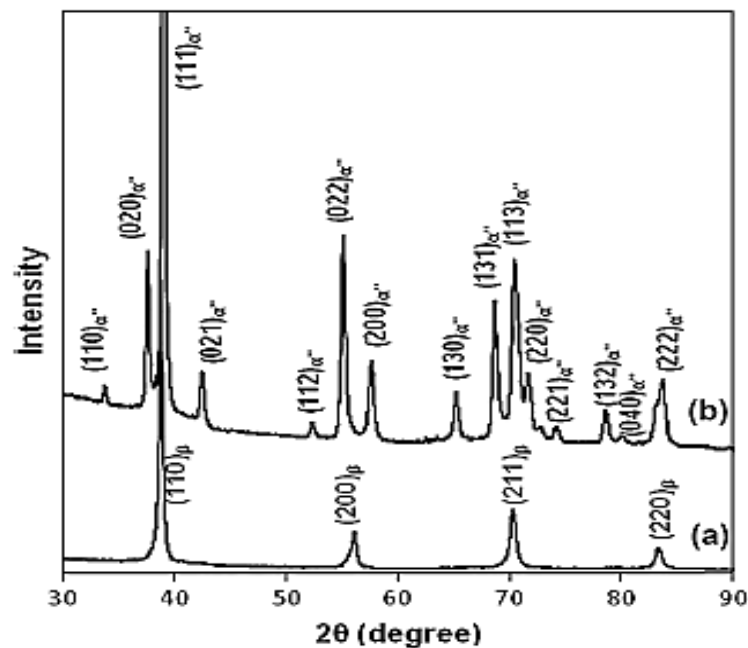


Figure 2.13. X-ray diffraction profile of a) Ti at 26% Nb b) Ti-24Nb alloys after solution treatment (ST) (Elmay et al., 2014).

Figure 2.14 shows X-ray diffraction with indexed patterns achieved by different process (Cremasco.,2013). α , β and ω phases were detected in the as-cast condition. α'' martensite phase and β phase were identified after plastic deformation. When the alloys

contain high Nb concentration and plastically deformed or rapidly cooled from high temperature cause formation of the orthorhombic martensite phase α'' .

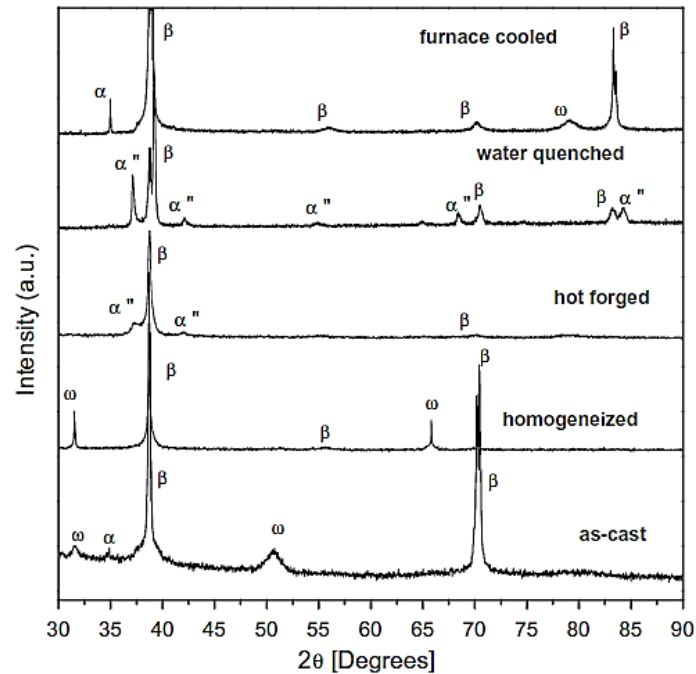


Figure 2.14. X-ray diffraction for Ti-35Nb alloy subjected to different processing step (Cremasco et al., 2013).

2.3.4. Mechanical properties

The type of material that can be used for a particular application depends on the mechanical properties. Some importance of these properties is elastic modulus, hardness, tensile strength and elongation (Geetha et al., 2009; Viteri and Fuentes., 2013). Chemical composition and thermo mechanical processing determine the mechanical behavior of titanium alloys.

The alloys with Nb concentrations of 5% and above have a higher hardness than that of titanium, and the alloys with Nb concentrations of 10% and above also have higher yield strength and tensile strength than those of titanium, while the elongation is considerably lower. Young's modulus decreases as the concentrations of niobium increase until 20%. The value for the Ti-Nb alloys with Nb concentrations from 5% to 25% are significantly lower than that for the titanium, while for the Ti- 30%Nb is significantly higher. Ti-20%Nb and Ti-30%Nb exhibit the lowest and the highest

Young's modulus, respectively as shown in Figure 2.15 and Figure 2.16 (Kikuchi et al., 2003).

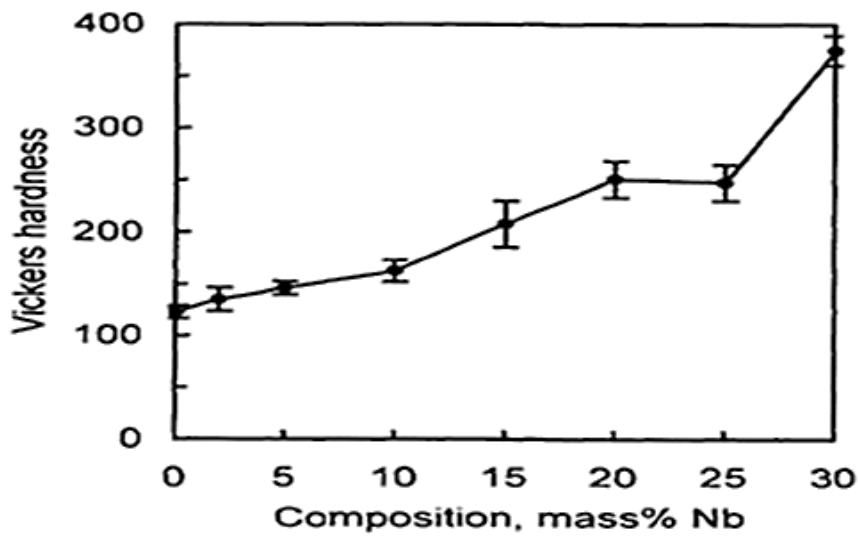


Figure 2.15. Hardness of the Ti-Nb alloys.

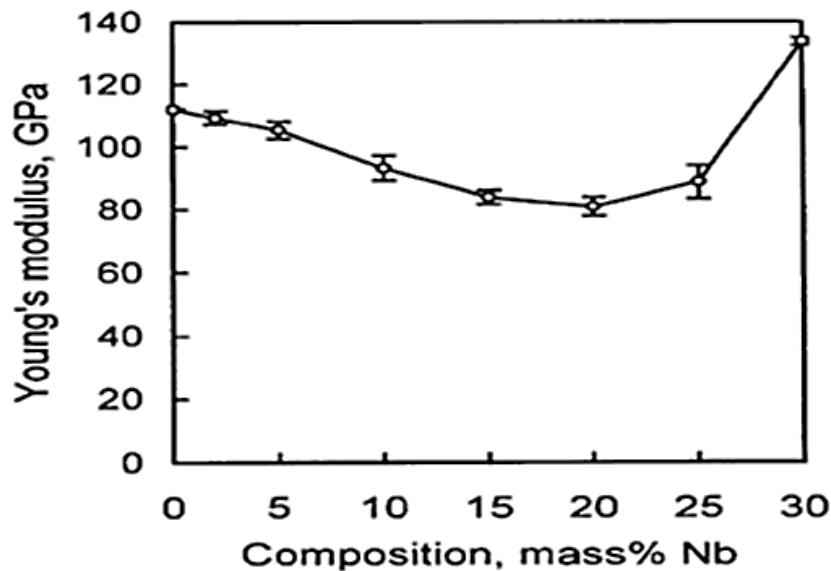


Figure 2.16. Young's modulus of the Ti-Nb (Kikuchi et al., 2003).

In a Ti-20 at % Nb alloy a large elongation of 40% was obtained. The yield stress and elongation decrease with increasing of Nb content from 20 at% to 26 at%. The Ti-26 at% Nb alloy displays double yielding as shown in Figure 2.17 (Kim H. Y. et al, 2004).

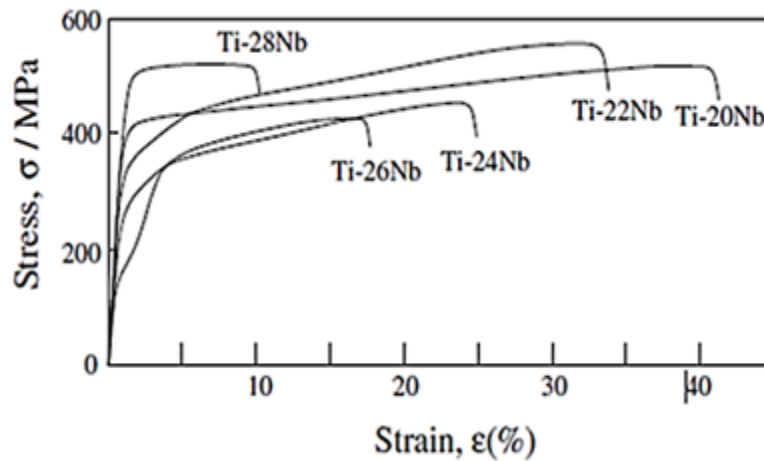


Figure 2.17. Stress-strain curves of Ti-(20–28) at %Nb alloys obtained at room temperature after the solution treatment at 1173K for 1.8 ks (Kim et al., 2004).

Figure 2.18 shows the relation between elastic modulus and Nb content. From 14 to 26 mass% Nb, the elastic modulus decreases with increases of Nb content, after that the elastic modulus increase with increases of Nb content and reached to a maximum value at 34 mass% Nb. The decrease in the elastic modulus with the increasing Nb content from 14 to 26 mass% is related with a gradual decrease in the ratio of the phase in the microstructure (Hon et al., 2003).

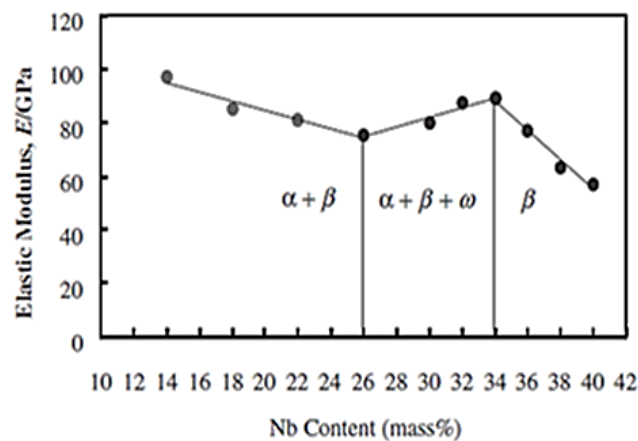


Figure 2.18. Elastic modulus and Nb content curve (Hon et al., 2003).

Comparison in mechanical properties between some Ti alloys shows in Table 2.1.

Table 2.1 Mechanical Properties of Different Ti-Nb alloys (Mittal K and Kaushik , 2016)

Alloys	Phase composition	Symbols	Tensile strength (MPa)	Modulus of Elasticity (GPa)	Yield Strength(MPa)
Ti-6Al-7Nb	$\alpha+\beta$	A	900-1050	114	880-950
Ti-26Nb	β	B	420	50	350
Ti-24Nb-2Zr	β	C	440	62	345
Ti-22Nb-4Zr(Super Elastic)	β	D	480	Super-elastic	320
Ti-20Nb-6Zr	β	E	470	60	365
Ti-18Nb-8Zr	β	F	550	75	455
Ti-16Nb-10Zr	β	G	520	70	485
Ti-13Nb-13Zr	β	H	1030	69—79	900
Ti-15Mo-3Nb	B	I	1020	82	1020
Ti-35.3Nb-5.1Ta-7.1Zr	Metastable β	J	597	55	547
Ti-35.3Nb-5.1Ta-7.1Zr-0.40O	Metastable β	K	1010	66	976
CP Ti	A	L	785	105	692
Bone		M	90—140	10—40

2.4. Fundamentals of Shape Memory Alloy (SMA)

The ability to recover shape when a material undergoes a suitable thermo mechanical treatment is called shape memory effect and the materials exhibiting this behavior are called shape memory alloys (SMA) (Machado and Savi, 2003). SMAs have two phases with different crystal structure and properties. One is called austenite phase (A) at high temperature and low stress, and the other is called martensite phase

(M) which has low temperature and high stress (Krishnan., 1985; Stoeckel., 1995; Mohammed et al., 2012; Lester et al., 2015). One-way shape memory means that materials which exhibit shape memory only upon heating, but two-way shape memory included that material also undergoes a change in shape upon re cooling (Hodgson et al., 1990).

Phase transformations in crystalline materials can be categorized into two groups; one is diffusional transformation and the other is diffusionless transformation. In the case of diffusional transformation, atoms leave one crystal structure to form another structure by diffusion. Martensitic transformation goes to second group, it is a phase transformation escorted with shear deformation and changing in the shape resulting from diffusionless cooperative movement of atoms (Brunette et al., 2001).

Diffusionless transformations do not require such long range movements; in these cases atoms are helpfully reorganized into a new, more stable crystal structure, but without changing the chemical nature of the matrix (Duerig. et al .,1990). Thermo elastic and non-thermo elastic are two groups of martensitic transformations. Thermo elastic occurs in shape memory alloys but non-thermo elastic transformations occur mostly in ferrous alloys (Aydoğmuş, 2010).

There are two main phenomena occurring in shape memory alloys: shape memory effect and superelasticity. They are closely connected to each other. Both behaviors are visible for the same material depending on the temperature. Under (A_s) only shape memory effect occurs but above (A_f) simply superelasticity is observed. Both mechanisms are active partially between (A_s) and (A_f). Critical stress to induce martensite and critical stress for slip with temperature are schematically drawn in

Figure 2.19 (Otsuka, and Shimizu, 1986). Ti–V-based alloys, Ti–Mo based alloys and Ti–Nb-based alloys are various β -type of Ti alloys exhibiting SME and SE. Shape memory effect and superelastic behavior appear in Ti-Nb based alloys at room temperature in a range between (16.7- 50 wt. %) of Nb content (Kim et al., 2005; Chai et al., 2008; Al-zain Yet al., 2010; Aleksanyan et al., 2012).

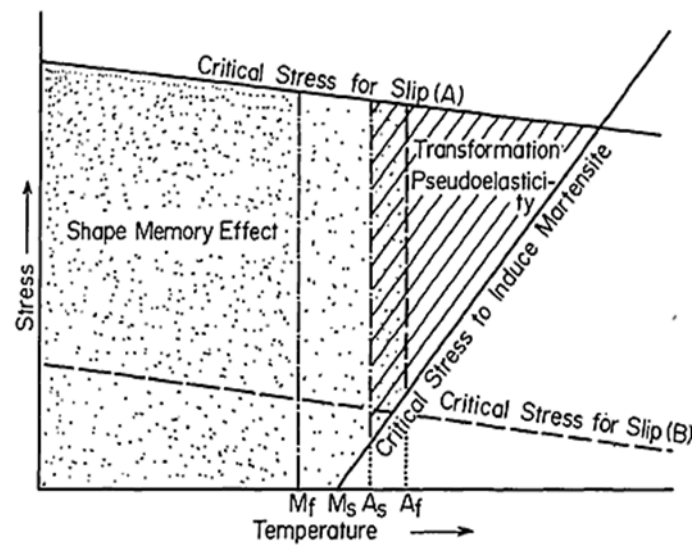


Figure 2.19. Diagram suggesting region of shape memory effect and transformation pseudo elasticity in temperature-stress coordinates (Otsuka and Shimizu, 1986; Otsuka and Ren, 2005).

2.4.1. Shape memory effect

SME is the phenomenon which happens in some alloys basically related with thermos-elastic martensitic transformations. NiTi, for example consists of austenite with a body centered cubic lattice, when it is exposed to high temperature, the austenite transforms to martensite on the cooling. Four temperatures can be defined during this transformation;

M_s : start temperature for martensite transformation on cooling.

M_f : finish of martensite transformation.

A_s : start temperature for austenite transformation on heating.

A_f : finish of austenite transformation.

Temperature and stresses are two factors playing the main role in the transformation mechanisms and represent the origin of the shape memory effect and superelasticity. The representative stress-strain curve of (SME) and (SE) are shown in Figure 2.20.

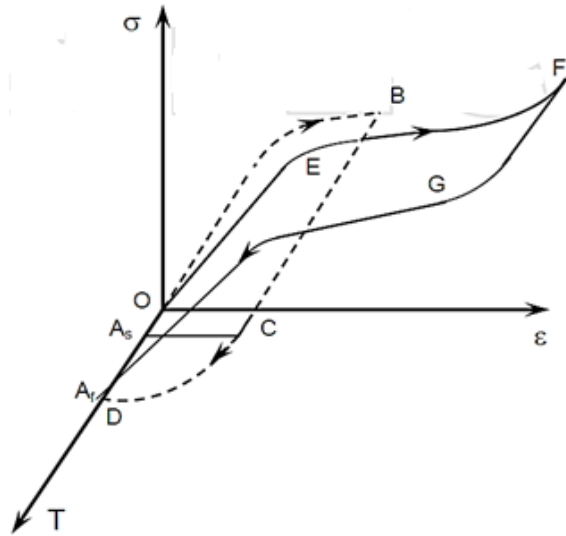


Figure 2.20. Graphic of stress-strain curve exemplifying the shape memory effect (OBCDO) and super elasticity (DEFGD) (Akselsen, 2004).

Good shape memory effect, biocompatibility, mechanical properties, and superior cold workability are properties that are displayed by Ti-based shape memory alloys (Horiuchi Y et al., 2006). Some non-toxic elements, such as Nb, Zr, Ta, Sn, Mo and Pt in Ti-based alloys exhibit shape memory effect (SME) and superelasticity (SE), which can be used in biomedical applications (Chai et al., 2008; Al-zain et al., 2010).

2.5. Production of Ti-Nb Alloys

2.5.1. Vacuum arc melting (VAM)

The Vacuum Arc Melting is an older device as shown in Figure 2.5.1, probably manufactured in the 1960's (Boehm, 1998). Alloys can be shaped by using this process. In this process metals are placed in the crucible to form alloy. Electric arc is used to generate heating; argon gas does not react with molten metal, so it is used to fill the chamber after evacuated. There are several problems assistant with graphite crucibles in vacuum arc melting that eliminated using the copper molds in this process, due to the absence of enough rousing, chemical homogeneity of the ingots requires several remitting procedures. Ti-Nb-Zr-Sn alloys were melted three times using a Ti-Sn master alloy and pure Ti, Nb and Zr as raw materials by using VAM technique. Three optical micrographs as-quenched quaternary alloys showed in Figure 2.5.2, represented

by Ti-24Nb-4Zr-7.5Sn, Ti-24Nb-4Zr-3.5Sn and Ti-20Nb-4Zr-7.5Sn alloys. Single β microstructure appear (Figure 2.5.2 (a)) or β matrix with high and low amount of the α'' martensite shown in (Figure 2.5.2 (b and c)). The small dark spots in Figure 2.5.2 (a) are often observed on metallographic samples of heavily deformed β -phase titanium alloys and are probably dislocation etch pits (Hao et al., 2006).

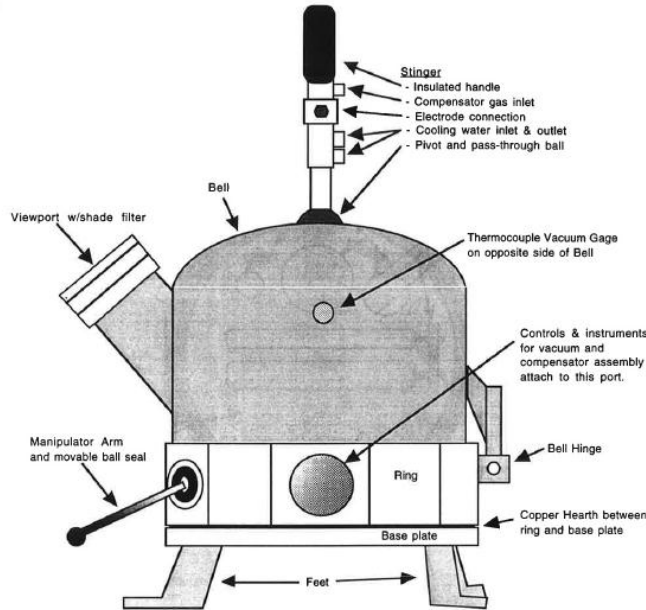
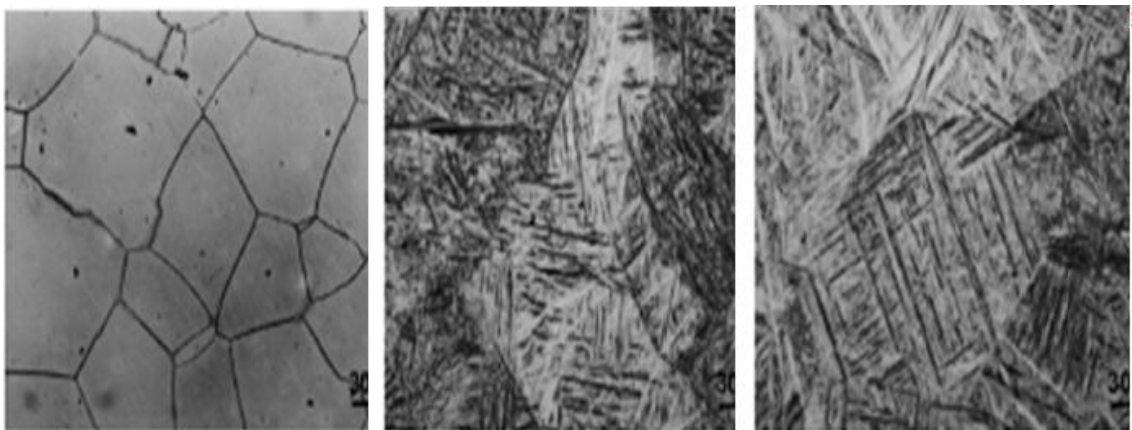


Figure 2.5.1. Right side view of Vacuum Arc Melting furnace with main parts (Boehm, 1998).



(a)

(b)

(c)

Figure 2.5.2. Characteristic graphic microstructures of water quenched quaternary Ti-Nb-Zr-Sn alloys: (a) Ti-24Nb-4Zr-7.5Sn, (b) Ti-24Nb-4Zr-3.5Sn and (c) Ti-20Nb-4Zr-7.5Sn alloys (Hao et al., 2006).

2.5.2. Vacuum induction melting (VIM)

Many complex alloys can be produced by Vacuum induction melting especially that is used in aerospace engineering. This process takes place in a graphite crucible inside a steel shell that is connected to a high speed vacuum system. VIM method is also used frequently for fabrication of the Ti alloys. Generally, VIM and VAR processes are combined to get sufficient homogenization of the melt (Capek et al., 2012).

VAR is essentially a constant voltage and constant resistance process. Heat for remelting is generated by a DC vacuum between the electrode and the forming ingot. In VAR, the molten metal droplets rapidly transfer from the electrode to the ingot. It is not capable of producing a rectangular ingot; however, by means of press forging or extrusion, rectangular billets can be made from round ingots for flat product applications. The majority of titanium alloys is produced by the VAR process

2.6. Powder Metallurgy

2.6.1. General

A conventional powder metallurgy process consists of four basic sub-processes namely powder production, blending or mixing, compaction and sintering (Kapil, 2016)

Powder mixing is a neutral type of mixing. It is a process in which two or more solid substances are mixed in a mixer by continuous movement of the particles or by hand. The length of time at which mixing is done increases the degree of mixing (Bhawna and Agrawal, 2007). Different lubricants can be used as binder with mixed powders. Generally, lubricant reduces die wall friction with powders and reduces friction between powders together, so more uniform product density is achieved (Jonsén, 2006). Three levels of homogeneity exist, large scale segregation from stratified mixtures, partial homogenization for agglomerated, and ideal of dispersed homogeneous structure as shown in Figure 2.5.3.

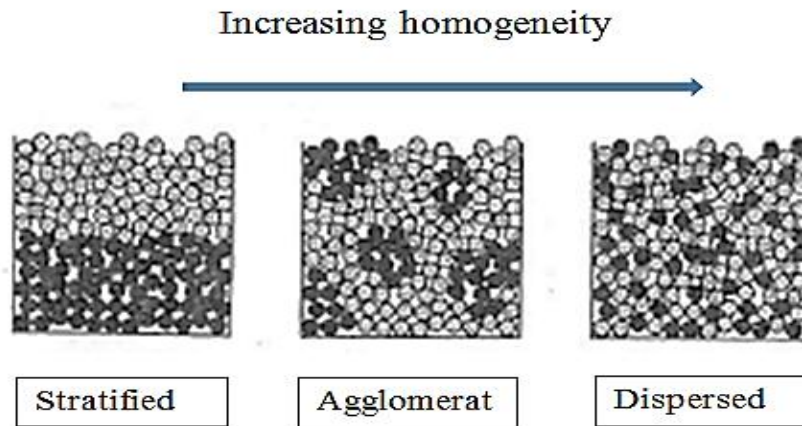


Figure 2.5.3. Graphic explained three levels of the increasing homogeneity (German, 1994)

Powder rearrangement, die filling, and compaction are the different stages in the die pressing process which play an important role in PM. The enclosed volume between punches and the die is reduced during powder compaction (Jonsén, 2006).

Figure 2.5.4 shows methods of die pressing. It can be done by two processes, single and double action pressing. The compacting pressure is highest on the edge of pressing tools and lowest on the bottom during single pressing. Using a movable upper and bottom punch in double action pressing makes the pressure distribution better than single pressing, but the die walls are also affected by friction (Sktiniovam et al., 2014).

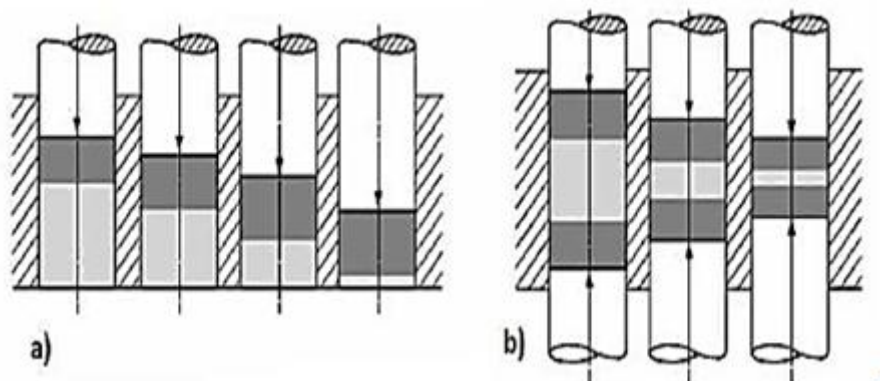


Figure 2.5.4. Methods of die pressing a) single pressing and b) double pressing (Sktiniovam et al., 2014).

Density gradients result from the pressure gradients in die pressed powder compacts, the density gradients with two types of single and double action pressing are shown in Figure 2.5.5 . These types of pressure applications control the density in the

compact and its strength. The density is the lowest at the bottom of the compact and increase towards the top in single action pressing, But, in double action pressing the density decreases towards the center and minimum density is reached at the center of the compact, so double action pressing is more homogenous if it compared with the single action pressing (German, 1994).

The height to diameter ratio of the compact is another important factor effecting the densification. Density of the compacts decreases with the increasing height to diameter ratio as shown in Figure 2.5.6 (German, 1984).

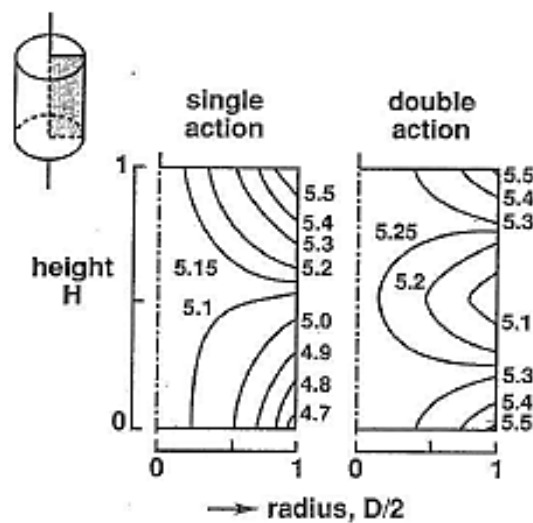


Figure 2.5.5. Density distribution in single and double action pressing (German, 1984).

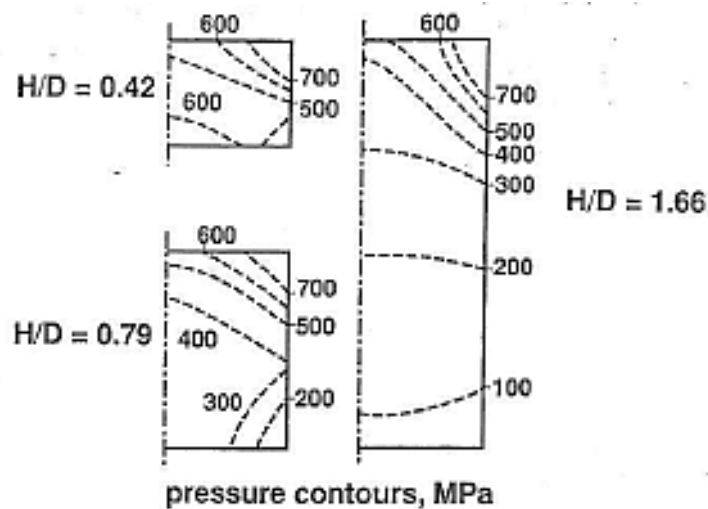


Figure 2.5.6. Pressure distributions in single-action pressing of three height to diameter ratios (German,1984).

Mechanical and hydraulic are two main types of compacting press. The particles of some metal powders are very hard and have limited plasticity, so rigid die compaction is not suitable for consolidating. Hot pressing, extrusion, or hot isostatic pressing, are other methods to process such powders (James, 2015; ElRakayby et al., 2015).

Figure 2.5.7 shows the compaction steps in uniaxial pressing. Arrangement of particles with considerable increase in density occurs in stage one. The contact between the particles increases in stage two, and individual particles are deformed at higher pressure, as a result more defined elastic-plastic deformation occurs at inter particle contact areas. In stage three, when pressure increases, cold welding occurs between particles (Eksi and Saritas , 2002; Sktinicovam et al., 2014; Suresh et al., 2015). Figure 2.5.8 displays the mechanisms for processing metal powders to full density as a function of temperature. Hot pressing or (HIP) is an example of diffusional creep processes which works at intermediate temperature, extrusion and forging are processes which work at high strain rates and lower temperatures. Liquid-phase sintering is low-stress process which works at high temperature and controlled by diffusion process. Dynamic compaction and explosive compaction are applications of ultrahigh-stress at ambient temperature which attain high density.

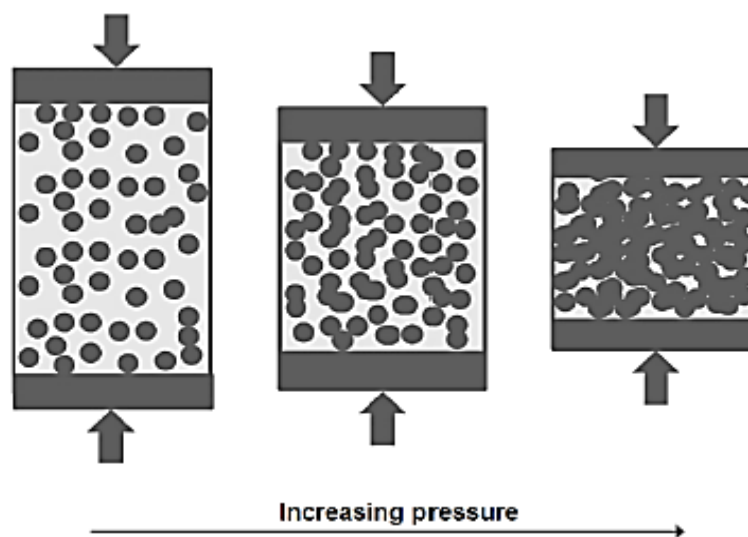


Figure 2.5.7. Simple view of the stages of metal powder compaction (Sktinicovam et al., 2014).

When metal powder is compressed and heated in a controlled atmosphere furnace, the temperature of the furnace will be somewhat below melting point of the metal powder but above the recrystallization temperature which is enough to allow bonding of the particles. This process is called sintering. Normally, strength, density and ductility increase and other mechanical properties are enhanced during sintering (German, 1984; Suárez et al., 2013; Sktinicovam et al., 2014).

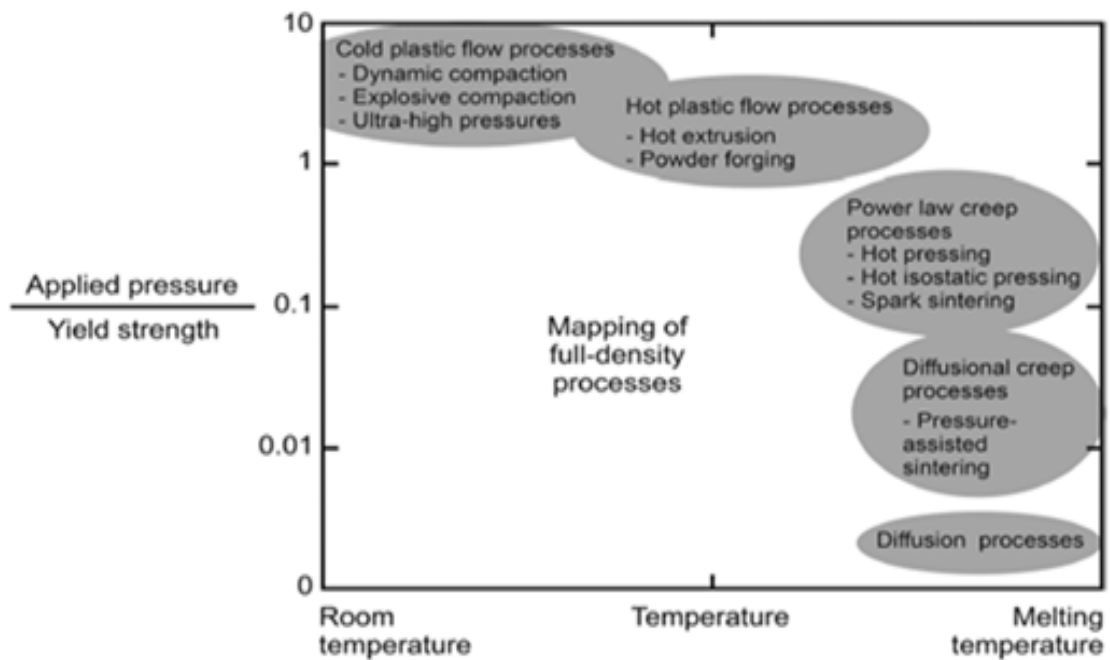


Figure 2.5.8. Options for processing metal powders to full density (James, 2015).

In general, a temperature of 0.6-0.75 of the melting point for one component system is suitable to occur sintering, but for multi-component systems, sintering is done at a temperature near or slightly higher than the melting of a component with the lowest melting point (Jonsén, 2006; Sktinicovam et al., 2014).

The changes of the pore structure with sintering are shown in Figure 2.5.9. The process passes during four stage, point contact, initial stage, intermediate stage, and final stage. The pore size decrease and approaches a cylindrical shape and the grain boundary increases with increasing of temperature. Different developed techniques for material sintering are shown in Figure 2.5.10.

The main purpose of sintering atmosphere is to keep the powder compacts from oxidation. Vacuum, hydrogen or inert gases such as argon can be used to produce Ti

and its alloys. A pre-alloyed titanium alloy powder and alloying elements or a pure titanium powder mixture and alloying elements are the main elements to prepare the titanium-based sintering products.

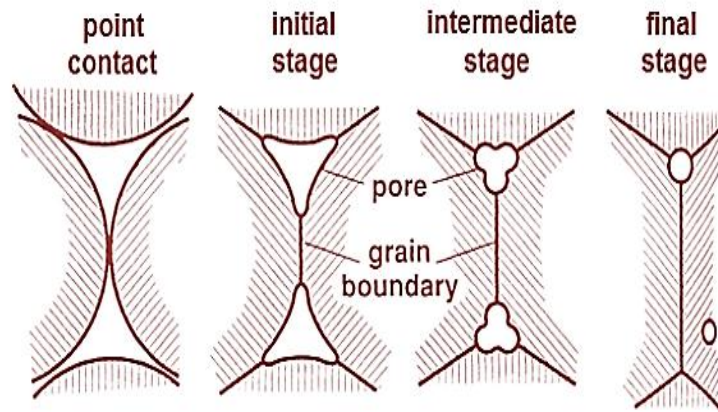


Figure 2.5.9. A diagram of pore structure and grain boundaries between particles during sintering (Geeman, 1994)

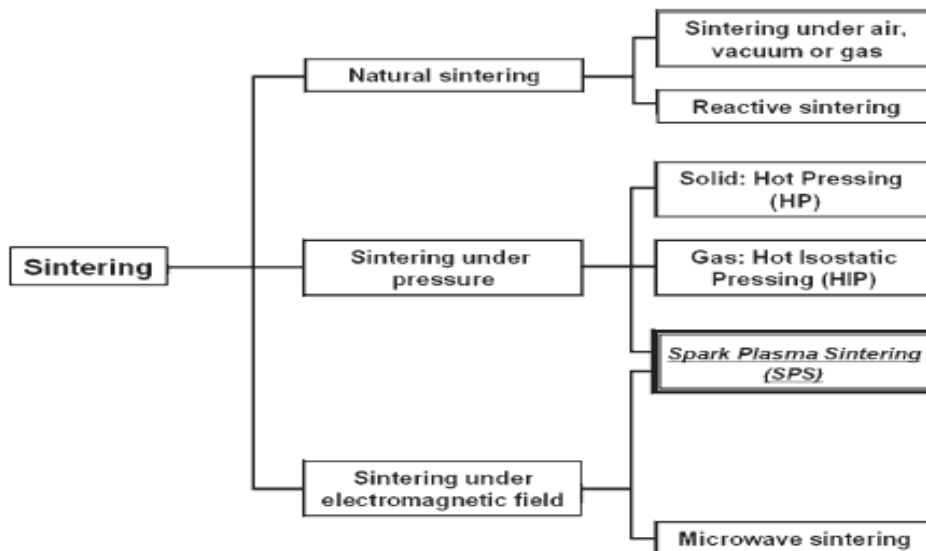


Figure 2.5.10. Different developed techniques for material sintering (Hungria et al., 2009).

To enhance mechanical properties and high densification of titanium powders, generally these powders must be vacuumed during sintering processes under pressure of 10^{-2} Pa or lower, to control the reaction between titanium and oxygen, nitrogen or carbon (Yu et al., 2017). With decreasing of gas pressure in the sintering chamber, the

surface contaminations are decreased on the powder particles (Guillon et al., 2014). High densification level can be achieved using fine particles, high compaction pressure and suitable sintering conditions (Yu et al., 2017).

Powder metallurgy is one of the available and suitable techniques for preparation of the Ti-Nb-based alloys using elemental powders because preparation of alloys with high content of Nb, which is a high melting point metal has difficulties with use of conventional methods (Štěpán et al., 2010).

2.7. Powder metallurgy of Ti Nb alloys

Pressing and sintering; pressing, sintering and hot working; hot pressing (HP), hot isostatic pressing (HIP), spark plasma sintering (SPS), metal injection molding (MIM), conventional sintering (CS), 3D printing are typical techniques used to prepare titanium and its alloys especially Ti-Nb alloys. The pressing and sintering is technically the simplest and economically the most attractive between all techniques above (Qian and Schafferm, 2010).

2.7.1. Hot pressing

Hot pressing is a type of sintering which is done under pressure. Induction heating, indirect resistance heating and direct hot presses are the three different types of heating which can be used in hot pressing technology. Hot pressing is much slower than the conventional press and sinter process and it has lower tolerance. In hot pressing process, the force and the heat are applied to the specimen at the same time. In this manufacturing process good mechanical properties can be achieved. This process requires extreme temperature and pressure. For this reason, the mold material that is selected must be capable to work under this condition. Graphite molds may be used for hot pressing technique. Fine green pressed powders can be consolidate in to partially or fully sintered components by hot pressing in elevated temperature and compressive stress. Titanium and titanium alloys can be consolidate by using hot pressing. Figure 2.5.11 shows hot pressing technique (Yang and Qain, 2015).

Titanium powders can be reached with a high density in less time with using inductive hot-pressing when compared it with pressing and sintering process (Bolzoni, 2012).

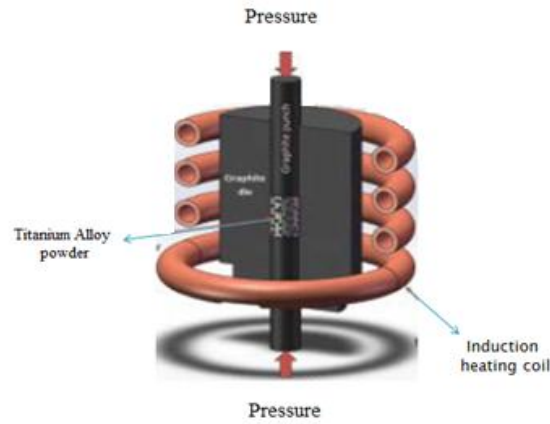


Figure 2.5.11. The hot pressing process: graphic of the device (Henriques et al., 2014).

2.7.2. Hot Isostatic Pressing (HIP)

In (HIP), a metal powder is strained using inert gas in a metal container and heated under vacuum to remove volatile contaminants. Pressure is applied from all directions at the same time. Powders must be processed to the point where they have no surface-connected and interconnected porosity (James, 2015). Excellent mechanical properties, good metallurgical bonding and 100% density can be obtained by using (HIP) process. HIP can be used for improvement of castings, consolidating powders and HIP provides better mechanical properties of parts than those produced by different manufacturing processes. Grain boundary diffusion, lattice diffusion and surface diffusion are different mechanisms of matter transport to fill the pores. In hot isostatic pressing a combination of pressure and temperature are used to dense the porous powders (ElRakayby et al., 2015).

HIP process was used to fabricate samples from elemental titanium and titanium alloys with relative density as high as %99 where relative density is the ratio of the compact density to the density of the same material without porosity (Bolzoni et al., 2012).

2.7.3. Spark plasma sintering (SPS)

(SPS) also known as field assisted sintering (FAST), is another sintering technique that uses force and direct electrical current (DC) under low atmospheric pressure to do high speed consolidation of the powder. High sintering speed, ease of operation, and control of sintering energy, safety and accuracy are the many advantages of SPS when compared with HP sintering, HIP or atmospheric furnace (Suárez et al., 2013). Different types of materials can be used in SPS process like nanostructured materials, intermetallic compound, metal matrix and ceramic matrix composites which are difficult to sinter by common methods. SPS is alike to hot pressing technique but the difference is the way to produce the heat and how transmitted to the sintering material (Suárez et al., 2013; Guillon et al., 2014).

SPS is more effective for superfine and nano crystalline structured materials because they have more surface area per volume compared to the same material that has larger particles. Most conventional powdered material sintering technologies require pre-forming and binders but sintering of materials by SPS processes is done without using binders. Generally high-density powder-metallurgy products and high mechanical properties of titanium alloys can be achieved by using SPS. Uniaxial press, punch electrodes, vacuum chamber, DC pulse generator, temperature, and pressure measuring units are the main parts of an SPS machine as shown in Figure 2.5.12..

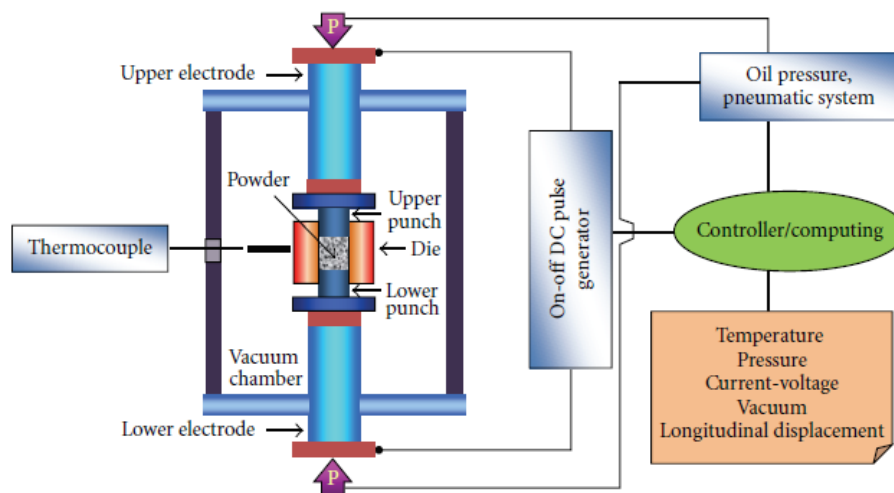


Figure 2.5.12. Main parts for SPS device (Saheb et al., 2012).

A high-temperature is generated, when a spark discharge appears in a gap or at the contact point between the particles of a material. This causes evaporation and melting on the surface of powder particles in the SPS process, and necks are formed around the area of contact between particles as shown in Figure 2.33

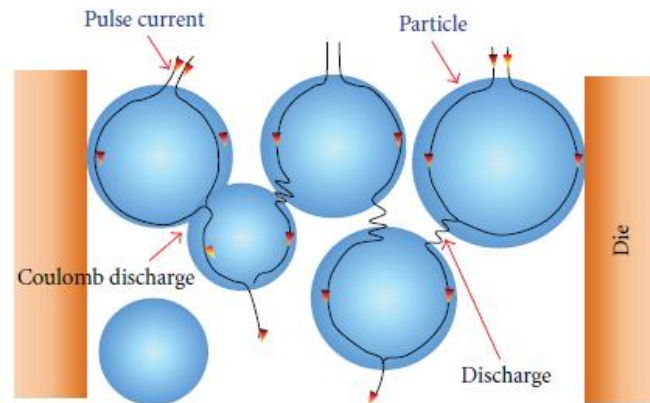


FIGURE 3: DC pulse current flow through the particles.

Figure 2.5.13. DC pulse current flow through the particles (Saheb et al., 2012).

Four main stages of SPS are indicated in Figure 2.34. Process starts with vacuuming after that pressure is applied followed by heating and sintering and finally cooling step finishes the cycle.

Both sintering temperature and applied pressure affect the sintered density of CP-Ti until full densification is achieved. Their influences are interconnected. Figure 2.35 shows the consolidation of CP-Ti powders ($<45\ \mu\text{m}$) by SPS technique under a pressure of 60 MPa and vacuum condition and isothermal hold: 5 min at each temperature. Increasing sintering temperature was effective before reaching 950°C but not afterwards because of the rapid achievement of full densification.

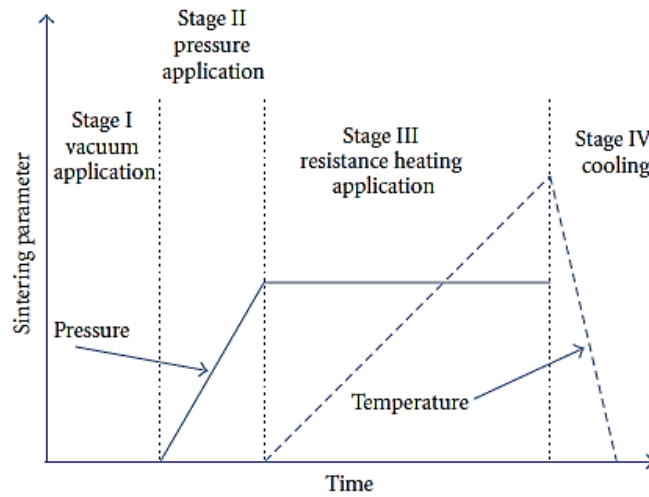


Figure 2.5.14. Four stages of spark plasma sintering (Saheb et al., 2012).

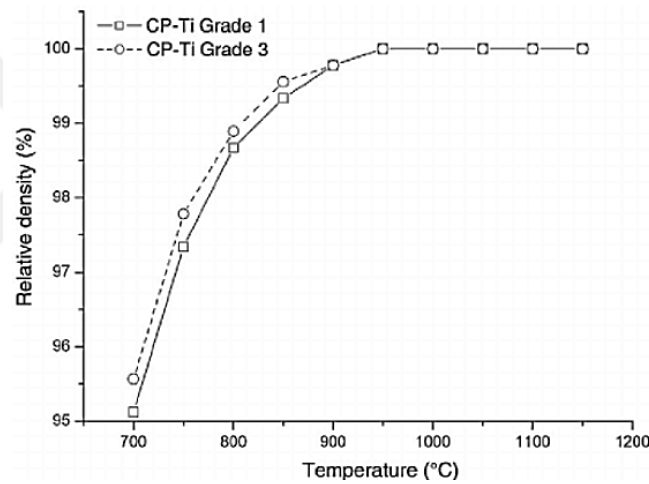


Figure 2.5.15. Consolidation of CP-Ti powders by SPS (Yang and Qain, 2015).

SPS techniques were used to prepare Ti-Nb samples using pure Ti and Nb powders. Spark-plasma sintering was used to consolidate the mixed powders into a cylindrical billet with a diameter of 50mm and 20mm height, and the sintering was done at a temperature of 1100°C for 60 min and under a pressure of 30 MPa under a vacuum of 5Pa. After that to increase the solid-state inter diffusion the homogenization process was carried out at 1500 °C for 12h. The XRD pattern of Ti-23 at% Nb for the sintered sample shows α and β phase, after the sintering process the peak intensity of the (α) phase decreases and β is the main phase in the alloy as shown in Figure 2.5.16 (Bahador., et al., 2017).

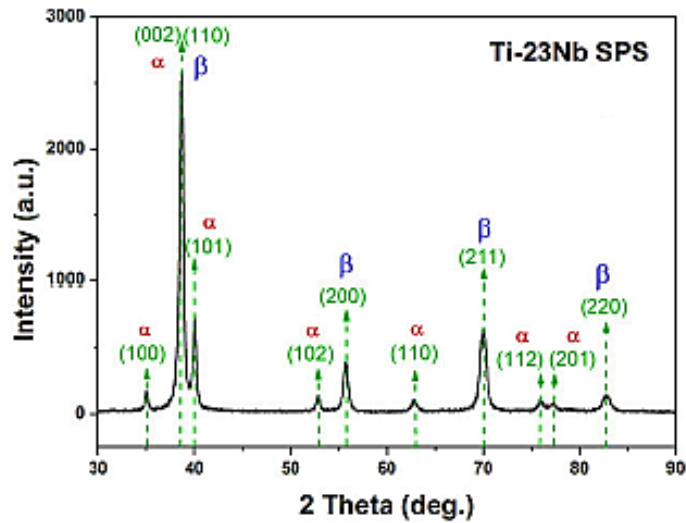


Figure 2.5.16. XRD diffraction pattern of sintered sample of Ti-23 at% Nb alloy (Bahador et al., 2017).

2.7.4. Metal injection molding (MIM)

A net-shape process for the manufacturing of high volume, very complex-shaped parts, and high accuracy components for use in a multiplicity of industries is called as MIM. It attracts growing interest for the processing of Ti and Ti alloys as biomaterial (Zhao et al., 2013). MIM process shows in Figure 2.5.17.

(Itoh et al., 2007) stated that the metal injection molding (MIM) process can be used to fabricate complex shape of Ti or its alloy parts with higher functionality and significant cost reduction using mixed powders. Ti-6Al-7Nb alloys using 3 types of mixed powders were produced by metal injection molding process, using mixture of Ti+Al-Nb (Al-53.8Nb), Ti+Ti-Al+Nb (Ti-35.7Al) and Ti+Al+Nb (all particles sizes are $-45\mu\text{m}$). Figure 2.38 shows the effect of sintering temperature on the relative density of Ti-6Al-7Nb alloy compacts for the 3 types of mixed powders. The relative density of the powders increases with increasing sintering temperature for all types of mixed powders. The tensile strength and elongation of the compacts using a mixture of Ti-6Al-7Nb alloy powders increase with the sintering temperature, but it remains nearly constant with increasing sintering temperature above 1423K as shown in Figure 2.39.

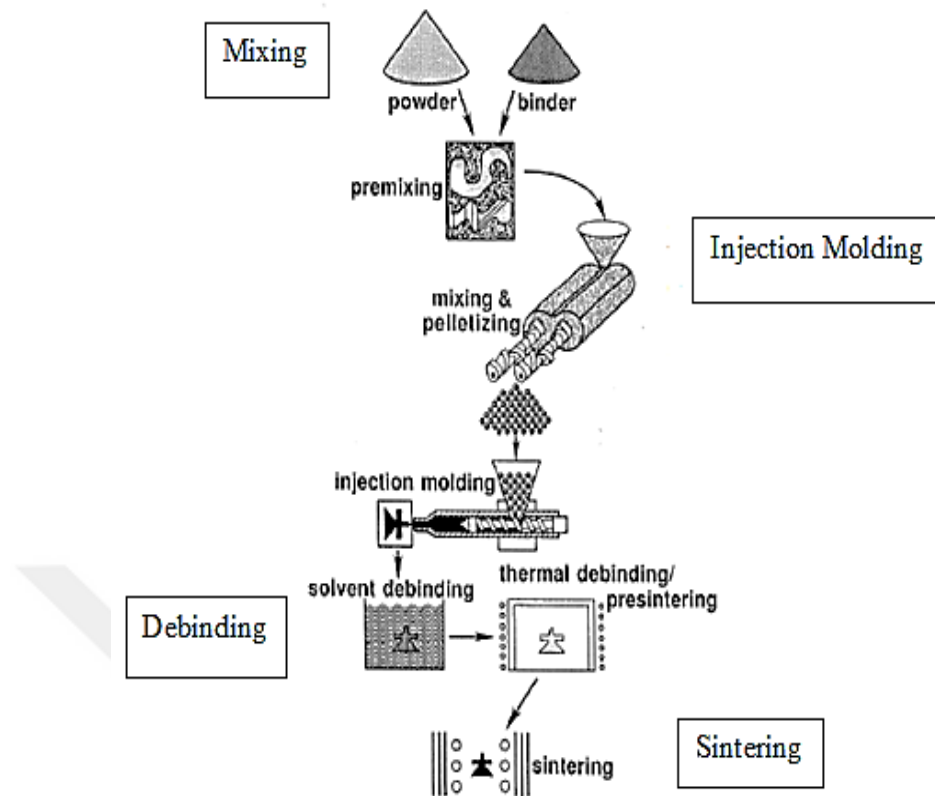


Figure 2.5.17. MIM processes process (Zhao et al., 2013).

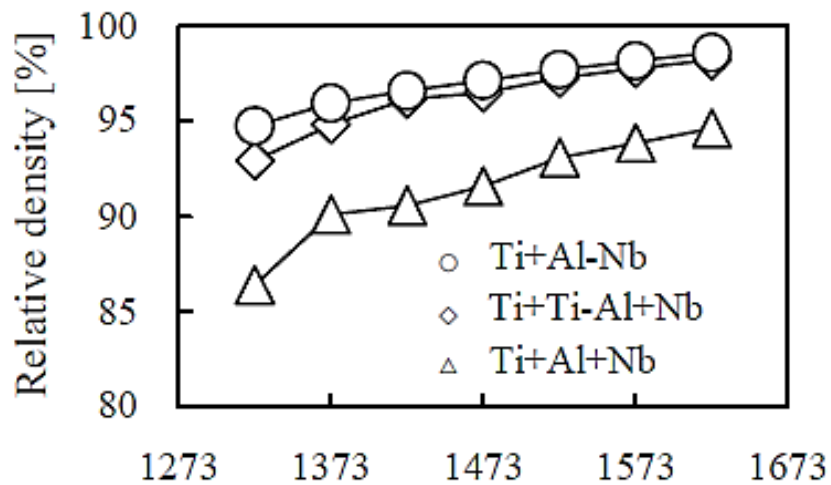


Figure 2.5.18. Effect of sintering temperature on the relative density of Ti-6Al-7Nb alloy compacts for 3 types of mixed powders (Itoh et al., 2007).

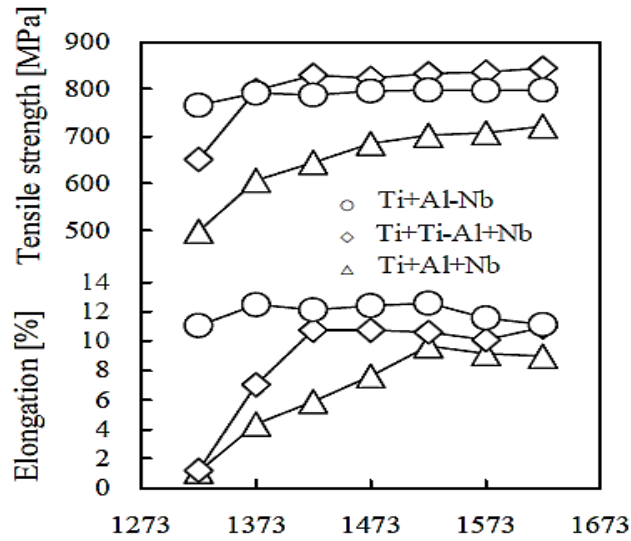


Figure 2.5.19. Effect of sintering temperature on the tensile properties of Ti-6Al-7Nb alloy compacts for 3 types of mixed powders (Itoh et al., 2007).

(Zhao et al., 2015) used Ti (-325 mesh) and Nb (-120 mesh) powders to fabricate Ti-16Nb (wt. %) alloys by metal injection molding process. The powders were mixed with the polymer binder; all specimens were sintered at different temperatures. Sintering temperatures ranged between 900 °C and 1500 °C with a heating rate of 5°C/min. After reaching the sintering temperature, the samples were held for 2 h and then furnace cooled to room temperature with a cooling rate of 10°C/min. The XRD spectra of the Ti-16Nb of all samples are shown in Figure 2.5.20. Figure 2.5.21 presents the microstructural evolution of the samples sintered at temperatures from 900 °C to 1500 °C. The Ti-16Nb (900) samples were apparently composed of Ti particles and Nb particles, resembling their original particle morphologies. High sintering temperature and longtime effected on the microstructure and mechanical properties of alloy in final products. The result of alloy sintered at 1500 °C showed a good grouping of high strength and low Young's modulus which can be used for biomedical applications. Sintering temperature also affected the porosity of TiNb alloys fabricated by MIM technique, the porosity decreased from about 25% to 6% as shown in

Table 2.5.1.

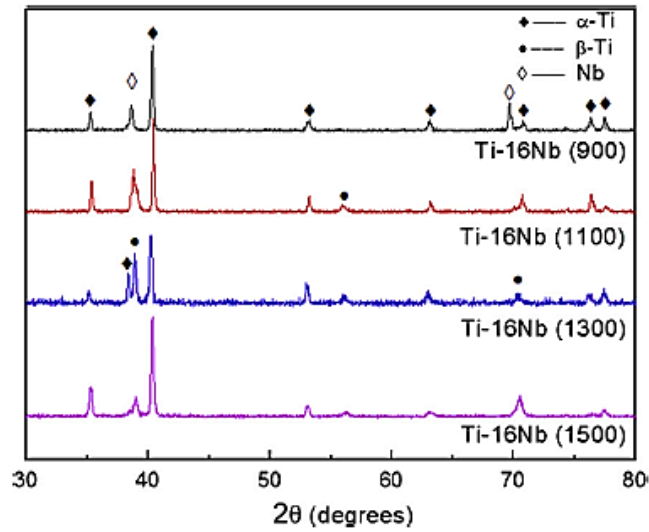


Figure 2.5.20. XRD results for the Ti–16Nb alloys sintered at different temperatures (Zhao et al., 2015).

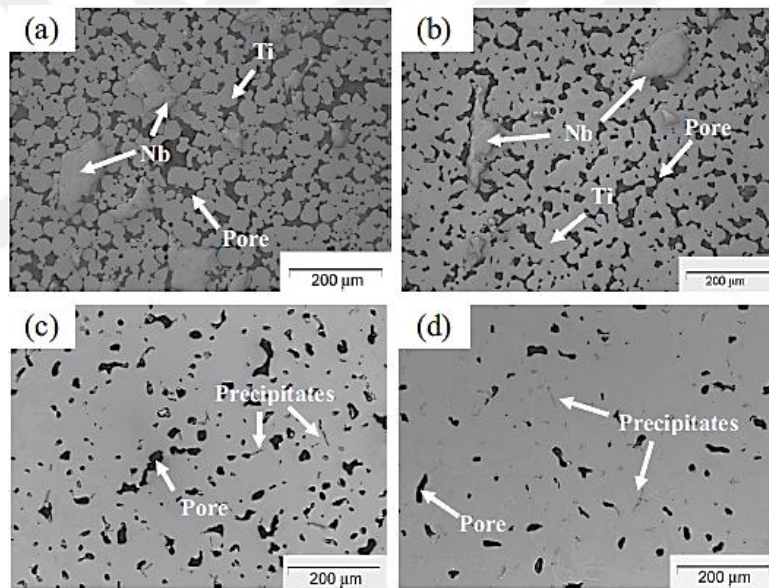


Figure 2.5.21. Optical micrographs of Ti–16Nb at (a) 900°C; (b) 1100°C; (c) 1300°C and (d) 1500°C (Zhao et al., 2015).

Table 2.5.1 The porosity of Ti–Nb alloys fabricated by MIM and sintered at different temperatures (Zhao et al., 2015)

Samples	Ti-16Nb (900)	Ti-16Nb (1100)	Ti-16Nb (1300)	Ti-16Nb (1500)
Porosity (%)	23.8±2.4	15.6±1.6	8.9±1.3	5.7±0.8

2.7.5. Conventional sintering (CS)

Densification and grain growth occur together through atomic diffusion mechanisms during the conventional sintering of a compacted powder. CS method provides higher production capacity and lower cost when compared to other sintering methods such as (HP), (SPS), and (HIP), but mechanical properties are lower compared to other sintering methods. It is still a more attractive sintering method to produce ceramic products, mainly due to its ease and low cost compared to other methods. In conventional sintering of Ti and Ti alloys mixed elemental or pre-alloyed powders requires compacting and sintered under high vacuum or Ar gas atmosphere at elevated temperatures around (1200-1400°C) for long times usually varying in the range of 2-72 hours (Aydoğmuş, 2010).

3. MATERIALS AND METHODS

3.1. Powders Used

In the present study, elemental pure Ti (99.5%) and pure Nb (99.8 %) powders (both of them -325 mesh, smaller than $45\mu\text{m}$) supplied by Alfa Aesar, Germany were used to fabricate Ti-40Nb (wt. %) corresponding to $\text{Ti}_{74}\text{Nb}_{26}$ alloy by atomic %. SEM images given in Figure 3.1 show the morphological properties of as-received powders. The shapes of Ti and Nb powder particles were irregular since they were produced by hydride dehydride conversion technique. In this powder production method firstly a ductile solid pure metal or an alloy is subjected to hydrogenation process and made brittle. After that for granulation mechanical milling is applied. When the desired powder size is reached milling is terminated and the powders obtained are exposed to final dehydrogenation step and ductile, hydrogen free pure or alloy powders are attained.

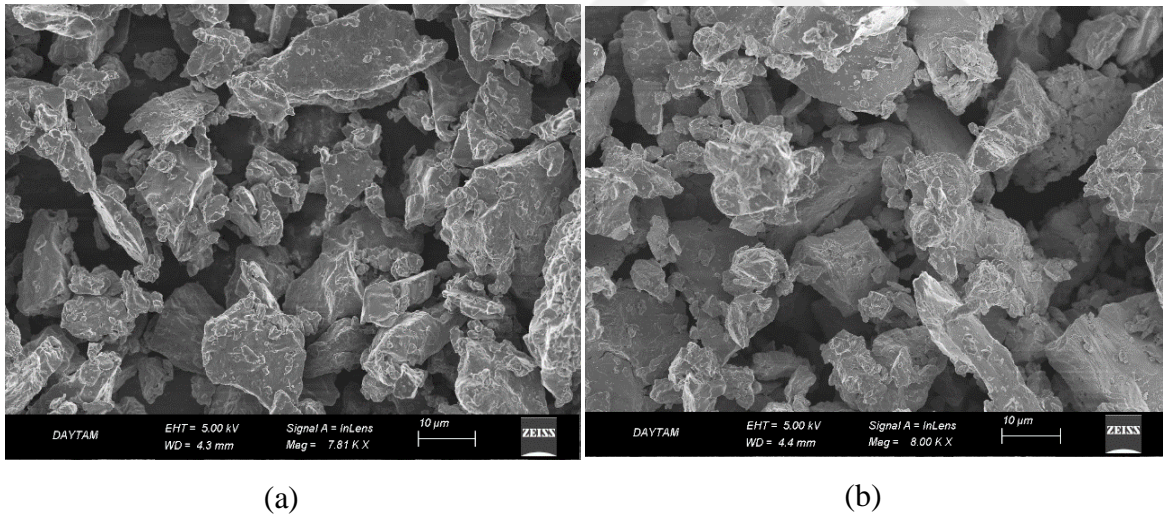
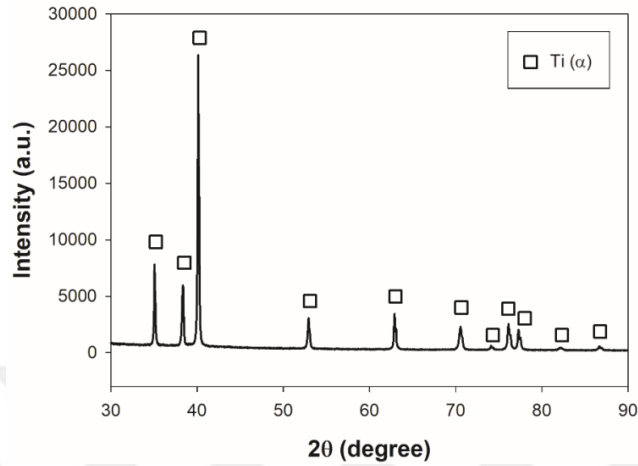


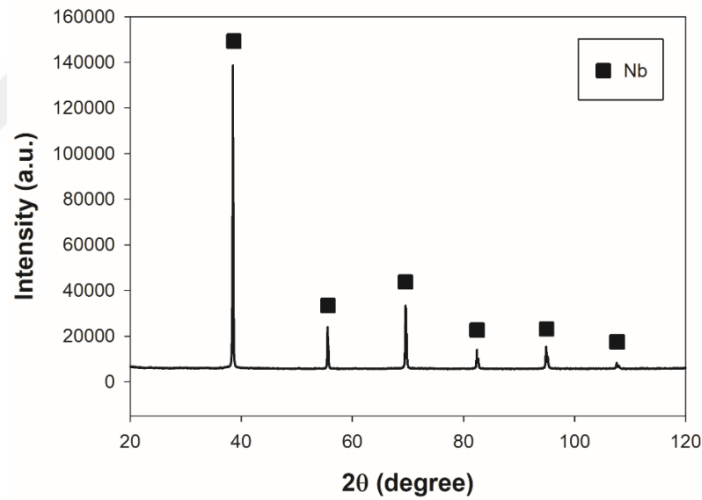
Figure 3.1. SEM micrographs of pure (a) Ti and (b) Nb powders.

Figure 3.2 presents the XRD results of starting raw powders. The phases existing in the microstructure of Ti and Nb powders were pure α -Ti with a hexagonal close packed (HCP) crystal structure and pure Nb with a body centered cubic (BCC) structure. None of the powders contained oxide or carbide phases so that they were free from any type

of contamination. Raw powders were stored in a glove box under high purity argon gas as shown in Figure 3.3 to prevent oxide layer formation on their surfaces.



(a)



(b)

Figure 3.2. XRD patterns of as-received (a) Ti powders and (b) Nb powders

3.2. Sample Production

3.2.1. Hot Pressing

Composition of the Ti-Nb alloy is selected to be $\text{Ti}_{74}\text{Nb}_{26}$ (atomic percent) because this composition has the lowest elastic modulus value and displays shape

memory and superelasticity properties. Weights of raw powders were calculated considering the selected composition and final dimensions of the cylindrical samples (15mm in diameter and 10mm in height). It was assumed that hot pressed samples would attain full density (zero porosity) in order to get the predetermined height or thickness of 10 mm. Powders were weighted (5.86 g Ti and 4 g Nb) using an electronic balance as shown in Figure 3.4 and mixed manually with the help of a binder, ethylene, for 15 minutes to obtain a homogeneous mixture. Afterwards, the mixture was charged into a hollow cylindrical graphite die with inner diameter of 15 mm as presented in Figure 3.5.



Figure 3.3 The argon-filled glove box used to store Ti and Nb powders.



Figure 3.4. The electronic balance employed to measure weight of the raw powders.

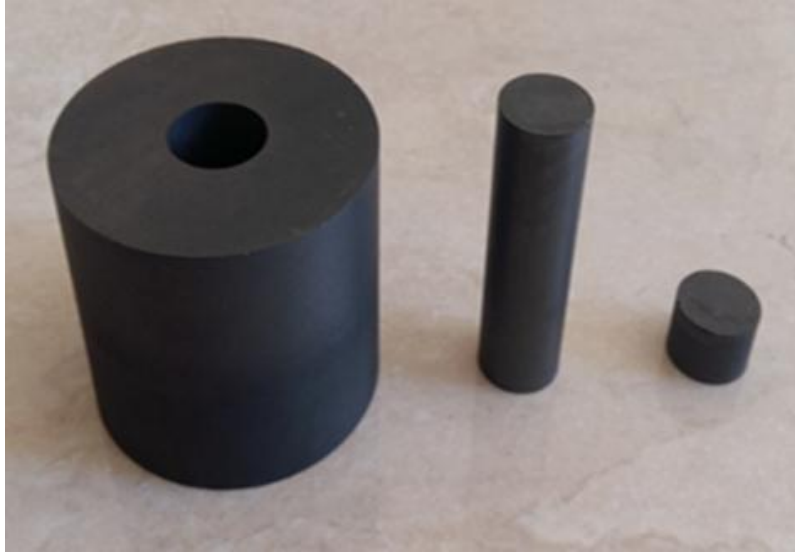


Figure 3.5. Graphite dies with the inner diameter of 15 mm and its accessories, top and bottom punches

The graphite die tool filled with Ti and Nb powder mixture was put into the pressing chamber and positioned as it can be seen in Figure 3.6. Then the door of hot pressing chamber was closed and the chamber was vacuumed up to 10^{-1} mbar. Following vacuuming the chamber was filled with pure argon gas. This procedure was repeated 3 times and all the residual air was swept away from the chamber. Specimens were heated to the hot pressing temperatures predetermined, pressed and sintered at those temperatures simultaneously for 1 hour of constant time. Heating rate used was $10^{\circ}\text{C}/\text{min}$ and the pressure applied during heating, pressing and cooling steps kept constant as 50 MPa. An MSE_ M_HP_1300 model hot press was employed to obtain full density samples and hot pressing operation was carried out at 600°C , 650°C and 800°C . All the hot pressing experiments were done under flowing argon gas atmosphere to prevent oxidation of samples. Finally, hot pressed samples were cooled inside the chamber slowly and taken from the chamber when the temperature decreased to 150°C . The graphite deposited as a thin layer on the hot pressed sample surfaces were removed applying grinding Figure 3.8.

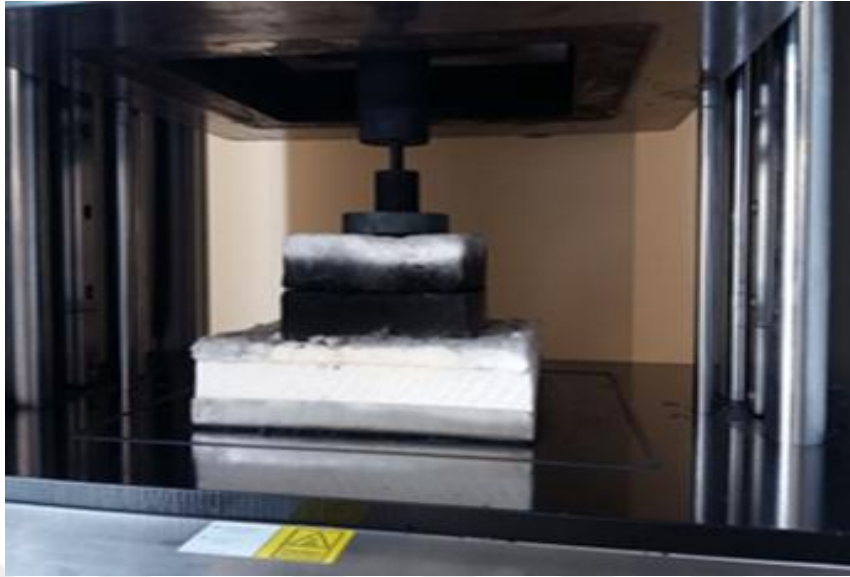


Figure 3.6. Location of the graphite die filled with powder mixture inside the hot pressing chamber.



Figure 3.7. Grinding wheel rotating type machine.

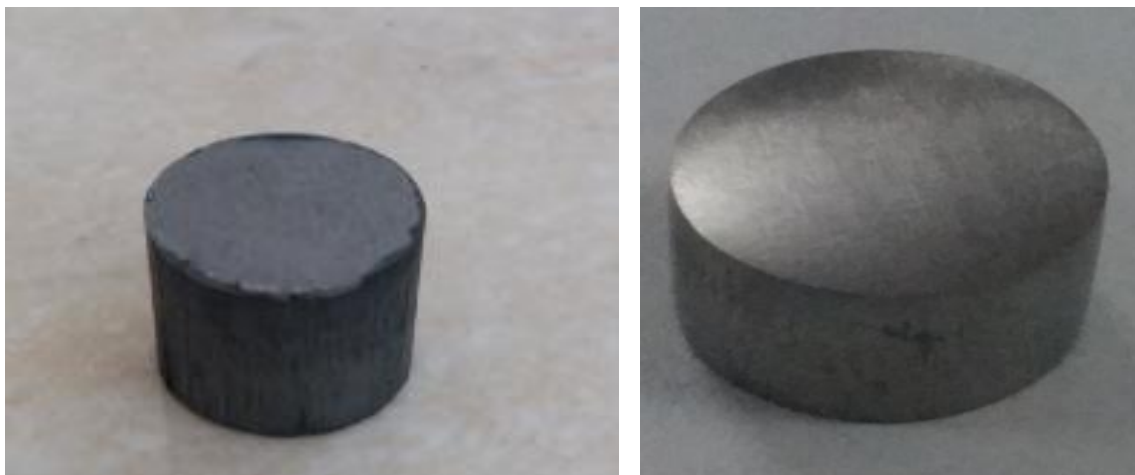


Figure 3.8. Hot pressed Ti-Nb specimen before and after grinding.

3.2.2. High Temperature Sintering

After grinding samples were cleaned in an ultrasonic cleaner for 10 minutes to remove possible residues and left drying. Next, samples put in an alumina (Al_2O_3) crucible were further sintered at $1200\text{ }^\circ\text{C}$ in a vertical tube furnace (Protherm PTF 14/50/450) for 1, 2, 3 and 4 hours under flowing argon gas to obtain desired β phase providing Nb dissolution in Ti. Sintering temperature ($1200\text{ }^\circ\text{C}$) was kept constant for all the specimens. The vertical tube furnace and experimental set-up used for high temperature sintering processes are shown in Figure 3.9. Having sintering completed, the samples were cooled inside the furnace slowly and removed from the furnace at 200°C . Heating rate for sintering was $8^\circ\text{C}/\text{min}$ which was lower than that of hot pressing. Heating, sintering and cooling curves are given in Figure 3.10. Temperature-time curve of hot pressing has also been added into that figure for comparison. Initial linear region in the curves represent heating step where the heating rates were kept constant as 10 and $8^\circ\text{C}/\text{min}$ for hot pressing and sintering, respectively. Horizontal second region corresponds to hot pressing or sintering time and finally the third region shows the cooling step where the slopes of the curves at different points are variable, not constant. This means that cooling rate is not constant during cooling; it is maximum just after sintering completed (at the beginning of cooling stage) and decreases with time.

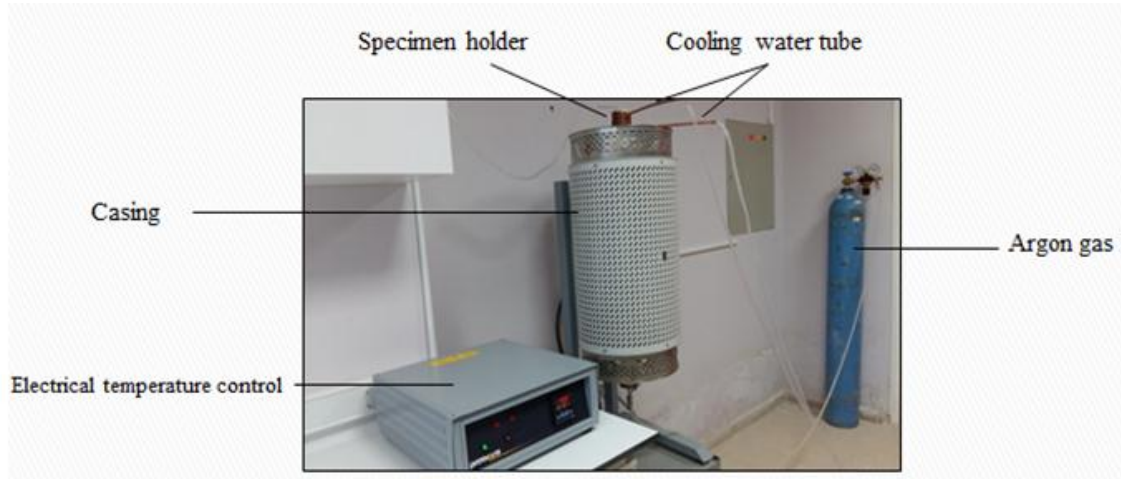


Figure 3.9. Experimental set-up including vertical tube furnace used for high temperature sintering operations.

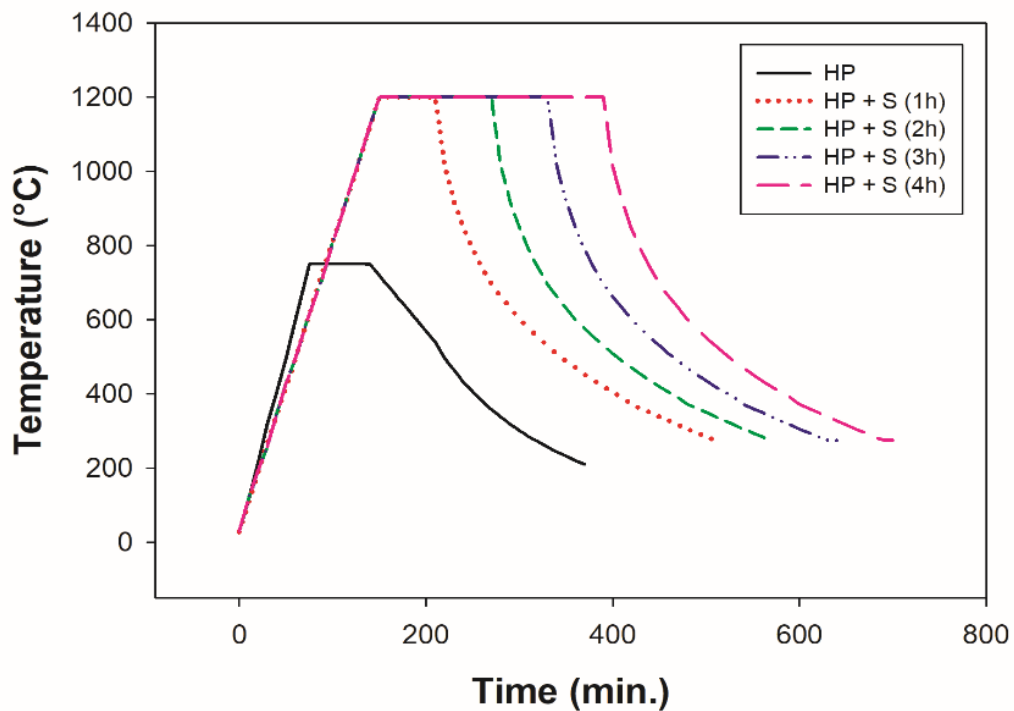


Figure 3.10. Temperature-time curves of hot pressing (HP) for 1h and following sintering (HP+S) processes for different times.

Figure 3.11 presents a picture of the sample sintered for 1 hour without using Ti getter particles. A very thin oxide layer that can be removed by grinding easily occurred on the surface of the sample during sintering and cooling. The sample which was sintered at the same temperature for 2h, surface oxidation occurred was more as shown

in Figure 3.12 compared to the sample sintered for 1h. Different colors correspond to different oxides of Ti.



Figure 3.11. The macrograph of the sample sintered at 1200 °C for 1h without using Ti getters.



Figure 3.12. The sample sintered at 1200 °C for 2h without using Ti getters.

In order to prevent or minimize oxidation during sintering, pure Ti sponge particles were used as shown in Figure 3.13 as oxygen getters. Figure 3.14 shows the sample produced sintering at the same temperature for 2h using Ti getters. Less oxidation was observed compared to the sample sintered at the same conditions without using Ti getters. Surface oxidation occurred was similar to one that formed on 1h sintered sample without using Ti getters. Consequently, it was decided to use Ti getters during sintering lasting 2h and more. Ti getters were placed just above the samples to be

sintered. During sintering and cooling these getters behaved as sacrificing materials to minimize oxidation and they were oxidized, Figure 3.15 instead of the samples.



Figure 3.13. Ti sponge getters used during sintering.



Figure 3.14. The sample sintered at 1200 °C for 2h using Ti getters.



Figure 3.15. Oxidized Ti getters after high temperature (1200 °C) sintering process.

3.3. Density Measurements

Density and the porosity of the samples in hot pressed and sintered conditions were measured using Archimedes' principle employing an electronic precision balance (X Precisa 321) equipped with a density determination kit by using the water replacement (suspension) method. The device used for the measurements is shown in Figure 3.16.

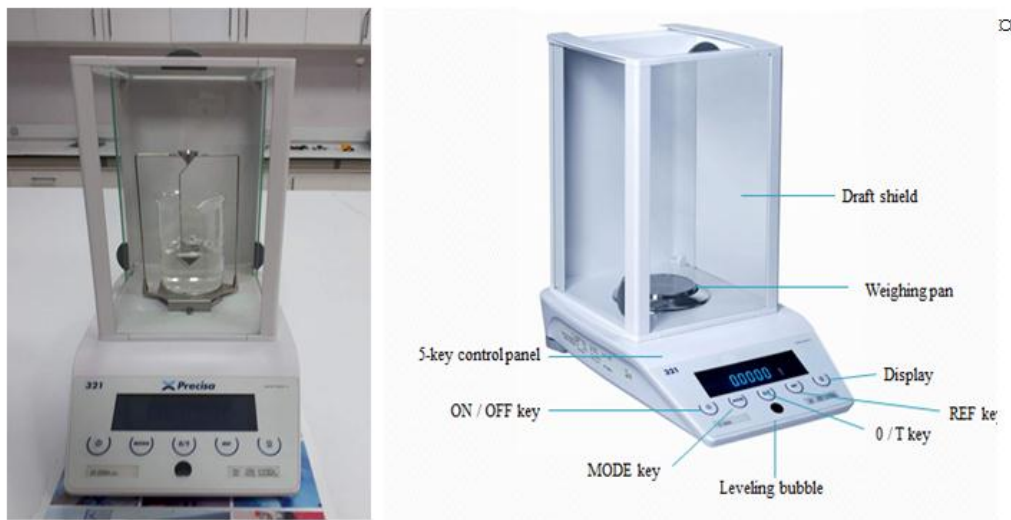


Figure 3.16. Precision balance and the density determination kit.

3.4. Metallographic Sample Preparation

The samples (Figure 3.17) for microstructural and mechanical characterization were cut in the dimensions of 5x5x10 mm using electrical discharge machine systems

(EDM), Charmilles Robofil 290 and 310, with electrical sparks between 8000-12000°C as shown in Figure 3.18. A special liquid was used to control sparking, cooling and flushes during cutting. Samples in compression tests were used as they were cut. For XRD studies surface of the samples were grinded with 320 SiC papers to remove contamination residues left after cutting operation. For micro hardness and SEM investigations specimens were subjected to full metallographic preparation steps in which grinding (240-1200 grinding papers), polishing (diamond suspension, 3 μ m) and finally etching was applied, respectively. Kroll's reagent (3 ml HF + 6 ml HNO₃ + 100 ml H₂O) was used to etch the samples for about 15 seconds.



Figure 3.17. Processing of cutting samples with dimensions 5x5x10mm

3.5. Microstructure

3.5.1. X-ray Diffraction (XRD)

X-ray diffraction (XRD) as shown in Figure 3.19 is a quick method used for phase identification of a crystalline material and it can give information on unit cell dimensions. The diffraction pattern of a substance is its "fingerprint" allowing identifying the substance and determining its crystalline structure. XRD analysis were carried out using a PANalytical Empyrean model X-ray diffractometer with CuK α radiation ($\lambda=1.540598 \text{ \AA}$) at 45 kV, 40 mA within a range of diffraction angles 2θ from 20° to 90° at a scan speed of 2 degree/min.



Figure 3.18 Two electrical discharge machines used for cutting samples.

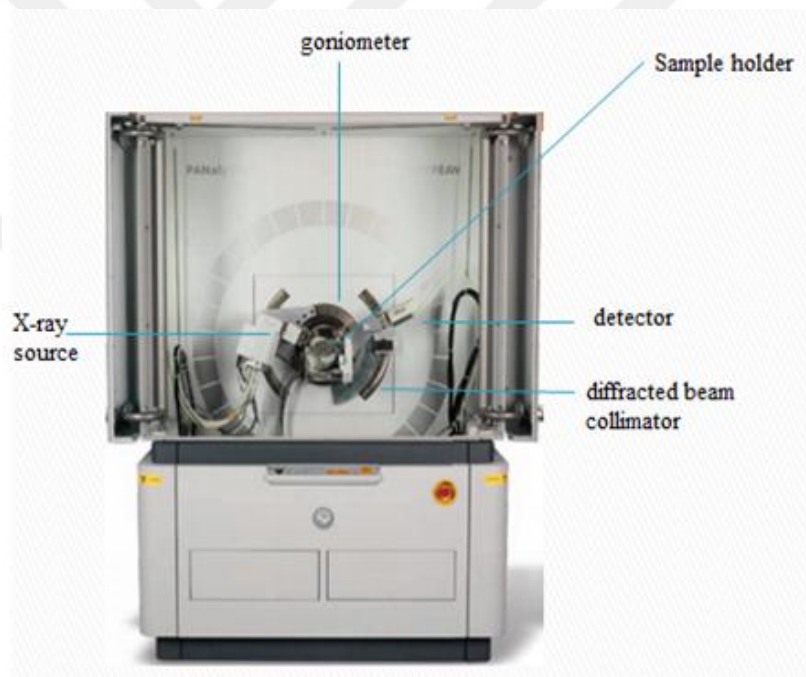


Figure 3.19. X-ray diffraction (XRD) device.

3.5.2. Scanning Electron Microscopy (SEM)

A scanning electron microscope is a kind of electron microscope that produces images of a sample by scanning it with a focused beam of electrons. Several signals can

be noticed containing information about the sample's surface topography. It can provide a variety of imaging techniques with resolutions in the range 1 μm to 1 nm, depending on the microscope and the signal used to form the image (Vernon-Parry, 2000). Microscopic investigation was performed by a Zeiss Sigma 300 scanning electron microscope equipped with an EDS detector as shown in Figure 3.20. Both secondary electron and backscattered electron modes were applied to identify the different phases in the microstructure. Compositional analysis was done employing EDS point analysis technique.



Figure 3.20. Scanning electron microscope (SEM).

3.6. Mechanical Tests

Mechanical tests consisted of uniaxial compression and micro hardness. Both surfaces of the compression specimens were mechanically ground to render them parallel. Graphite was used to reduce friction between the samples and the compression plates and also to prevent or minimize barreling during uniaxial compression testing.

3.6.1. Micro hardness testing

A load which is applied on the indenter is not greater than 1 kg in micro hardness tests. The hardness is evaluated by the amount of permanent deformation or plastic flow of the material. The quantity of flow may be determined by gauging the depth of the indentation or by measuring the area. (Chandler, 1999). Vickers hardness

was measured on the polished specimens using a digital micro hardness tester (HVD-1000AP) as shown in Figure 3.21. With a load of 100 grams force (981mN) and 20 second dwell time. The hardness value could be displayed directly and it did not need to enter the length of the diagonal. Four specimens sintered at 1200 °C for variable times were used to measure the hardness.

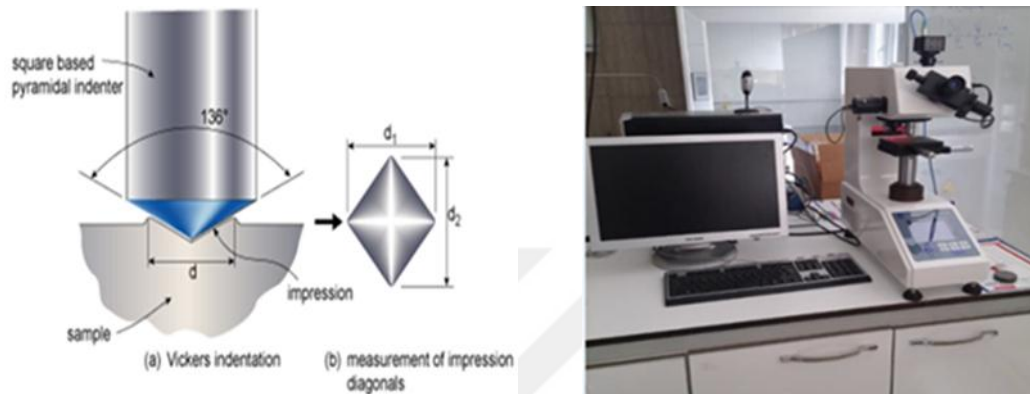


Figure 3.21. Vickers hardness testing machine

3.6.2. Uniaxial Compression Tests

A simple and effective way to characterize material's response to loading can be provided by the uniaxial compression tests. The change in dimensions and resulting load can be recorded to calculate a stress-strain profile by subjecting a sample to a controlled compressive displacement along a single axis. Young's modulus, yield strength, compressive strength, elastic and plastic material properties can be determined from the obtained curve. Uniaxial compression tests at ambient temperature (25 ± 5 °C) were conducted using a universal Raagen tension-compression testing device. Elastic modules were determined by applying least squares curve fitting to the linear portion of the stress-strain diagram while yield strengths of the sintered samples were determined using the 0.2%-offset method. Compression strengths were the maximum stresses achieved and as a measure of ductility fracture strains were used. The testing frame used for the experiments is shown in Figure 3.22.



Figure 3.22. Uniaxial compression testing machine equipped with a heating-cooling system.



4. RESULTS AND DISCUSSION

4.1. Density and Porosity

Theoretical density of $Ti_{74}Nb_{26}$ alloy is calculated as 5.578 g/cm^3 . Measured density and calculated porosity of the samples in hot pressed and sintered conditions are shown in Table 4.1. The density of the sample hot pressed at $600 \text{ }^\circ\text{C}$ was only 4.52 g/cm^3 and its porosity was close to 17%. $50 \text{ }^\circ\text{C}$ increment in hot pressing temperature decreased the porosity to 12.5% so that hot pressing temperature was increased to $800 \text{ }^\circ\text{C}$ providing almost full density. Hot pressing at $800 \text{ }^\circ\text{C}$ resulted in a porosity of only 0.85%. This little amount of porosity would be eliminated during following high temperature sintering. Consequently, hot pressing temperature was optimized to be $800 \text{ }^\circ\text{C}$ and all the samples were pressed at that temperature prior to sintering. Actually, this was the idea behind combining hot pressing with high temperature sintering. Previous studies (Yang and Qain., 2015) present in the literature showed that, conventional cold pressing and sintering could not eliminate the porosity. On the other hand, only hot pressing is not sufficient for complete dissolution of Nb in Ti and accordingly getting β phase desired due to its limited temperature. As expected sintering carried out for different times eliminated the porosity remained from hot pressing and full density was achieved for all the sintering durations of 1 to 4 hours.

Table 4.1. Density and porosity of the samples produced in different condition

Specimen	Density (g/cm^3)	Porosity (%)
600 $^\circ\text{C}$ 1h (HP)	4.52	16.89
650 $^\circ\text{C}$ 1h (HP)	4.88	12.53
800 $^\circ\text{C}$ 1h (HP)	5.53	0.85
1200 $^\circ\text{C}$ 1h (HP+S)	5.58	0
1200 $^\circ\text{C}$ 2h (HP+S)	5.59	0
1200 $^\circ\text{C}$ 3h (HP+S)	5.59	0
1200 $^\circ\text{C}$ 4h (HP+S)	5.60	0

4.2. X-ray Diffraction

X-ray diffraction patterns of sintered samples revealed that β phase formed as a result of Nb dissolution in Ti as it can be seen from Figure 4.1. In addition to main phase β (BCC) little amount of α phase (HCP) were also detected in the microstructure. Longer sintering times increased the intensity of β peaks while α phase peak decreased. Even 4 hours of sintering at 1200 °C was not enough to eliminate all the α phase and to get single β phase. Nevertheless, amount of α phase was very low which can be seen comparing main peak intensities of two phases.

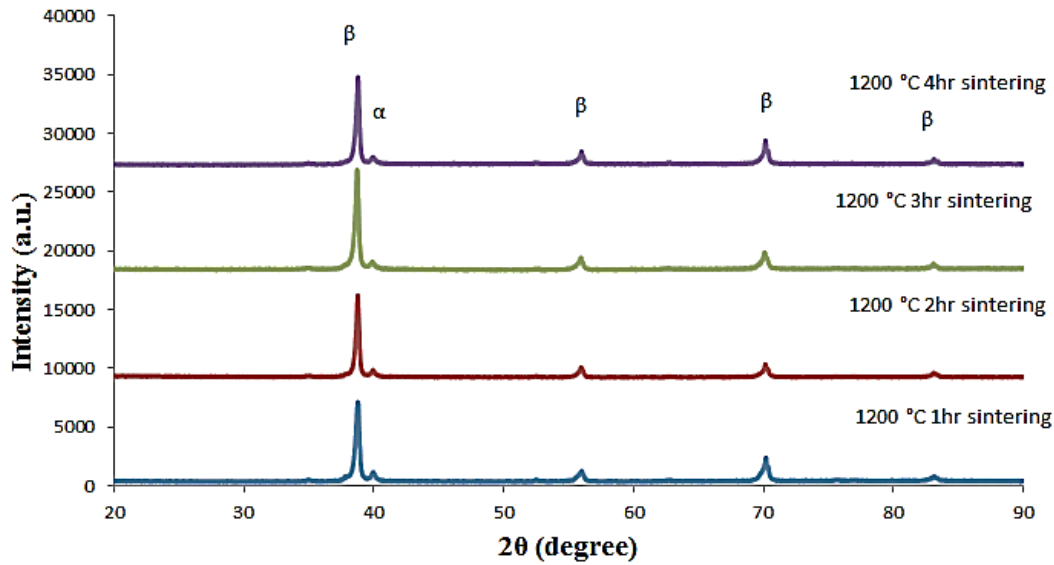
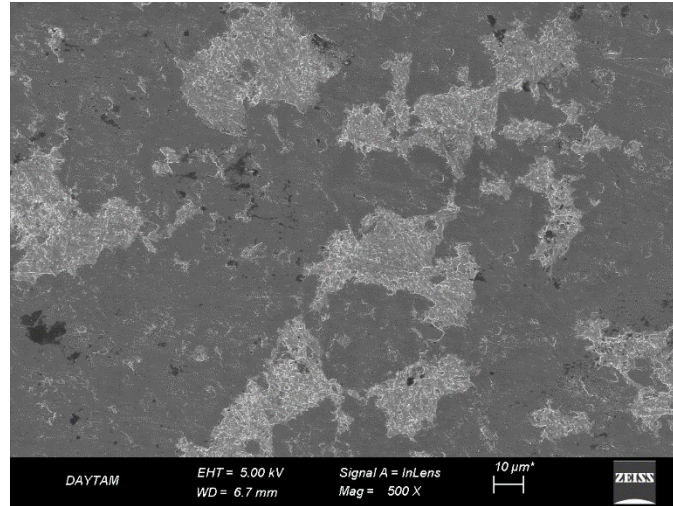


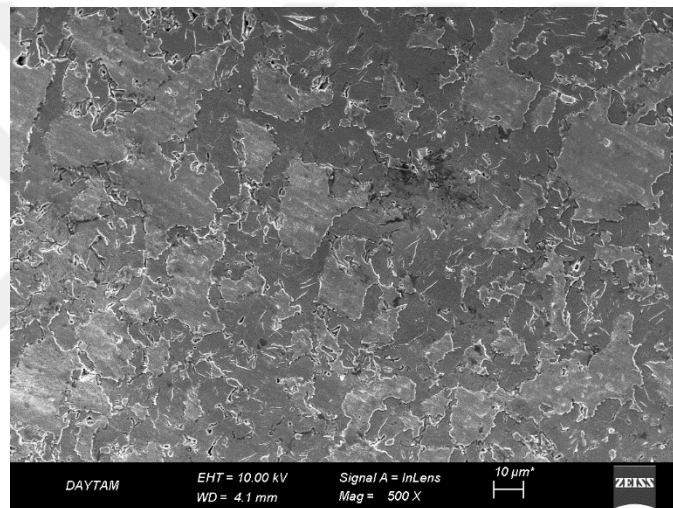
Figure 4.1. XRD patterns of specimens hot pressed at 800 °C for 1h and then sintered at 1200 °C for different times

4.3. Scanning Electron Microscopy

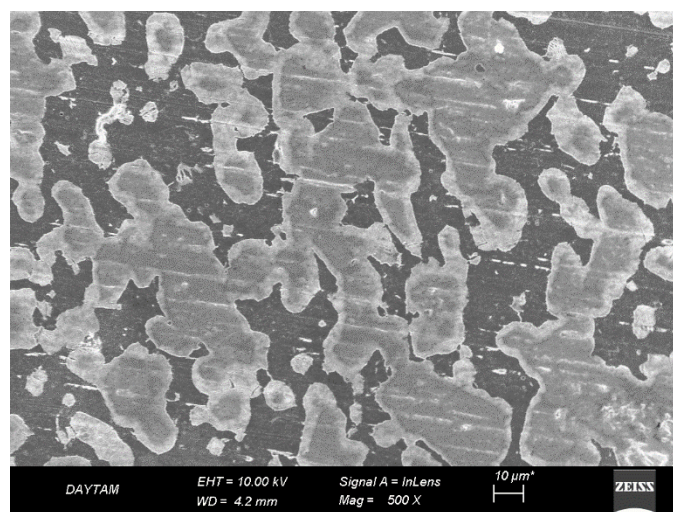
Figure 4.2 presents the SEM micrographs of hot pressed samples at 600, 650 and 800 °C for 1h. Dark regions in the micrographs correspond to pure Ti phase whereas light grey regions correspond to pure Nb. 600 and 650 °C were not sufficient for dissolution of Nb in Ti. Almost none of the Nb was dissolved in Ti at these temperatures as can be followed by Figure 4.2 (a) and (b). On the other hand, Nb dissolution occurred at 800 °C and as a result of Nb dissolution β phase was also observed (Figure 4.2c).



(a)



(b)



(c)

Figure 4.2. SEM images of hot pressed samples at a) 600, b) 650, c) 800 °C for 1h.

EDS point analysis taken from the grey region in Figure 4.3 also confirmed β phase formation. Amount of Nb at that point was 23.7% by weight percentage (13.8% as atomic percentage). Figure 4.4 represent the EDS point analysis results taken from pure Ti region. This dark phase was consisting of 100% Ti.

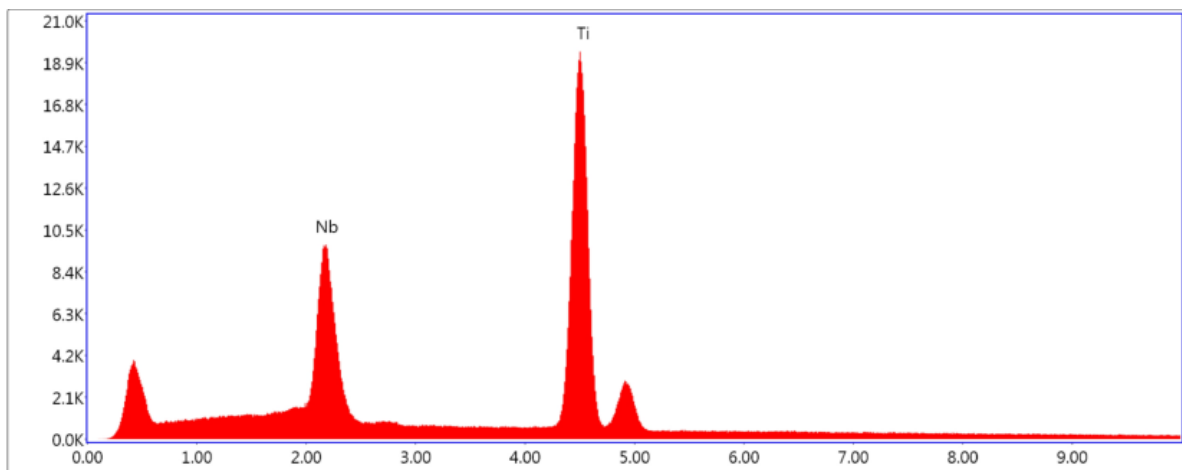
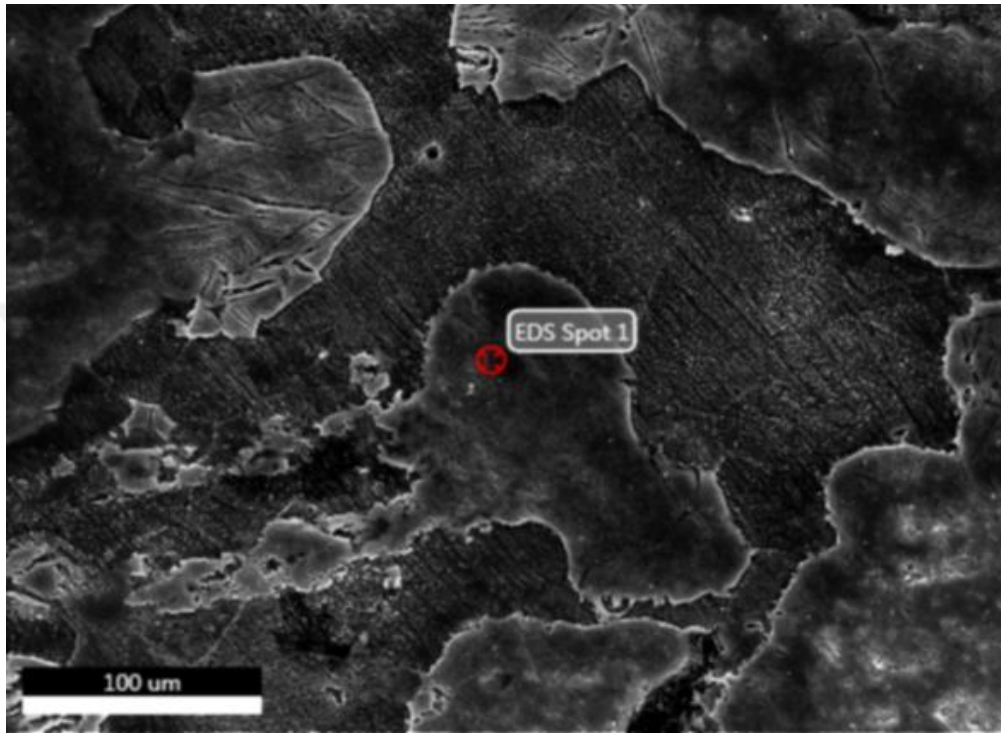


Figure 4.3. EDS point analysis showing Nb dissolution in Ti and β phase formation at 800 °C. (Nb: 23.7 wt. %).

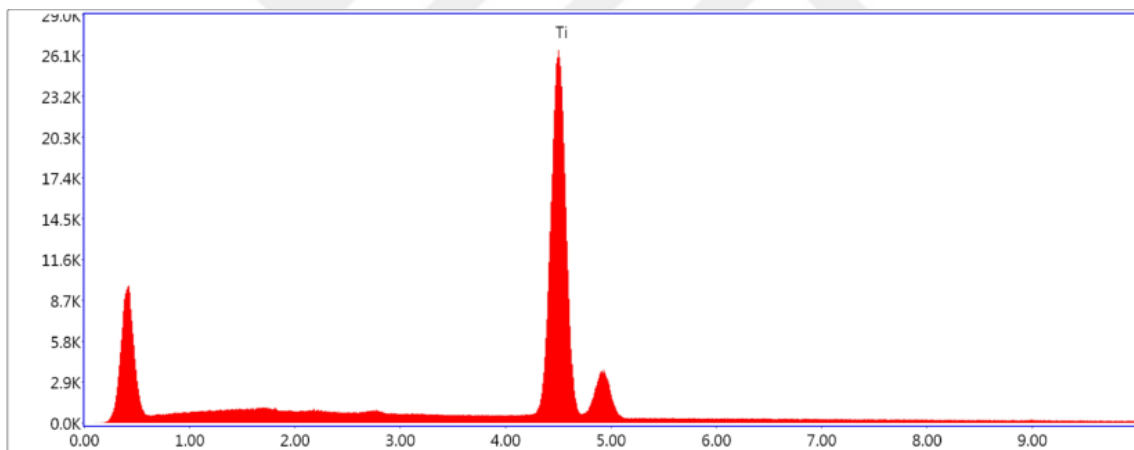
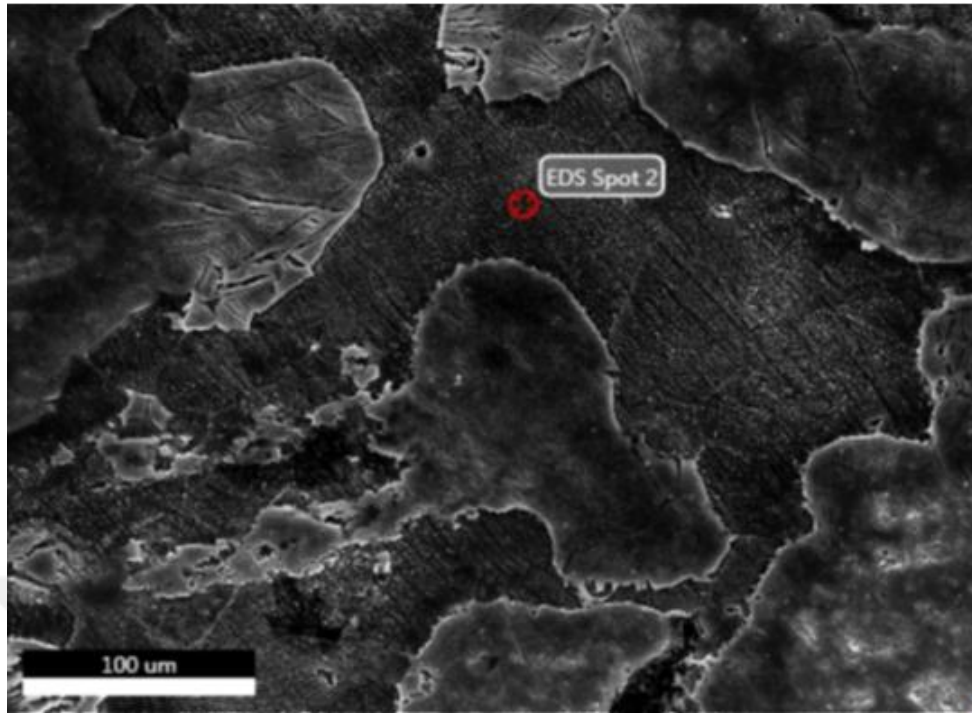


Figure 4.4. EDS point analysis showing pure Ti region (Nb: 0 wt. %).

Hot pressing performed at 800 °C not only provided almost full density but also caused partial dissolution of Nb and β phase formation. However, aim of the study was to obtain single β phase so only hot pressing at 800 °C for 1h was not enough to get single β phase. High temperature sintering was also necessary for complete dissolution of Nb in Ti. Since the temperature of hot press used in this study is limited high temperature sintering experiments were performed in a vertical furnace capable of working continuously at 1200 °C.

The morphological characteristics of the sintered samples at 1200 °C for different times after hot pressing at 800 °C for 1h were examined with the scanning electron microscope and the microstructures are presented in Figure 4.5 to Figure 4.8. SEM micrographs revealed that with increasing sintering time from 1h to 4h amount of α phase decreased and the amount of β phase increased. The results were in good agreement with those obtained from XRD.

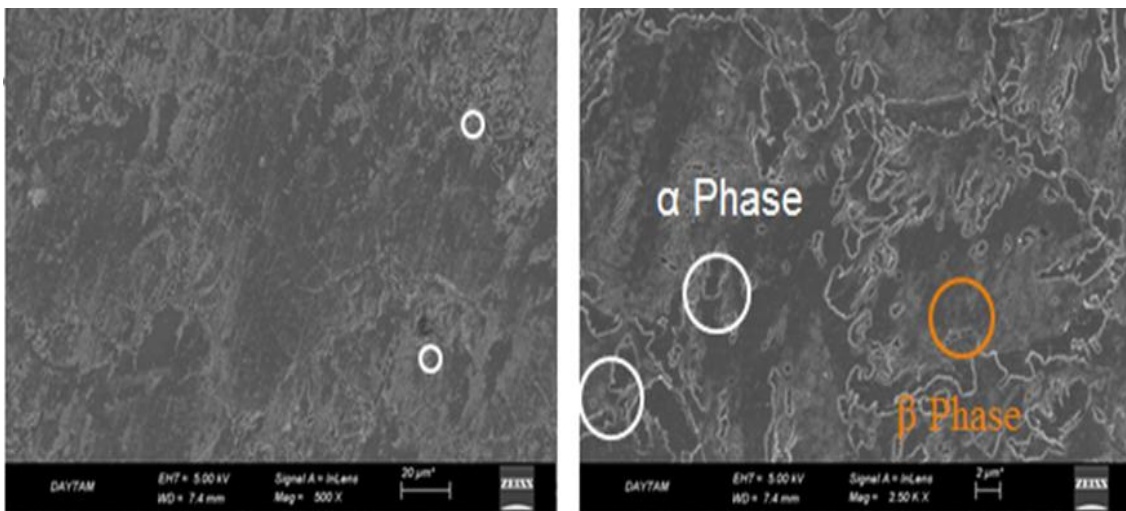


Figure 4.5. SEM images of $\text{Ti}_{74}\text{Nb}_{26}$ alloy sintered for 1h at 1200 °C.

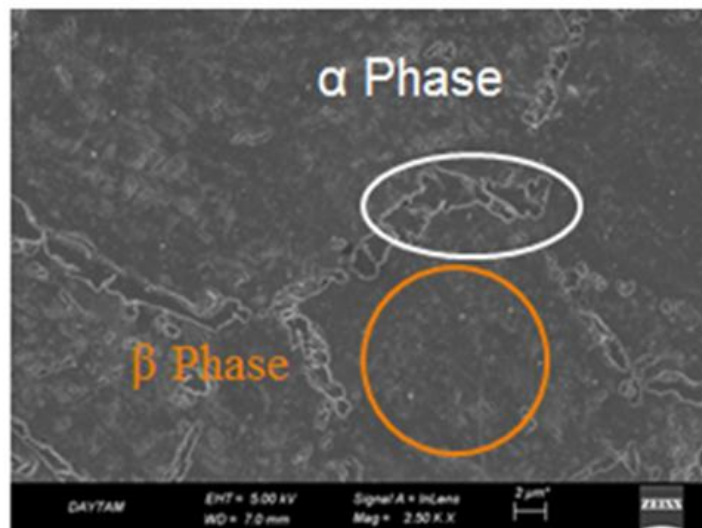


Figure 4.6. SEM image of $\text{Ti}_{74}\text{Nb}_{26}$ alloy sintered for 2h at 1200 °C.

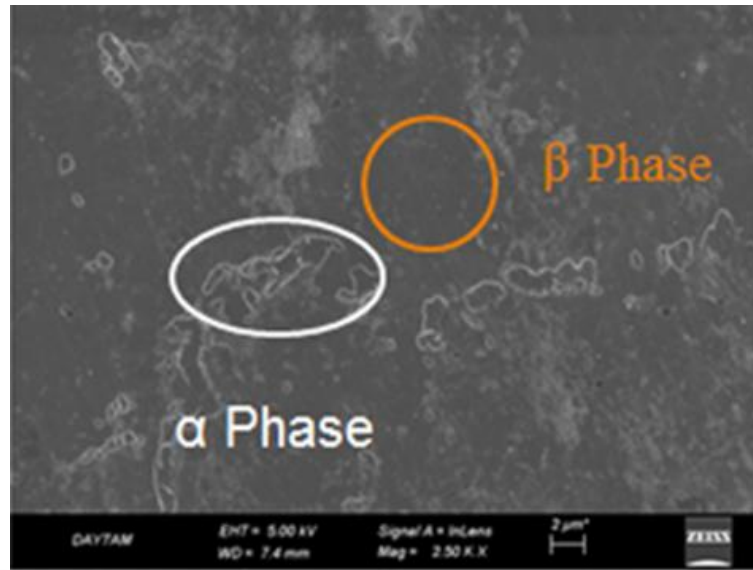


Figure 4.7. SEM image of $Ti_{74}Nb_{26}$ alloy sintered for 3h at 1200 °C.

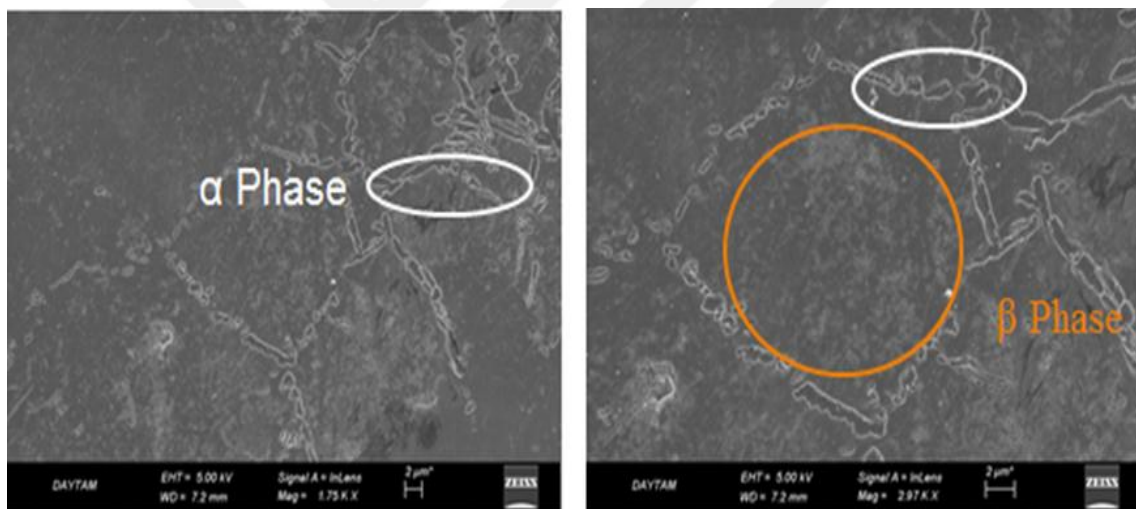


Figure 4.8. SEM images of $Ti_{74}Nb_{26}$ alloy sintered for 4h at 1200 °C.

BSE mode was used in order to ensure whether undissolved pure Nb existed or not in the microstructure of the samples since it was quite difficult to differentiate in secondary electron mode. BSE micrographs of bulk $Ti_{74}Nb_{26}$ alloys are given in Figure 4.9 to Figure 4.12. The micrographs are similar and the microstructure consists of the same phases. The amount of α phase is very small as detected by XRD and secondary electron mode in SEM, β is the main phase and a little undissolved pure Nb in white color was also observed. EDS point analysis shown in Figure 4.13 proves that all the white regions in BSE images correspond to pure Nb. Although amount of pure

Nb decreased with increasing sintering time its complete elimination was not possible by sintering at 1200 °C even for the longest sintering time of 4h used in the present study.

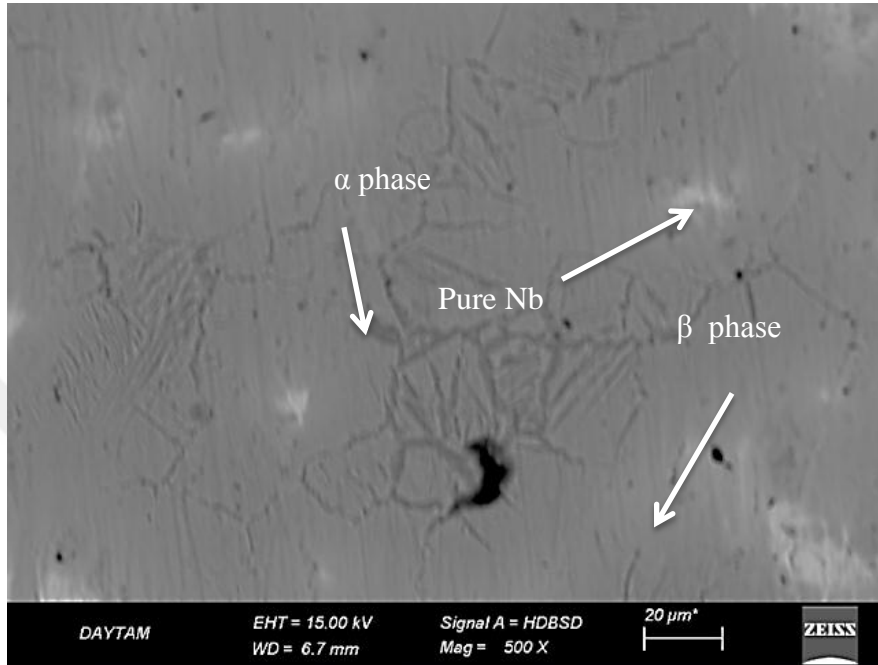


Figure 4.9. BSE micrograph of bulk $Ti_{74}Nb_{26}$ alloy sintered at 1200 °C for 1h.

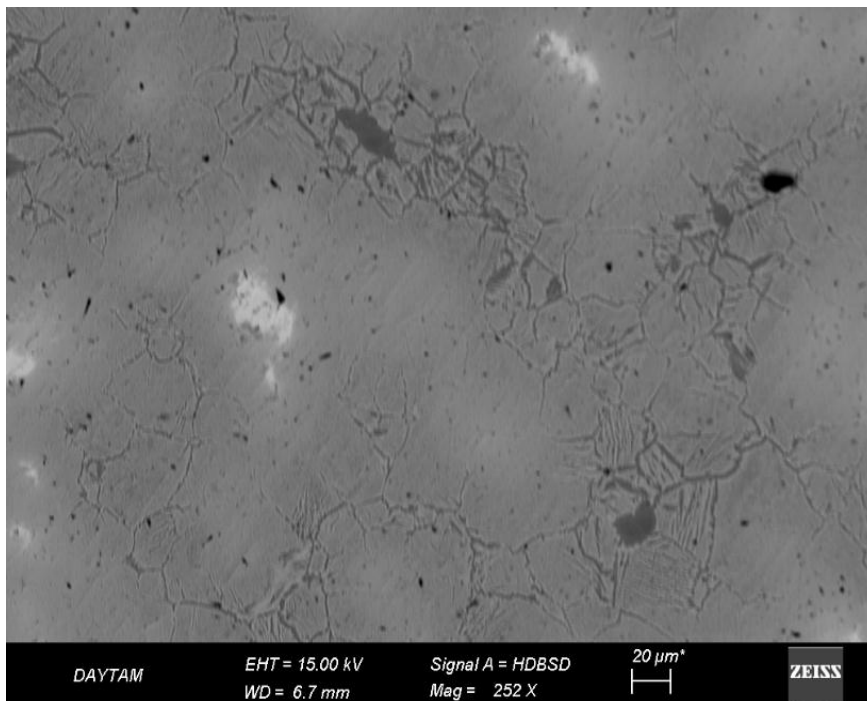


Figure 4.10. BSE micrograph of bulk $Ti_{74}Nb_{26}$ alloy sintered at 1200 °C for 2h.

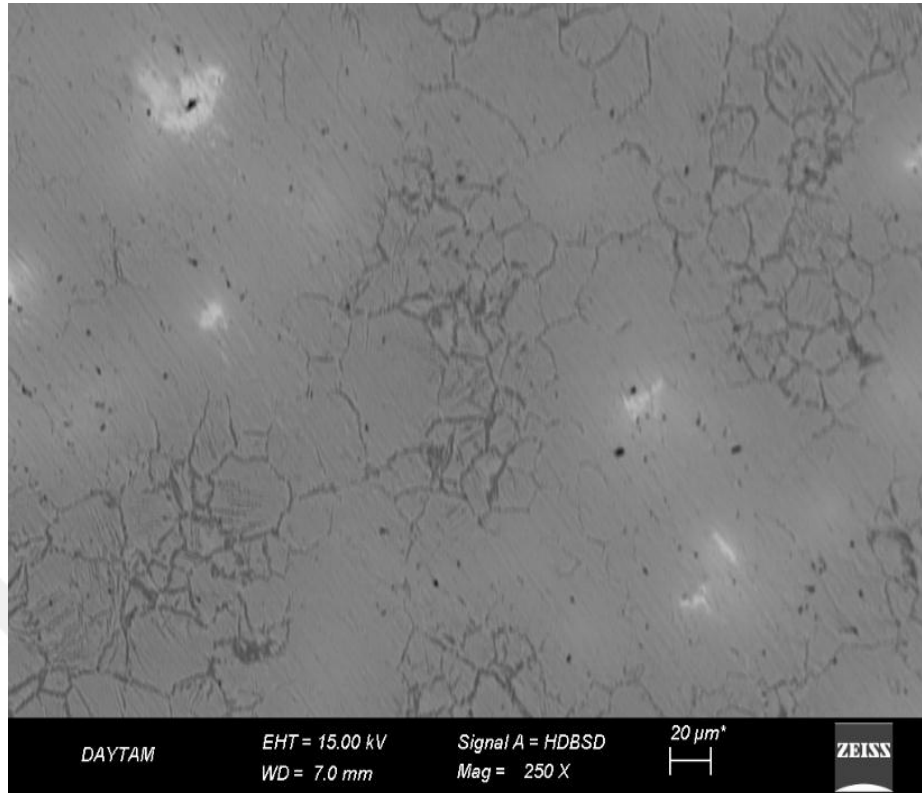


Figure 4.11. BSE micrograph of bulk $\text{Ti}_{74}\text{Nb}_{26}$ sintered at 1200 °C for 3h.

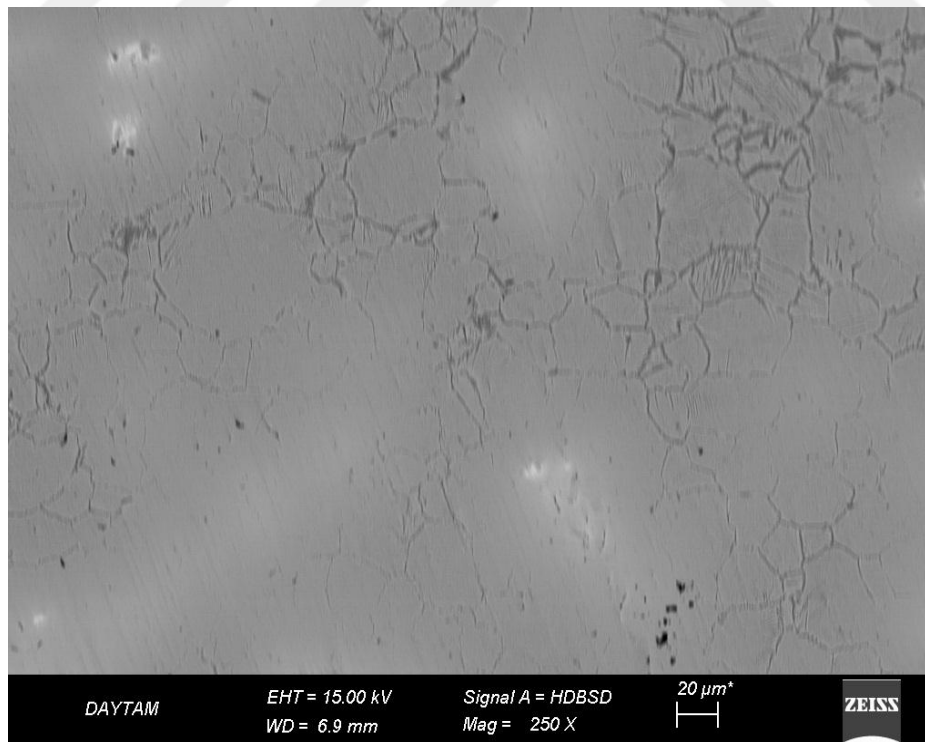


Figure 4.12. BSE micrograph of bulk $\text{Ti}_{74}\text{Nb}_{26}$ sintered 1200 °C for 4h.

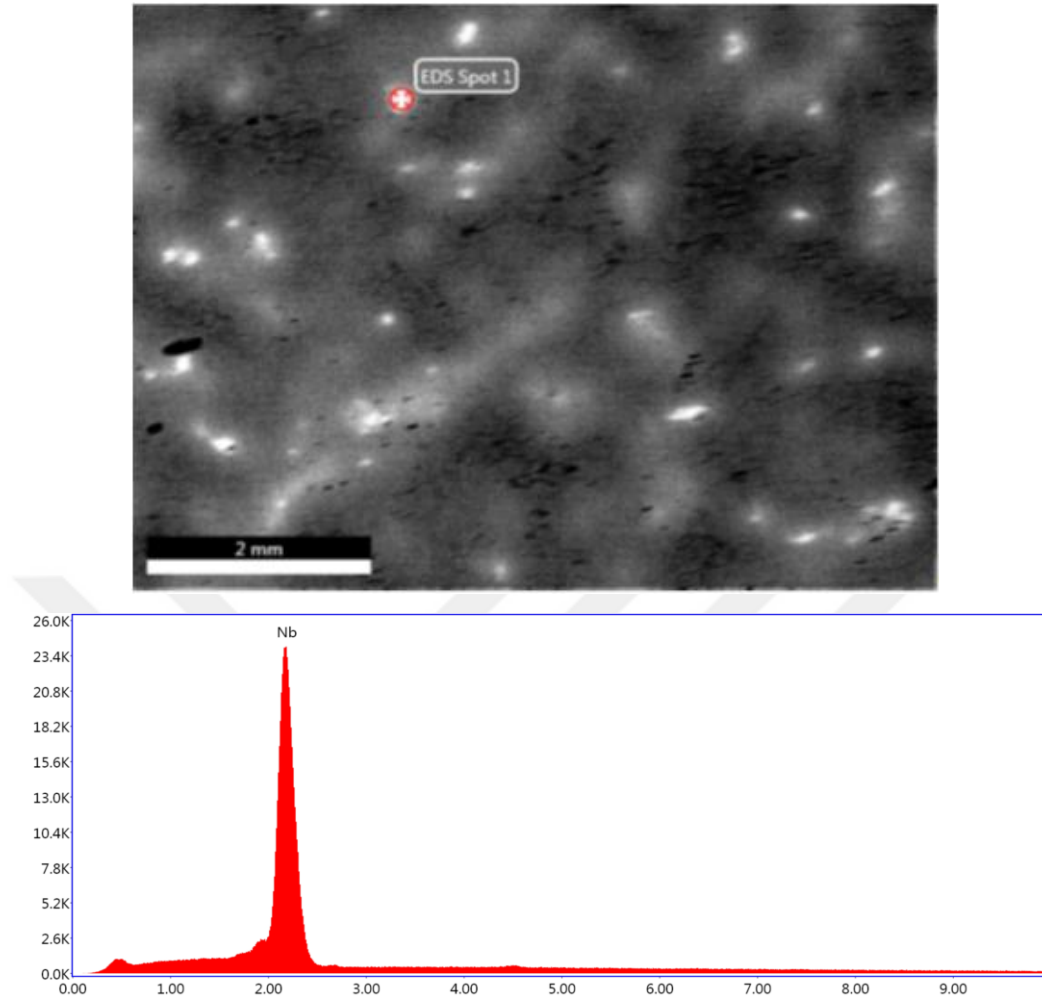


Figure 4.13. EDS point analysis result showing undissolved pure Nb.

EDS point analysis results obtained from α and β phases in the specimens sintered at 1200 °C for 3h are displayed in Figure 4.14 and Figure 4.15, respectively as examples. Table 4.2 gives all the results of EDS analysis. Combining EDS results and BSE images it can be concluded that Nb distribution in β phase is quite homogeneous and homogeneity increases with increasing sintering time. Nb distribution in α phase is also similar for all the sintering durations. Nb content of β phase is normally should be 26% (atomic) considering starting composition, however EDS technique as a semi-quantitative method is generally not capable of providing exact compositional information.

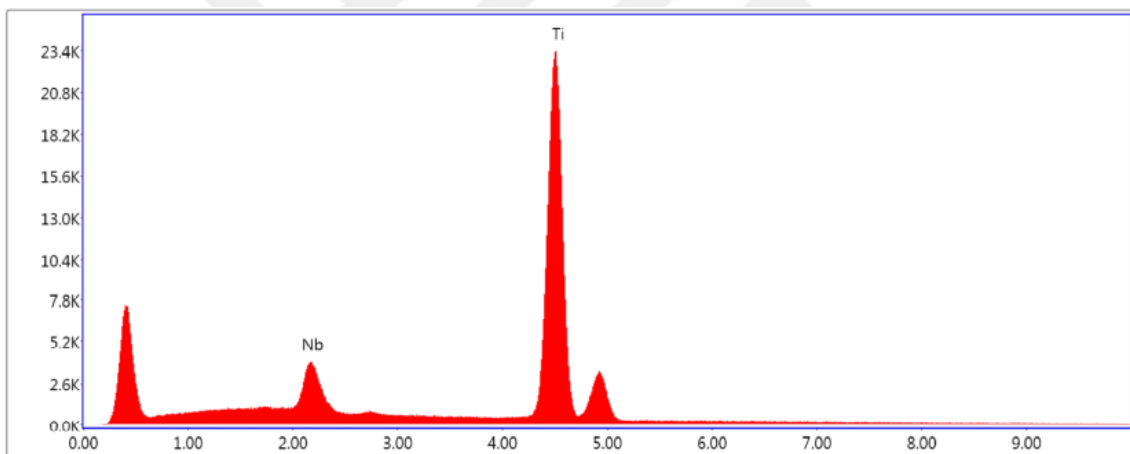
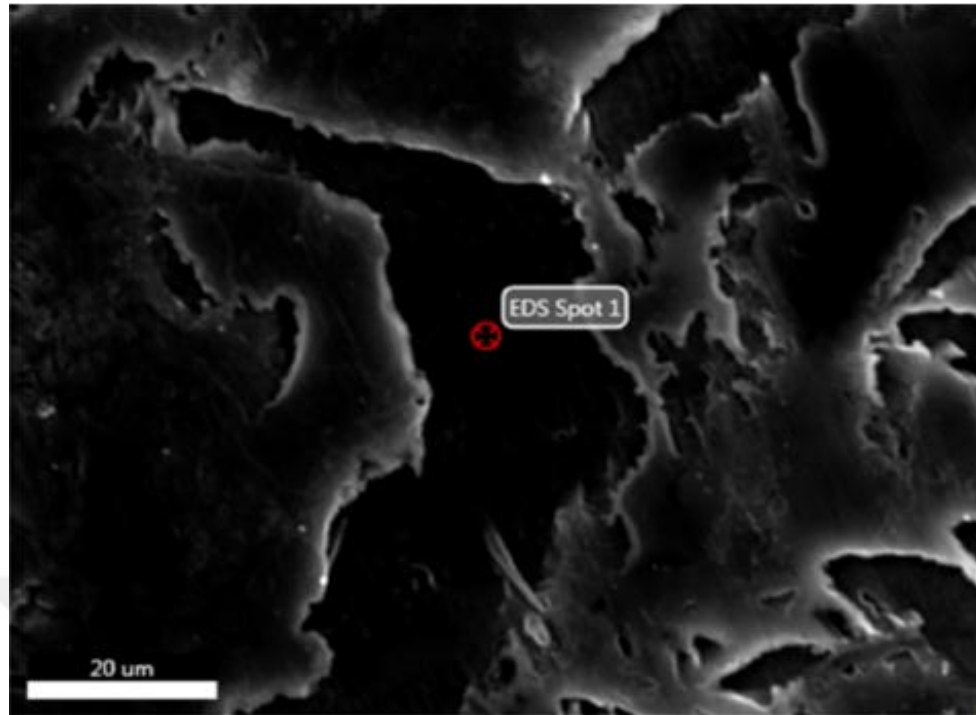


Figure 4.14. EDS point analysis result for α phase (3h sintering), Ti% (atomic) = 95.7 and Nb% (atomic) = 4.3.

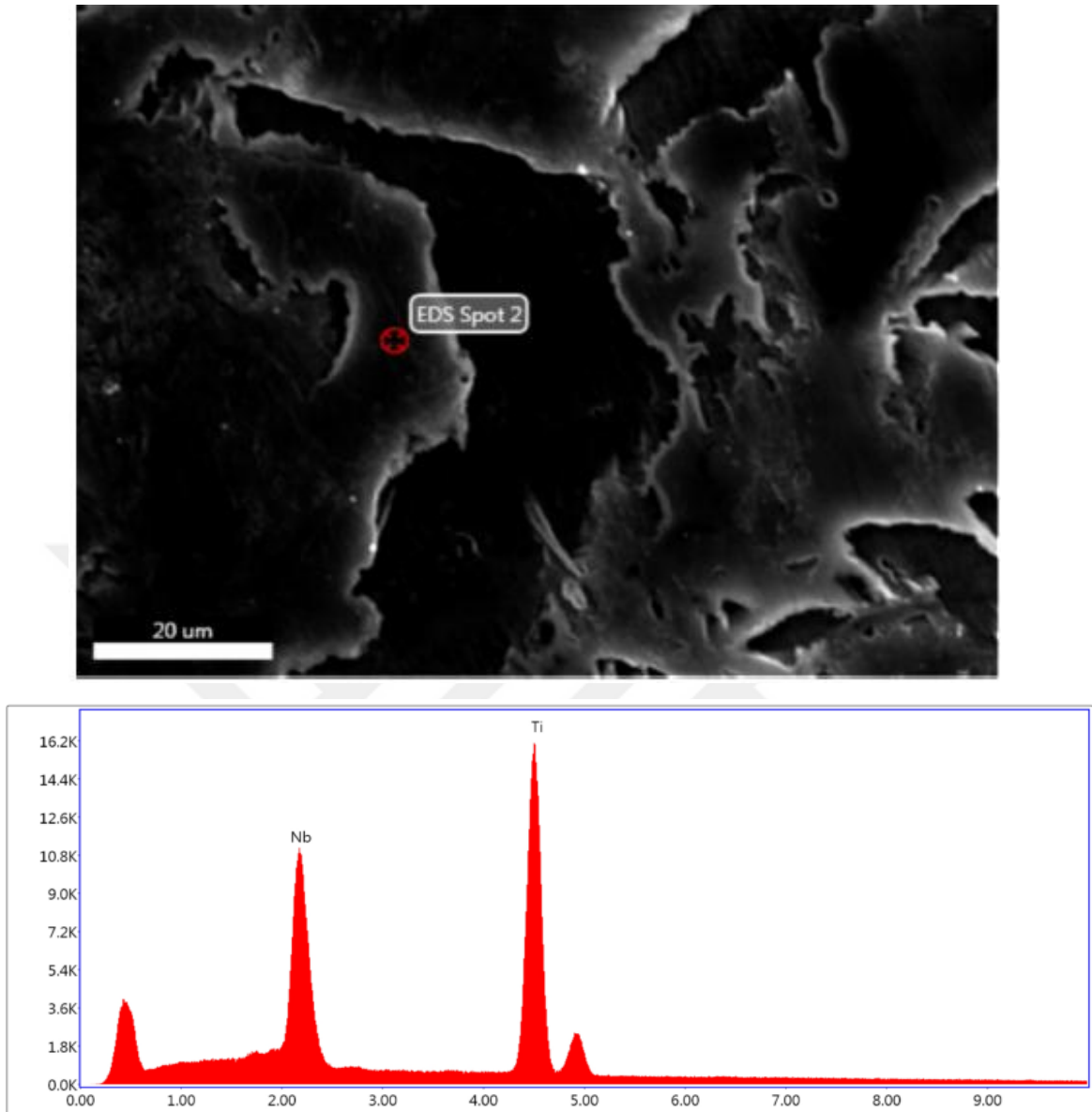


Figure 4.15. EDS point analysis result for β phase (3h sintering), Ti% (atomic) = 81.7 and Nb% (atomic) = 18.3.

4.4. Micro Hardness Tests

The micro hardness values presented a clear relation with sintering duration. Longer sintering times resulted in higher hardness as observed in Table 4.3. As expected, 4hr of sintering at 1200 °C exhibited the highest hardness value of 332 HV. The lowest hardness measured was 309 HV of 1h sintered sample at the same temperature. Increase in sintering time increased the amount of β phase which is harder than α phase and consequently, hardness value also increased.

Table 4.2. EDS point analysis results obtained from α and β phases in the samples sintered at 1200 °C for different times

Sintering time (h)	α phase		β phase	
	Ti% (atomic)	Nb% (atomic)	Ti% (atomic)	Nb% (atomic)
1	95.2	4.8	76.4	23.6
			70.2	29.8
2	95.3	4.7	80.9	19.1
			81.7	18.3
3	95.7	4.3	81.7	18.3
			79.1	20.9
4	96.2	3.8	79.9	20.1
			78.2	21.8
			79.3	20.7

4.5. Uniaxial Compression Tests

The stress-strain curves of hot pressed samples obtained from compression tests conducted at room temperature are shown in Figure 4.16. It is clear from the figure that elastic modulus, yield strength and compressive strength increase with increasing hot pressing temperature due to decreasing porosity. Ductility on the other hand increases when the hot pressing temperature is increased from 600 °C to 650 °C but further increase in temperature (800 °C) decreases the ductility and gives the lowest fracture strain. Lower pressing temperatures could not form β phase so only variable for ductility is porosity. With decreasing porosity ductility increases. However, at 800 °C porosity was almost zero and some β phase formed, therefore, ductility decreased.

Figure 4.17 presents the stress-strain curves of sintered samples at 1200 °C for different times. The curve belonging to hot pressed sample at 800 °C for 1h is also included for comparison. Mechanical properties obtained from these curves are summarized in Table 4.4

Table 4.3. Vickers micro hardness tests results

Sintering time (h)	Measurement #	Hardness (HV)	Mean Hardness (HV)
1	1	290	308.8
	2	285	
	3	315	
	4	318	
	5	336	
2	1	281	315
	2	310	
	3	323	
	4	330	
	5	331	
3	1	298	330.8
	2	310	
	3	325	
	4	353	
	5	368	
4	1	328	332
	2	330	
	3	333	
	4	333	
	5	336	

All the mechanical properties enhanced as a result of sintering done at high temperature of 1200 °C for 3 and 4 hours. Interestingly, yield strength of hot pressed sample was higher than those of sintered for 1 and 2 hours and compressive strength (1007 MPa) was a few tens of MPa lower. However, ductility of the hot pressed sample was less than half of the sintered samples.

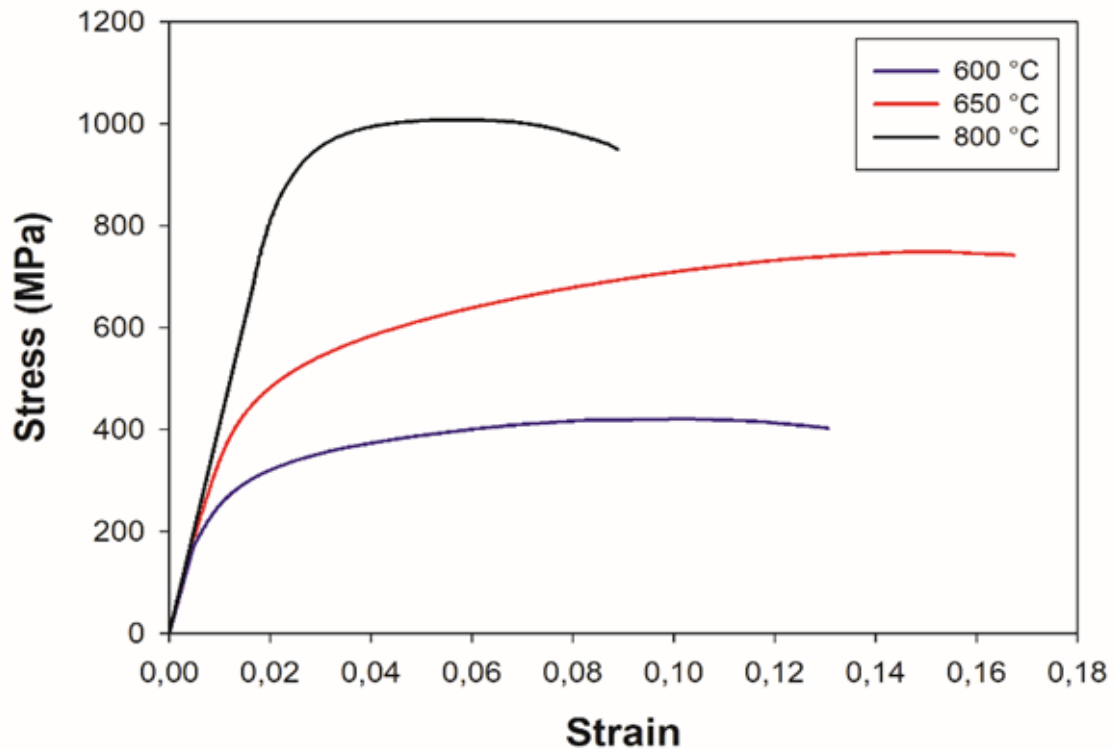


Figure 4.16. Stress-strain curves of samples hot pressed at different temperatures for 1h.

Young's modulus of the samples sintered for 1, 2, 3 and 4h were 40, 41, 41.4 and 44 GPa, respectively as shown in

Table 4.4. The lowest yield strength was measured to be 789 MPa for 1h sintered sample and increased with increasing sintering time up to 894 MPa for the sample sintered for 4h. Compressive strength values were also increased from 1020 (1h) to a maximum of 1178 MPa (4h). Fracture strains as a measure of ductility were very similar for all the sintering times and changing in the range of 18-21%. The value of elastic modulus (44 GPa), yield strength (894 MPa) and compression strength (1178 MPa) were the highest mechanical properties all obtained for 4 hours of sintering.

The relations between mechanical properties and sintering time are plotted in Figure 4.18 and 4.19. Elastic modulus increases as the sintering time gets longer since the extended sintering times provides better bonding between the initial powders.

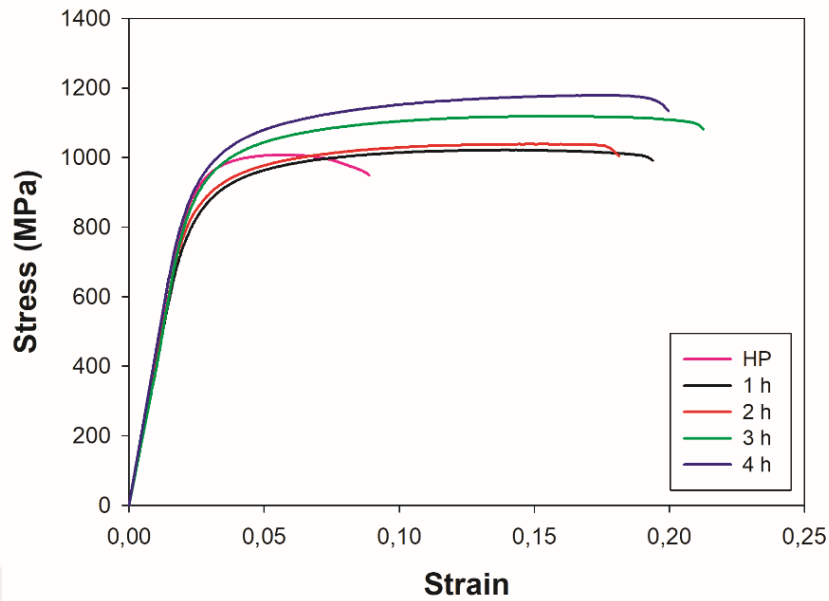


Figure 4.17. Stress-strain curves of sintered samples at 1200 °C for different times (1, 2, 3 and 4h). The curve of hot pressed sample at 800 °C for 1h (HP) is also included for comparison.

Table 4.4. Mechanical properties of $Ti_{74}Nb_{26}$ alloys sintered at 1200 °C for variable times

Sintering time (h)	Elastic modulus (GPa)	Yield strength (MPa)	Compression strength (MPa)	Fracture strain (%)
1	40.1	789	1020	19,4
2	41	803	1038	18.1
3	41.4	856	1118	21.3
4	44	894	1178	19.9

However, in the present study increase of Young's modulus was only 4 GPa with the increment of sintering time from 1h to 4h. This is due to low elastic modulus of β phase. α has a higher elastic modulus and longer sintering times decreased the α phase amount. As a result, the increase in elasticity modulus was limited just too a few GPas. Yield and compressive strengths enhanced especially after 2h of sintering. This can be understood comparing the slope of the linear curves between 1 and 2h, and after 2h up to 4h. As it can be seen from Figure 4.17 the slope of the both curves increase after 2h.

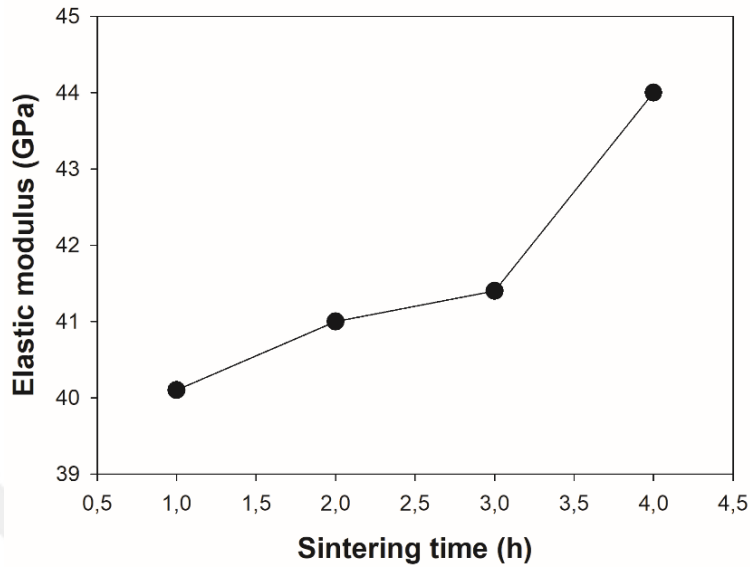


Figure 4.18. Elastic modulus-sintering time relation.

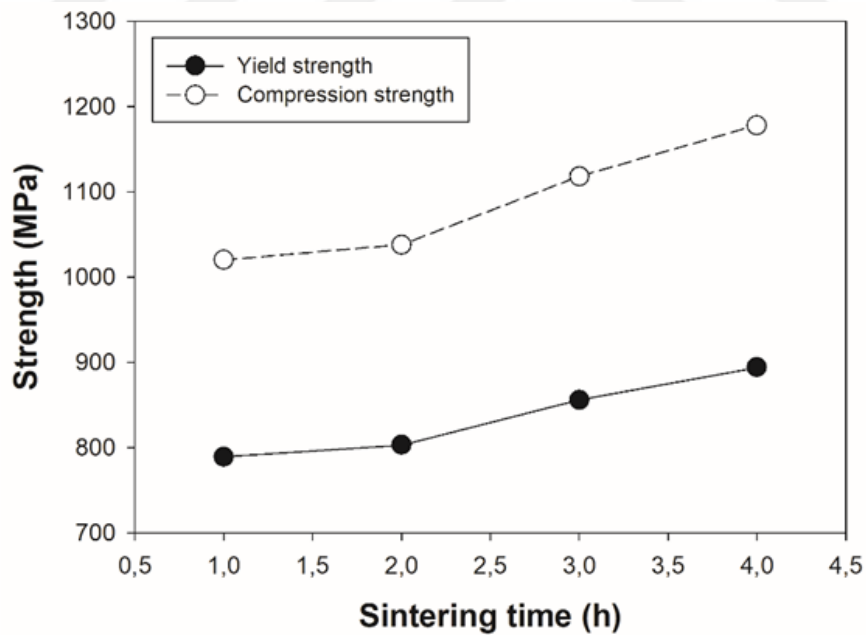


Figure 4.19. Yield and compressive strength as a function of sintering time

Figure 4.20 shows the effect of using Ti getters during sintering on the mechanical properties of the sample sintered for 2h. Elastic modulus and yield strength were similar for the sintering treatment done with or without Ti getters. Compressive

strength on the other hand was slightly higher for the sample sintered without using Ti getter particles. Ti getter usage during sintering provided a better ductility since oxidation strengthens Ti alloys while decreasing ductility. The difference in strength and ductility of the two samples were not too much so that it can be concluded that oxidation occurred during sintering without using Ti getters was not severe.

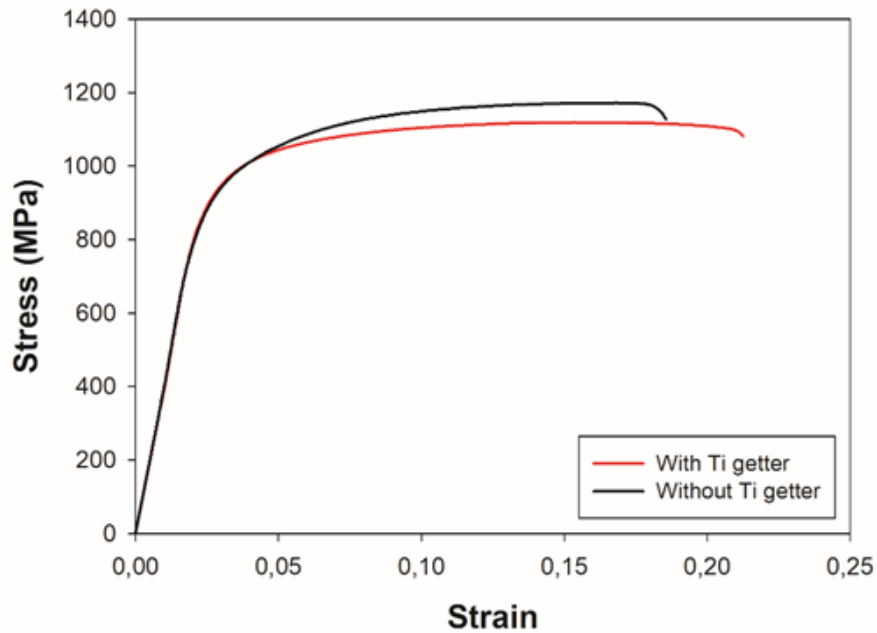


Figure 4.20. Effect of Ti getter usage during sintering at 1200 °C for 2hr on stress-strain curves.

In Table 4.5 mechanical properties of the samples produced in the present study has been compared to the results published already. The sample hot pressed at 800 °C for 1h and sintered at 1200 °C for 4h exhibited the lowest Young's modulus (44 GPa) and highest yield strength (894 MPa). It is clear from the table that, similar compositions (signed with bold style in the table) produced with casting methods resulted in elastic modulus values of 45-95 GPa. Yield strength values (250-722 MPa) on the other hand were quite low compared to the results of the present study. Hardness values were also in the range of (188-323 HV) comparable to our result of 332 HV. As a result it can be concluded that hot pressing following high temperature sintering is a quite efficient method to produce bulk Ti-Nb alloys with superior mechanical properties.

Table 4.5. Comparison of mechanical properties with the ones existing in the literature

Alloy comp.	Elastic Modulus (GPa)	Yield strength (MPa)	Hardness (HV)	Fabrication method and condition	Reference
Ti-35Nb (wt. %)	94.9 ± 5.7	722 ± 21	323 ± 15	VAM, 1000 °C / 24 h, (FC)	Creiasco, 2013
	75.2 ± 15.7	343 ± 1	188 ± 4	HT, 1000 °C / 1 h, (WQ)	
Ti-10Nb (wt. %)	85.2±9.0	552±19		
Ti-16Nb (wt. %)	78.4±5.6	589±20	MIM at 1550 °C/4h	
Ti-22Nb (wt. %)	70.9±7.2	649±31		Zhao et al, 2013
Ti-10Nb (wt. %)	90.1±6.1	612±3.6		
Ti-16Nb (wt. %)	82.2±5.0	661±14	HIP at 915 °C / 2h	
Ti-22Nb (wt. %)	75.6±7.6	687±34		
Ti-16Nb (at. %)	58	461	SST at 750 °C / 0.5 h	Wang et al 2008
	56	382	SST at 850 °C / 0.5 h	
	60	386	SST at 950 °C / 0.5 h	
Ti-24Nb (at. %)	45	250	VAM at 1223 K / 72h	Elmay et al., 2014
Ti-26Nb (at. %)	50	300	VAM at 1223 K / 72h	
Ti-5Nb (wt. %)	127±7	358±27	Arc melting furnace, different temperatures	Han et al. 2015
Ti-10Nb (wt. %)	149±6	338±24		
Ti-15Nb (wt. %)	114±5	413±21		
Ti-20Nb (wt. %)	127±5	332±13		
Ti-22Nb (at. %)	272	Plasma melting,	Štěpán et al. 2010
	621	HT at 1100 °C / 12h	
	235	Plasma melting	
Ti-25Nb (at. %)	410	HT at 1100 °C / 12h	Štěpán et al. 2010
	273	EBFZM	
	244	HT at 200 °C/ 1h	
	292	HT at 400 °C/ 1h	
.....	271	HT at 600 °C/ 1h		
Ti₇₄Nb₂₆	44	894	332	HP (800°C, 1h) and HTS (1200 °C, 4hr)	Present study

HT – heat treatment; EBFZM – electron beam floating zone melting; SST-Solid solution treated; VAM-Vacuum arc melting; HT-Heat treatment.



5. CONCLUSIONS

In this study, binary $\text{Ti}_{74}\text{Nb}_{26}$ alloys were produced combining, for the first time, hot pressing with high temperature sintering. General conclusions obtained from the study are as follows:

- Density measurements (Archimedes' technique) showed that optimum hot pressing temperature of Ti-Nb alloys for 1h is 800 °C. Almost full density (over 99%) was achieved at 800 °C.
- The microstructures of $\text{Ti}_{74}\text{Nb}_{26}$ alloys sintered at 1200 °C for different times consist of small amount of α and very little undissolved pure Nb in addition to the main phase β and amount of β increases with increasing sintering time according to XRD and SEM investigations.
- Even 4 hours of sintering at 1200 °C was not sufficient to obtain single β phase. Therefore, sintering temperature should be higher than 1200 °C to get only β phase free from α and pure Nb.
- Mechanical properties enhanced by increasing sintering time. 4h of sintering exhibited the highest mechanical properties including elastic modulus (44 GPa), yield strength (894 MPa), compression strength (1178 MPa) and microhardness (332 HV). Ductility (18-21%) on the other hand was almost the same for all the sintering temperatures.
- Samples produced combining hot pressing and high temperature sintering were found to be suitable in terms of mechanical properties for bone replacement applications although they have higher elastic modulus (40-44 GPa) compared to that of bone (> 20 GPa).



REFERENCES

- Afonso, C.R.M., Aleixo, G.T., Ramirez, A.J., Caram, R., 2007. Influence of cooling rate on microstructure of Ti-Nb alloy for orthopedic implants. *Materials Science and Engineering C*, **27**: 908-913.
- Akselsen, O.M., 2004. Joining of shape memory alloys. *SINTEF Materials and Chemistry Norway*, 183-211.
- Aleksanyan. A.G., Dolukhanyan, S.K., Shekhtman. V.Sh., Khasanov. S.S., Ter-Galstyan, O.P., Martirosyan, M.V., 2012. Formation of alloys in the Ti - Nb system by hydride cycle method and synthesis of their hydrides in self-propagating high-temperature synthesis. *International Journal of Hydrogen energy*, **37**: 14234-14239.
- Al-Zain, Y., Kim, H.Y., Hosoda, H., Namc, T.H., Miyazaki, S., 2010. Shape memory properties of Ti – Nb – Mo biomedical alloys. *Acta Materialia*, **58**: 4212-4223.
- Andrade, D. P. D., Vasconcellos, L. M. R. D., Carvalho, I. C. S., Forte, L. F. D. B. P., Santos, E. L. D. S., Prado, R. F. D., Santos, D. R. D., Cairo, C. A. A., Carvalho, Y. R., 2015. Titanium-35niobium alloy as a potential material for biomedical implants: In vitro study. *Materials Science and Engineering C*, **56**: 538–544.
- Aydoğmuş, T., 2010. *Processing and Characterization of Corous Titanium Nickel Ahape Memory Alloys* (Ph.D thesis). Middle East University, Ankara..
- Bahador, A., Hamzah, E., Kondoh, K., Abu Bakar, T.A., Yusof, F., Imai, H., Saud, S.N., Ibrahim, M.K., 2017. Effect of deformation on the microstructure, transformation temperature and superelasticity of Ti–23 at% Nb shape-memory alloys. *Materials and Design*, **118**: 152–162.
- Bhawna, B., Agrawal, S.S., 2007. **Mixing**. Pharmaceutical Engineering, New Delhi.
- Boehm, J.J., 1998. The vacuum arc melter, history, theory and operating instructions. *Material Group*.1-19.
- Bönisch M., Calin, M., Humbeeck, J.V., Skrotzki, W., Eckert, J., 2015. Factors influencing the elastic moduli, reversible strains and hysteresis loops in martensitic Ti–Nb alloys. *Materials Science & Engineering C*, **48**: 511-520.
- Bonisch, M., Waitz, T., Calin, M., Skrotzki, W., Eckert, J., 2016). Tailoring the Bain strain of martensitic transformations in Ti e Nb alloys by controlling the Nb content. *International Journal of Plasticity*, **85**: 190-202.
- Bönisch, M., Calin, M., Waitz, T., Panigrahi, Zehetbauer, M., Gebert, Skrotzki, W., Eckert, J., 2016. Thermal stability and phase transformations of martensitic Ti–Nb alloys. *Science and Technology of Advanced Materials*, **14**: 1-9.
- Bolzoni, L., Ruiz-Navas, E.M., Neubauer, E., Gordo, E., 2012. Inductive hot-pressing of titanium and titanium alloy powders. *Materials Chemistry and Physics*, **131(3)**: 672-679.
- Brunette, D.M., Tengvall, P., Textor, M., Thomsen, P., 2001. *Titanium in Medicine*. Springer-Verlag Berlin Heidelberg.
- Chai, Y.W., Kim, H.Y., Hosoda, H., Miyazaki, S., 2008. Interfacial defects in Ti – Nb shape memory alloys. *Acta Materialia*, **56**: 3088-3097.
- Chandler, H. (1999). Introduction to Hardness Testing. ASM International.

- Cai, C., Song, B., Xue, P., Wei, Q., Wu, J.-M., Li, W., Shi, Y., 2016. Effect of hot isostatic pressing procedure on performance of Ti6Al4V: Surface qualities, microstructure and mechanical. *Journal of Alloys and Compounds*, **686**: 55-63.
- Callister, W.D. Jr., Rethwisch, D.G., 2009. *Fundamentals of Materials Science and Engineering: An Integrated Approach*. United States of America: John Wiley & Sons, Inc.
- Capek, J., Vojtech, D., Novak, P., 2012. Preparation of the NiTi alloy by a powder metallurgy technique. *Metal*, **23**: 1-7.
- CreMASCO, A., Lopes, E.S.N., Cardoso, F.F., Contieri, R.J., Ferreira, I., Caram, R., 2013. Effects of the microstructural characteristics of a metastable β Ti alloy on its corrosion fatigue properties. *International Journal of Fatigue*, **54**: 32-37.
- Da Silva, L.M., Paes, A.C., Donato, T.A.G., Grandini, C.R., Claro, A.P.R.A., 2009. Preparation, structural, and elastic characterization and biocompatibility of Ti-Nb alloys used as biomaterial. *11th International Conferanc on Advanced Material*, 20-25.
- Duda, T., Raghavan, L. V., 2016. 3D metal printing technology. *IFAC-PapersOnLine*, **29**: 103–110.
- Duerig, T.W., Melton, K.N., StÖckel, D., Wayman, C. M., 1990. *Engineering Aspects of Shape Memory Alloys*. London: Butterworth-Heinemann Ltd.,
- Eksi, A., Saritas, S., 2002. Effects of powder hardness and particle size on the densification of cold isostatically pressed powder. *Turkish J. Eng. Env. Sci.*, **26**: 377-384.
- Elias, C.N., Lima, J.H.C., Valiev, R., Meyers, M.A., 2008. Biomedical Applications of Titanium and its Alloys. *Biological Materials Science*, 46-49.
- Elias, L.M., S.G. Schneider, S.G., Schneider, S., Silva, H.M., Malvisi, F., 2006. Microstructural and mechanical characterization of biomedical Ti – Nb – Zr (– Ta) alloys. *Materials Science and Engineering A*, **432**: 108-112.
- Elmay, W., Patoor, E., Gloriant, T., Prima, F., Laheurte, P., 2014. Improvement of Superelastic Performance of Ti-Nb Binary Alloys for Biomedical Applications. *Journal of Materials Engineering and Performance*, **23**: 2471-2476.
- ElRakayby, H., Kim, H., Hong, S., Kim, K., 2015. An investigation of densification behavior of nickel alloy powder during hot isostatic pressing. *Advanced Powder Technology*, **26**: 1314-1318.
- Farooq, M.U., Khalid, F.A., Zaigham, H., Abidi, I.H., 2014). Superelastic behaviour of Ti–Nb–Al ternary shape memory alloys for biomedical applications. *Materials Letters*, **121**: 58-61.
- Fri'ak, M., William Art Counts , W.A Ma, D., Sander, B., David Holec, D., Raabe,D., Neugebauer ,J .2012. Theory-Guided Materials Design of Multi-Phase Ti-Nb Alloys with Bone-Matching Elastic Properties. *Materials*, **5**: 1853-1872.
- Fukui. Y., Inamura, T., Hosoda, H., Wakashima, K., Miyazaki, S., 2004. Mechanical Properties of a Ti-Nb-Al Shape Memory Alloy. *Materials Transactions*,, 1077-1082.
- Geetha, M., Singh, A. K., Asokamani, R., Gogia, A. K., 2009. Ti based biomaterials, the ultimate choice for orthopaedic implants–A review. Progress in *Materials Science*, **54**: 397–425.
- German, R. M., 1994. *Powder Metallurgy Science*, Metal powder industries federation, Princeton, New Jersey.

- Guillon, O., Gonzalez-Julian, J., Dargatz, B., Kessel, T., Schierning, G., Rathel, J., and Herrmann, M., 2014. Field-Assisted Sintering Technology/Spark Plasma Sintering: Mechanisms, Materials, and Technology Developments. *Advanced Engineering Materials*, 1-20.
- Guo, S., Zhang, J., Cheng, X., Zhao, X., 2015. A metastable b -type Ti – Nb binary alloy with low modulus and high strength. *Journal of Alloys and Compounds*, **644**: 411-415.
- Hammes, G., Binder, C., Galiotto, A., Klein, A.N., Al-Qureshi, H.A . Relationship between Cold Isostatic Pressing and Uniaxial Compression of Powder Metallurgy. *gisele@pg.Materials.ufsc.br*. 1-6.
- Han et al. (2015). Effect of Nb on the microstructure, mechanical properties, corrosion behavior, and cytotoxicity of Ti-Nb alloys. *Materials*, **8**: 5986-6003.
- Hao, Y.L., Li, S.J., Sun, S.Y., Yang, R., 2006. Effect of Zr and Sn on Young's modulus and superelasticity of Ti–Nb-based alloys. *Materials Science and Engineering A*, **441**: 112-118.
- Hartl, D. J., and Lagoudas, D. C., 2008. Thermomechanical Characterization of Shape Memory Alloy Materials. *Springer Science*.
- Henriques, B., Soares, D., Teixeira, J.C., Silva, F.S. 2014. Effect of Hot Pressing Variables on the Microstructure , Relative Density and Hardness of Sterling Silver (Ag-Cu alloy) Powder Compact. *Materials Research.*, **17 (3)**: 664-671.
- Hermawan, H., Ramdan, D., Djuansjah, J.R.P., 2009. Metals for Biomedical Applications. *Biomedical Engineering*, 411-430.
- Hodgson, D.E., Wu, M.H., Biermann, R.J., 1990. Shape Memory Alloy. *Properties and Selection: Nonferrous Alloys and Special-Purpose Material*, 897-902.
- Holz, M., Walker, G.P., Gabriele, M.C., 2011. Ti Facts. *International Titanium Association Education Committee*. 1-24.
- Hon, Y.-H., Wang, J.-Y., Pan, Y.-N., 2003. Composition/Phase Structure and Properties of Titanium-Niobium Alloys. *Materials Transactions*, **44**: 2384-2390.
- Horiuchi, Y., Inamura, T., Kim, H.Y., Miyazaki, S., Wakashima, K., Hosoda, H., 2006. X-ray Diffraction Analysis of Ti-18 mol%Nb Based Shape Memory Alloys Containing 3d Transition Metal Elements. *Materials Transactions*, **47**: 1209-1213.
- Hungria, T., Galy, J., Castro, A., 2009. Spark Plasma Sintering as a Useful Technique to the Nanostructuring of Piezo-Ferroelectric Materials. *Advanced engineering materials*, **11**: 615-630.
- Itoh, Y., Miura, H., Sato, Niinomi, M., 2007. Fabrication of Ti-6Al-7Nb Alloys by Metal Injection Molding. *Materials Science Forum*, **534-536**: 357-360.
- James, W.B., 2015. Powder Metallurgy Methods and Applications. *Powder metallurgy*, **7**: 9-19.
- Jonsén, P., 2006. *Fracture and stress in powder compacts* (Ph.D thesis). Lulea university of technology, Lulea, Sweden .
- Kenta, D., Wanga, G., Dargusch, M., 2013. Effects of phase stability and processing on the mechanical properties of Ti – Nb based β Ti alloys. *Journal of the Mechanical Behavior of Biomedical Materials*, **28**: 15-25.
- Kikuchi, M., Takahashi, M., Okuno, O., 2003. Mechanical properties and grindability of dental cast Ti-Nb alloys. *Dental Materials Journal*, **22(3)**: 328-342.

- Kima, J.I., Kim, H.Y., Inamura, T., Hosoda, H., Miyazaki, S., 2005. Shape memory characteristics of Ti – 22Nb – (2 – 8) Zr (at .%) biomedical alloys. *Materials Science and Engineering, A* **403**: 334-339.
- Kim, H.Y., Satoru, H., Kim, J.I., Hosoda, H., Miyazaki, S., 2004. Mechanical Properties and Shape Memory Behavior of Ti-Nb Alloys. *Materials Transactions*, **45**: 2443-2448.
- Kim, H.Y., Kim, J.I., Inamura, T., Hosoda, H., Miyazaki, S., 2006. Effect of thermo-mechanical treatment on mechanical properties and shape memory behavior of Ti-(26-28) at.% Nb alloys. *Materials Science and Engineering A*, **438-440**: 839-843.
- Koike, M., And Okabe, T., 2007. Cast Titanium Alloys for Dental Applications. 1-32.
- Konopatskii, A.S., Zhukova, Yu. S., Dubinskii, S. M., Korobkova, A. A., Filonov, M. R., Prokoshkin, S. D., 2016. Microstructure of superplastic alloys based on ti – nb for medical purposes. *Metallurgist*, **60**: 89-93.
- Krishnan, R.V., 1985. Stress induced martensite transformations. *Material science Forum*, **3**: 387-398.
- Kuo, P.C.-H., Chou, H.-H., Lin, Y.-H., Peng, P.-W., Ou, K.-L., 2012. Effects of surface functionalization on the nanostructure and biomechanical properties of binary titanium-niobium alloys service effects of surface functionalization on the nanostructure and biomechanical properties of binary Titanium-Niobium Alloys. *J. Electrochem.Soc.*, **159**: 103-107.
- Kunčická, L., Štěpán, P., Kliber, J., Mamuzič, I., 2014. Influence of heat treatment on properties of ti-nb alloys. *Metallurgija*, **53**: 186-188 .
- Lester, B.T., Baxevanis, T., Chemisky, Y., Lagoudas, D.C., 2015. Review and perspectives : shape memory alloy composite. *Acta Mech*, **226**: 3907-3960.
- Leyens, C., Peters, M., 2003. *Titanium and Titanium Alloys: Fundamental and Applications*. Wiley-VCH.
- Machado, L.G., Savi, M.A., 2003. Medical applications of shape memory alloys. *Brazilian Journal of Medical and Biological Research*, **36**: 683-691.
- Mantani, Y., Kudou, K., 2013. Effect of plastic deformation on material properties and martensite structures in Ti – Nb alloys. *Journal of Alloys and Compounds*, **5775**:S448-S452.
- Mittal, K., Kaushik, P., 2016. A prospective analysis of mechanical properties of different Ti-Nb alloy compositions: A review. *Saudi Journal of Engineering and Technology*, **1**: 64-68.
- Moffat, D. L., Kattner, U. R., 1988. The stable and metastable Ti-Nb phase diagrams. *Metallurgical Transactions A*, **19A**: 2389–2397.
- Mohammed, M.T., Khan, A.Z. Arshad N. Siddiquee, A.N. 2012. Titanium and its Alloys , the Imperative Materials for Biomedical Applications. *International Conference on Recent Trends in Engineering & Technology*, 91-95.
- Mohammed, M.T., Khan, A.Z. Arshad N. Siddiquee, A.N., 2014. Beta Titanium Alloys: The Lowest Elastic Modulus for Biomedical Applications: A Review. *Materials and Metallurgical Engineering*, **8**: 814-819.
- Morgan, N.B., 2004. Medical shape memory alloy applications — the market and its products. *Materials Science and Engineering*, **378**:16-23.
- Murray, J.L., 1981. The Nb-Ti (Niobium-Titanium) System. *Bulletin of Alloy Phase Diagrams*, **2**: 55-61.

- Niinomi, M., Nakai, M., Hieda, J., 2012. Development of new metallic alloys for biomedical applications. *Acta Biomaterialia*, **8**: 3888-3903.
- Niinomi, M., 2008. Review article mechanical biocompatibilities of titanium alloys for biomedical applications. *Journal of the Mechanical Behavior of Biomedical Materials*, 30-42.
- Otsuka, K., and Ren, X., 2005. Physical metallurgy of Ti – Ni-based shape memory alloys. *Progress in Materials Science*, **50**: 511-678.
- Otsuka, K., and Shimizu, K., 1986. Pseudoelasticity and shape memory effects in alloys. *International Metals Reviews*, **31** :93-114.
- Otsuka, K., Ren, X., 1999. Martensitic transformations in nonferrous shape memory alloys. *Materials Science and Engineering A*, **273-275**: 89-105.
- Ozaki, T., Matsumoto, H., Watanabe, S., Hanada, S., 2004. Beta Ti alloys with low Young's modulus. *Materials Transactions*, **45**: 2776–2779.
- Panigrahi, A., Bönisch, M., Waitz, T., Schafler, E., Calin, M., Eckert, J., 2015. Phase transformations and mechanical properties of biocompatible Ti – 16 . 1Nb processed by severe plastic deformation. *Journal of Alloys and Compounds*, **628**: 434-441.
- Prashanth, K.G., Zhuravleva, K., Okulov, I., Calin, M., Eckert, J., Gebert, A., 2016. Mechanical and Corrosion Behavior of New Generation Ti-45Nb Porous Alloys Implant Devices. *Technologies*, **4**: 1-12.
- Prokoshkin, S., Brailovski, V., Dubinskiy, S., Zhukova, Y., Sheremetyev, V., Konopatsky, A., K. Inaekyan, K., 2016. Manufacturing , Structure Control , and Functional Testing of Ti–Nb-Based SMA for Medical Application. *Shape Memory and Superelasticity*, **2**: 130-144.
- Pathak, A., Banumathy, S., Sankarasubramanian, R., Singh, A. K., (2014). Orthorhombic martensitic phase in Ti – Nb alloys : A first principles study. *Computational Materials Science*, **83**: 222-228.
- Ping, D.H., Cui, C.Y., Yin, F.X., Yamabe-Mitarai, Y., 2006. TEM investigations on martensite in a Ti–Nb-based. *Scripta Materialia*, **54**: 1305-1310.
- Qian, M., Schafferm G. B., 2010. **Sintering of titanium and its alloys**. Woodhead publishing, Australia.
- Saheb, N., Iqbal, Z., Khalil, A., Hakeem, A.S., Al Aqeeli, N., Laoui, T., Al-Qutub, A., Kirchner, R., 2012. Spark plasma sintering of metals and metal matrix nanocomposites: a review. *Journal of Nanomaterials*, **2012**: 1-13.
- Sarin, V., Pal, U., Goplan, S., 2003. Development of hot pressing as a low cost processing technique for full cell fabrication. *Lockheed Martin Energy Research Corporation*. 1-44
- Seetharaman, S. 2005. Fundamentals of metallurgy. Wood head Publishing Limite.
- Sharma, B., Vajpai, S.K., Ameyama, K., 2016. Microstructure and properties of beta Ti - Nb alloy prepared by powder metallurgy route using titanium hydride powder. *Journal of Alloys and Compounds*, **656**: 978-986.
- Shymanski, V.I., Cherenda, N.N., Uglov, V.V., Astashynski, V.M., Kuzmitski, A.M., 2015. Structure and phase composition of Nb / Ti system subjected to compression plasma flow impact. *Surface & Coatings Technology*, **278**: 183-189.
- Sikka, V.K., Viswanathan, S., Loria, E.A., 1993. Processing and Properties of Nb-Ti-Base Alloys. *Journal of Materials Engineering and Performance*, **2**: 505-510.

- Sktiniovam, K., Kursá, M., Szurman, I., 2014. *Powder Metallurgy*. Ostrava Technická Univerzita, Ostrava.
- Štěpán, P., Losertová, M., Petlák, D., Jaromír, D., 2010. Methods of Preparation of TiNb Based Alloys. *Non-Ferrous Metals and Alloys*, **1**: 27-31.
- Štěpán, P., Losertová, M., Petlák, D. . Microstructure properties of tinb alloys prepared by plasma metallurgy. 51-57.
- Stoeckel, D., 1995. The Shape Memory Effect - Phenomenon, Alloys, and Applications. *NDC*, 1-13.
- Suárez, M., Fernández, A., Menéndez, J.L., Torrecillas, R., Kessel, H.U., Hennicke, J., Kirchner, R., Kessel, T., 2013. Challenges and Opportunities for Spark Plasma Sintering : A Key Technology for a New Generation of Materials. *Sintering Applications*, 319 -342.
- Suresh K.R., Mahendran S., Krupashankara, M.S., Avinash L., 2015. Influence of Powder Composition & Morphology on Green Density for Powder Metallurgy Processes. *International Journal of Innovative Research in Science*, **4**: 18629-18634.
- Tarniță, D., Tarniț, D. N., Bîzdoacă, N., Mîndril, Vasilescu, M., 2009. Properties and medical applications of shape memory alloys. *Romanian Journal of Morphology and Embryology*, **50**: 15-21.
- Terayama, A., Fuyama, N., Yamashita, Y., Shizaki, I., Kyogokuc, H., 2013. Fabrication of Ti – Nb alloys by powder metallurgy process and their shape memory characteristics. *Journal of Alloys and Compounds*, **577S**: S408-S412.
- Tobea, H., Kim, H.Y., Inamura, T., Hosoda, H., Nam, T.H., Miyazaki, S., 2013. Effect of Nb content on deformation behavior and shape memory properties of Ti – Nb alloys. *Journal of Alloys and Compounds*, **577S**: S435-S438.
- Viteri, V.S. and Fuentes, E., 2013. Titanium and Titanium Alloys as Biomaterials *InTech*, 156-181
- Wang, Y.B., Zheng, Y.F., 2009. Corrosion behaviour and biocompatibility evaluation of low modulus Ti–16Nb shape memory alloy as potential biomaterial. *Materials Letters*, **63**: 1293-1295.
- Wang, Y.B., Zheng, Y.F., 2008. The microstructure and shape memory effect of Ti – 16 at.% Nb alloy. *Materials Letters*, **62**: 269-272.
- Wood, R., 1972. **Titanium Alloys Handbook Metals and Ceramics Information Centre**. Battelle, Columbus: MCIC-HB-02.
- Wu, S.Q., Pinga, D.H., Yamabe-Mitarai, Y., Kitashima, T., Li, G.P., Yang, R., 2013. Microstructural characterization on martensitic α'' phase in Ti – Nb – Pd alloys. *Journal of Alloys and Compounds*, **577S**: 2011-2014.
- Yang, Y.F., Qain M., 2015. Spark plasma sintering and hot pressing of titanium and titanium alloys. *Titanium Powder Metallurgy*, 219-235.
- Yu, C., Cao, P., Jones, M.I., 2017. Titanium Powder Sintering in a Graphite Furnace and Mechanical Properties of Sintered Parts. *Metals*, **7**: 1-14.
- Yu, Z.-T., Zhang, M.-H., Tian, Y.-X., Cheng, J., MA, X.-Q., X-M, Liu, H.-Y., Wang, C., 2014. Designation and development of biomedical Ti alloys with finer biomechanical compatibility in long-term surgical implants. *Front. Mater. Sci.*, **8(3)**: 219-229.
- Zhao, D., Chang, K., Ebel, T., Qian, M., Willumeit, R., Yan, M., Pyczak, F., 2013. Microstructure and mechanical behavior of metal injection molded Ti–Nb binary

- alloys as biomedical material. *Journal of the Mechanical Behavior of Biomedical Materials*, **28**: 171-182.
- Zhao, D., Chang, K., Ebel, T., Nie, H., Willumeit, R., Pyczak, F., 2015. Sintering behavior and mechanical properties of a metal injection molded Ti–Nb binary alloy as biomaterial. *Journal of Alloys and Compounds*, **640**: 393-400.
- Zhuravleva, K., Bönisch, M., Prashanth, K.G., Hempel, U., Helth, A., Gemming, T., Calin, M., Scudino, S., Schultz, L., Eckert, J., Gebert, A., 2013. Production of Porous β -Type Ti – 40Nb Alloy for Biomedical Applications: Comparison of Selective Laser Melting and Hot Pressing. *Materials*, **6**: 5700-5712.





APPENDIX

EXTENDED TURKISH SUMMARY (GENİŞLETİLMİŞ TÜRKÇE ÖZET)

ÖZET

SICAK PRES YÖNTEMİ İLE TİTANYUM NİYOBYUM ŞEKİL BELLEKLİ ALAŞIMLARIN ÜRETİMİ

Al-ZANGANA Nuaman Jasim Filamarz
Yüksek Lisans Tezi, Makine Mühendisliği Anabilim Dalı
Tez Danışmanı : Doç. Dr. Tarık AYDOĞMUŞ
Ocak 2018, 101 sayfa

Geçmişten günümüze Ti-Nb alaşımlarının üretimi için genellikle döküm yöntemleri (vakum indüksiyon ergitme veya vakum ark ergitme) kullanılmıştır. Saf Ti ve Nb'un erime sıcaklıkları son derece yüksek olduğundan (1668 ve 2477 °C sırasıyla), döküm yoluyla Ti-Nb alaşımlarını üretmek ekonomik değildir. Toz metalurjisi yöntemi ile bu alaşımları çok daha düşük sıcaklıklarda (Ti erime sıcaklığından daha az) ve tamamen katı halde ekonomik olarak üretmek mümkündür. Bu çalışmada Ti₇₄Nb₂₆ alaşımları, ilk kez sıcak presleme ve yüksek sıcaklık sinterlemesinin kombinasyonu ile saf Ti ve saf Nb tozları kullanılarak üretilmiştir. Üretim sürecinde uygulanan işlem sıcaklığı ve zamanının yoğunluk, mikroyapı ve mekanik davranış üzerindeki etkileri araştırılmıştır. Yoğunluk ölçümleri 800 °C'de yapılan sıcak presleme işleminin tam yoğunluğu sağladığını göstermiştir. XRD ve SEM incelemeleri, sinterleme süresinin artmasıyla birlikte β fazı oluşumunun arttığını ortaya koymuştur. Ana faz β'ya ilaveten, mikroyapıda az miktarda α fazı ve çok az miktarda saf Nb gözlenmiştir. Mekanik özellikler tek eksenli basma ve Mikro Vickers sertlik testleri ile belirlenmiştir. Mekanik test sonuçları 1200 °C'de 4 saatlik sinterlemenin en yüksek sertlik (336 HV), elastik modül (44 GPa), akma mukavemeti (894 MPa) ve basma mukavemeti (1178 MPa) değerlerini sağladığını göstermiştir.

Anahtar kelimeler: Mekanik test, Mikroyapı, Sıcak Presleme, Sinterleme, Titanyum-Niyobyum alaşımları, Toz metalurjisi.



1. GİRİŞ

Paslanmaz çelik, kobalt-krom alaşımları ve titanyum alaşımları en çok kullanılan metalik biyomalzemelerdir. Ti alaşımları bu metalik biyomalzemeler arasında en yüksek biyo-uyumluluk seviyesine, yüksek mekanik dayanıma ve aşınma direncine sahiptir. Diğer malzemelere ve alaşımlara göre daha iyi yorulma direnci, yüksek aşınma dayanımı, üstün kırılma tokluğu direnci ve yüksek mukavemet/ağırlık oranı gibi özelliklere sahip olduklarından, titanyum ve alaşımları biyomedikal endüstrisi ve havacılık gibi pek çok alanda kullanılmaktadır (Han, M.-K. *et al*, 2015; Kim, H. Y. *et al*, 2006; Elias, L.M. *et al*, 2006; Niinomi, M. *et al*, 2012; Zhuravleva, K. *et al*, 2013; Sharma, B. *et al*, 2016; Yu, Z.-T. *et al*, 2014; Bolzoni, L. *et al*, 2012; Afonso, C.R.M. *et al*, 2007; Cremasco, A. *et al*, 2013).

Yüksek makine ve hammadde maliyetleri, titanyum ve alaşımlarının havacılık ve tıp alanlarında kullanımının yaygınlaşmasını zorlaştırmaktadır. Toz metalürjisi yöntemleri kullanılarak ilgili maliyetler ciddi oranlarda düşürülebilmekte ve daha kesin şekiller elde ederek ihtiyaç duyulan makine işlem zamanları ve atık malzeme oranları azaltılabilmektedir. Ni, Al ve V gibi ilave elementlerden kaynaklanabilecek zehirlilik sorunlarının çözümü için de Ti alaşımları önerilmektedir. Son zamanlarda Ti-Nb, Ti-Ta ve Ti-Zr gibi β titanyum alaşımları düşük elastiklik katsayısı, yüksek gerilim direnci, iyi süneklik ve potansiyel olarak toksik olabilecek unsurların yokluğu gibi üstün özellikleri nedeniyle umut vadetmektedir (Bolzoni *et al*, 2012; Kentet *et al*, 2013; Chai *et al*, 2008). Saf Ti düşük sıcaklıklarda sıkı paket hegzagonal kristal (HCP) yapıdaki α fazında bulunurken, denge faz diyagramına göre sıcaklık 882 ± 2 °C'ye ulaştığında alotropik bir dönüşüme uğrayarak hacim merkezli kübik (BCC) yapıdaki β fazına dönüşmektedir. Titanyum alaşımları genelde α , $\alpha+\beta$ ve β alaşımları olarak sınıflandırılmaktadır (Ping *et al*, 2006; Elmay *et al*, 2014). Vanadyum, molibden, tantal ve niyobyum gibi elementler β -izomorfiklere birer örnek olup, bunların alaşımdaki oranları artırılarak β -dönüşüm sıcaklığı düşürülebilmektedir. Bu elementler Ti'nin β fazında tamamen çözünebilir özelliktedir. Niyobyum, β fazı stabilizörü olarak işlev gösterebilen ve biyo-uyumlu bir elementtir ve Ti alaşımlarına katıldığında alaşımın Young katsayısını düşürür. Ayrıca zehirli olmayan bir element olup, insan vücudunda reaksiyona sebep olmaz (Wang, and

Zheng., 2008). Titanyuma niyobyum eklenmesi oksitlenme direncini artırdığı gibi, yoğunluğu da azaltmaktadır (Sikka *et al.*, 1993).

Ti ve Nb konsantrasyonları, alaşımın fiziksel ve mekanik özelliklerine ve dönüşüm karakteristiklerine de etki edebilir. Ti-Nb alaşımındaki Nb oranı artırılarak, sertlik, dayanım, ve ergime sıcaklığı yükseltilebilmektedir (Kikuchi *et al.*, 2003).

Ti-Nb alaşımları genellikle döküm ve dövme teknikleri ile üretilmektedir. Dökümün neden olduğu ana kusurlar gözeneklilik, kaba mikro-yapılar, ve bileşim ayrışmaları olup, bunlar alaşımın mekanik özelliklerini ciddi şekilde kötüleştirir. Ayrıca, Ti ve Nb'nin ergime noktaları sırasıyla 1668 ve 2477 °C olduğundan, döküm yöntemlerini kullanırken çok yüksek sıcaklıklara ulaşabilen özel fırınlara, başka pahalı cihazlara ve yüksek enerji tüketimine ihtiyaç duyulmaktadır. Dövme yöntemleri daha iyi mekanik sonuçlar vermektedir ancak, yüksek masrafları ve hammaddelerin görece daha bol kullanımına neden olması uygulama alanlarını daraltmaktadır. Öte yandan toz metalürjisi işleme yöntemleri düşük işleme sıcaklıkları (1000-1400 °C) gereksinimleri nedeniyle, üretim verimliliğini artıran ve karmaşık yapılarda küçük parçaların üretimine olanak sağlayan yöntemlerdir (Štěpán.*et al.*, 2010; Caiet *al.*, 2016; Andrade . *et al.*, 2015). Toz metalürjisi yöntemleri yüksek miktarlarda Ti-Nb numuneleri üretiminde kullanılabilir ve makine işlemlerini azaltıp, aynı sonucu elde etmek için normalde kullanılan hammaddenin yalnızca %90'ının kullanılmasına olanak sağlayarak, diğer üretim yöntemlerine kıyasla üretim masraflarının azaltılmasını sağlayabilir. Ayrıca bu yöntem ile daha kesin şekilli parçalar elde edilebilmektedir.

Üretim işlemlerine bağlı olarak, toz metalürji yöntemleri bütünleştirme işleminin yapıldığı sıcaklık esas alınarak iki grupta toplanabilir:

Soğuk bütünleştirme işlemleri: oda sıcaklığında preslenen tozlar, yüksek sıcaklıklarda sinterlenir.

Sıcak bütünleştirme işlemleri: tozlara aynı anda hem yüksek basınç hem de ısı uygulanır. Ayrıca, sıcak bütünleştirme işlemleri ile azami yoğunluk elde edilebilmektedir.

Bu çalışmanın amacı, $Ti_{74}Nb_{26}$ alaşımlarının sıcak presleme ve sonrasında uygulanan yüksek sıcaklık sinterleme işlemi ile üretilmesi ve bu alaşımın özelliklerinin tespit edilmesidir. Yoğunluk, nihai mikro-yapı ve arzu edilen mekanik özellikler, basınç, sıcaklık ve zaman gibi sıcak presleme değişkenlerinin ayarlanması ile kontrol

edilebilmektedir. Bu fikirle Ti ve Nb tozları bir karışım halinde 15 mm çapındaki silindir şeklindeki grafit kalıplara yerleştirilmiş ve 600, 650 ve 800 °C’de 1 saat boyunca 50 MPa basınçta gözeneksiz numuneler elde etmek için argon gazı altında sinterlenmiştir. Numuneler 10 mm yükseklikte olacak şekilde ayarlanmıştır. Numuneler işlem için en uygun ısı olan 800 °C’de sıcak preslendikten sonra 1200 °C’de 1, 2, 3 ve 4 saat boyunca sinterlenerek Nb’nin çözünmesi ve Ti’nin β fazına dönüşmesi sağlanmıştır. Uygulanan sıcak presleme ve sinterleme sıcaklıklarının numunelerin mikro-yapı, yoğunluk ve mekanik davranışları üzerindeki etkilerinin tespit edilmesi için Taramalı Elektron Mikroskobu (SEM), X-Işını Kırınımı (XRD), Arşimet yöntemi, tek eksenli basma testi ve Vickers mikro-sertlik testi kullanılmıştır.





2. TEORİK ALTYAPI

2.1. Titanyum ve Titanyum Alaşımları

Titanyum elementi 1790'da William Gregor tarafından İngiltere'de keşfedilmiştir, ancak titanyum ismi Klproth tarafından 1795'de konulmuştur (Viteri, and Fuentes., 2013). Titanyum düşük yoğunluklu bir elementtir. Yoğunluğu yalnızca 4.5 g/cm^3 olup, bu değer çeliğin yoğunluğunun (7.9 g/cm^3) yalnızca %60'ına denk gelmektedir. Yüksek sıcaklıklarda çalışması gereken ve özellikle yüksek dayanım/ağırlık oranı gerektiren parçalarda kullanılabilir (Hermawan,H. *et al.*, 2009; Hermawan *et al.*, 2009). Ti alaşımları kusursuz aşınma dirençleri, yüksek özgül dayanımları ve üstün biyo-uyumlulukları nedeni ile tıpta da kullanılmaktadır (Zhao et al, 2013). 5 g/cm^3 'lük yoğunluk değeri, ağır ve hafif metallerin ayrıldığı sınır olarak belirlenmiştir. Hafif metaller arasında en ağır metal titanyumdur (Leyens,. and Peters., 2003).

Titanyum alaşımlarının ana özellikleri mekanik ve biyo-uyumluluk, güvenilirlik, insan vücudunda yüksek aşınma direnci, yüksek yorulma direnci, üstün dayanıklılık ve yüksek özgül mukavemet olup, bunlar nedeniyle metalik implantlarda ve ortopedik ve diş protezlerinin üretiminde tercih edilmektedirler (Cai. *et a.*, 2016). Young katsayıları çeşitli alaşımlar tasarlanarak arzu edilen şekilde artırılıp azaltılabildiğinden, titanyum alaşımları aynı zamanda endüstriyel uygulamalarda da yaygın şekilde kullanılmaktadır. Fedotov ve Belousov, Ti'ye Nb eklenerek elastik katsayısının azaltılabileceğini belirtmişlerdir.

2.2. Ti Alaşımları: Yapı ve Özellikleri

Yüksek sıcaklıklarda hacim merkezli kübik β fazı ve düşük sıcaklıklarda sıkı paket hegzagonal α fazı, Ti esaslı alaşımların iki kararlı fazını teşkil ederken, (ortorombik) α'' ve hegzagonal ω fazları da, su verme ile elde edilen iki yarı kararlı fazı oluşturmaktadır. Ti, $882\pm 2^\circ\text{C}$ alotropik bir değişime uğrar; bu sıcaklığa kadar (HCP) yapıda bulunan α fazı, $882\pm 2^\circ\text{C}$ üzerine çıkıldığında (BCC) β fazına dönüşür; bu faz ergime noktasına kadar stabil kalmaktadır. İki fazın dizilim, hacim oranı ve kendilerine

has özellikleri titanyum alaşımlarının da özelliklerine etki etmektedir. (Leyens, and Peters., 2003; Elmay *et al*, 2014; Ping *et al*, 2006; Kim *et al*, 2005; Mantani,. and Kudou., 2013; Panigrahi, A., 2015; Bhadeshia,n.d).

2.3. Ti-Nb Faz Diyagramı

Bir sistemin eşit fiziksel ve kimyasal özellikler gösteren homojen kısmına faz denmektedir. Tüm saf malzemelerin katı, sıvı ya da gaz fazında oldukları kabul edilmektedir. Faz diyagramları kullanılarak her türden faz dönüşümleri anlaşılabilir gibi, bir alaşımın mikro-yapısı ve fiziksel özellikleri de anlaşılabilir (Otsuka, and Ren1999). Herhangi bir sisteme ait termodinamik bilginin bir varyasyonu da bu faz diyagramları tarafından çok sayıdaki fazın dengesi ve faz dağılımlarının ölçülebilir verileri aracılığı ile aktarılabilir (Seetharaman., 2005).

Bir alaşım sisteminin en kararlı halinin tespit edilebilmesi için faz diyagramları azami önem arz etmektedir. Ergime, kalıplama ve kristalleşme bilgileri faz diyagramları kullanılarak elde edilebilir (Callister, and Rethwisch., 2009). Denge ve dengesiz hal fazları, titanyum alaşımlarının öge elementlerine göre değişen iki faz dönüşümünü temsil etmektedir. α ve β fazları arasındaki denge, alaşımların uygun faz alanlarında ısıl işlemler kullanılarak ve ardından oda sıcaklığına soğumaya bırakılarak sağlanmaktadır (Pathak *et al*, 2014).

2.4. Nb Miktarının Faz ve Mikro-Yapıya Etkileri

Ti-Nb sisteminde farklı hızlarda soğutmanın sonucunda ortaya çıkabilen dengesizlik nedeniyle çeşitli yarı-kararlı fazla oluşabilmektedir. Bu eşitsizliklerden meydana gelecek nihai ürünün özellikleri hem soğuma hızına hem de bileşimdeki Nb miktarına bağlıdır. Ti-Nb alaşımındaki Nb içeriğinin artması β , α' , α'' ve az miktarlarda ω fazı gibi yarı kararlı fazların ortaya çıkmasına neden olmaktadır (Wu *et al*, 2013; Moffat, and Kattner., 1988;Tob *et al*, 2013).

2.5. Mekanik Özellikleri

Herhangi bir uygulamada kullanılacak malzemenin türü mekanik özelliklerine bağlıdır. Bu özelliklerden önemli olan bazıları elastik katsayı, sertlik, gerilim dayanımı ve uzama özelliğidir (Geetha *etl.*, 2009). Kimyasal bileşim ve termo-mekanik işlemler titanyum alaşımlarının davranışlarına etki edebilmektedir.

%5 ve üzerinde Nb içeriğine sahip olan alaşımların titanyumdan daha yüksek sertliği olmakta ve %10 ve üzerinde Nb içeren alaşımlar saf titanyuma göre daha yüksek akma ve çekme dayanımına ve belirgin şekilde daha düşük uzama özelliğine sahip olmaktadır. %20'ye varana kadar, niyobyum oranı arttıkça, Young katsayısı azalmaktadır. Nb yoğunluğu %5 ile %25 arasında olan Ti-Nb alaşımlarının Young katsayısı, saf Ti'ye göre belirgin şekilde daha düşüken, %30 ve üzerindeki Nb oranlarına sahip alaşımlarınki belirgin şekilde daha yüksektir.

2.6. Toz Metalürjisi

Toz karıştırma doğal tür bir karıştırma tekniğidir. Bu yöntemde iki veya daha fazla katı madde bir karıştırıcı yardımı ile ya da el kullanarak sürekli şekilde karıştırılmaktadır. Karıştırma süresinin artması karışma derecesini de artırmaktadır (Bhawna and Agrawal., 2007). Farklı kayganlaştırıcılar tutturucu olarak kullanılıp bu tozlara karıştırılabilir. Genellikle kayganlaştırıcılar tozların hem birbirleri ile hem de kalıp duvarları ile olan sürtünmesini azaltır, böylece daha muntazam bir yoğunluk elde edilmektedir (Jonsén ., 2006). Homojenliğin üç seviyesi vardır: katmanlı karışımlar için geçerli olan yüksek ölçek ayrışma, çökeltili karışımlar için geçerli olan kısmi homojenlik ve şekil 2.23'da gösterildiği üzere dağınık homojen adı verilen ideal homojenlik.

2.7. Ti-Nb Alaşımlarının Toz Metalürjisi

Presleme ve sinterleme; presleme, sinterleme ve sıcak işleme; sıcak presleme (hot pressing, HP), sıcak izostatik presleme (HIP), kıvılcım plazma sinterleme (SPS), metal enjeksiyon kalıplama (MIM), konvansiyonel sinterleme (CS) ve 3D yazdırma

titanyum alaşımlarının, özellikle Ti-Nb alaşımlarının hazırlanmasında genelde kullanılan yöntemlerdir. Presleme ve sinterleme yukarıda sayılan yöntemler arasında teknik olarak en basit ve ekonomik olarak en cazip yöntemdir (Qian and Schaffer.,2010).

2.7.1. Sıcak presleme

Sıcak presleme basınç altında gerçekleştirilen bir sinterleme yöntemidir. İndüksiyon ısıtması, dolaylı rezistans ısıtması ve doğrudan sıcak presleme, sıcak presleme teknolojisinin üç farklı uygulama türünü teşkil etmektedir. Sıcak presleme konvansiyonel preslemeden oldukça yavaş bir sinterleme sürecidir ve daha düşük tolerans seviyesine sahiptir. Sıcak presleme işlemlerinde, numuneye aynı anda hem güç hem de ısı uygulanmaktadır. Bu yaklaşım ile iyi mekanik özellikler elde edilebilmektedir. Öte yandan bu yaklaşım aşırı yüksek sıcaklıklara ve basınca ihtiyaç duymaktadır. Bu nedenle seçilen kalıp malzemesinin bu şartlarda çalışmaya uygun olması gerekmektedir. Grafit kalıplar bu iş için uygundur. Başlangıç tozları yüksek ısı ve basınç sayesinde sinterlenen bileşenlere kısmen veya tamamen bütünleşebilmektedir. Titanyum ve titanyum alaşımları bu şekilde sıcak presleme ile bütün haline getirilebilmektedir. Şekil 2.35 sıcak presleme tekniğini göstermektedir (Yang and Qain ., 2015).

Titanyum tozları indüktif sıcak presleme kullanılarak, yalın presleme ve sinterleme yöntemleri ile elde edilenden daha yüksek bir yoğunlukta ve daha kısa sürede alaşım haline getirilebilmektedir (Bolzoni, 2012).

3. MATERYAL VE YÖNTEM

3.1. Kullanılan Tozlar

Bu çalışmada element olarak Alfa Aesar, Almanya'dan tedarik edilmiş saf Ti (99.5 %) ve saf Nb (99.8 %) tozları (her ikisi de -325 mesh, 45µm'den küçük) kullanılarak, atomik yüzdesi Ti₇₄Nb₂₆ olan titanyum alaşımı elde edilmiştir. Şekil 3.1'de verilen SEM sonuçları elde edilen tozların morfolojik özelliklerini göstermektedir. Hidrat-dehidrat dönüşüm yöntemi ile elde edildiklerinden, Ti ve Nb tozlarının şekillerinin düzensiz oldukları görülmektedir. Bu toz üretim yönteminde önce sünek katı saf metal ya da alaşım hidrojenleme sürecine tabi tutularak kırılğan hale getirilir. Bundan sonra mekanik öğütme uygulanarak parçalama yapılır. İstenilen toz ebadına ulaşıldığında öğütmeye son verilir ve elde edilen tozlar nihai dehidrojenez sürecine tabi tutularak, sünek, hidrojenizsiz saf element veya alaşım tozları elde edilmiş olur.

3.2. Numune Hazırlanması

3.2.1. Sıcak presleme

Alaşımın Ti-Nb kompozisyonu Ti₇₄Nb₂₆ (atomsal yüzde) olarak belirlenmiştir, zira bu kompozisyon en düşük elastik katsayı değerini vermekte ve şekil hafızası ve süperelastiklik gibi özellikler göstermektedir. Ham tozların ağırlıkları bu yüzde göz önüne alınarak hesaplanmış ve silindir şeklindeki kalıpların son ebatları 15 mm çap ve 10 mm yükseklik olarak belirlenmiştir. Öngörülen 10 mm yüksekliği elde edebilmek için sıcak pres numunelerinin azami yoğunluğa (sıfır gözeneklilik) ulaşacakları varsayılmıştır. Tozlar elektronik terazi ile tartılmış (5.86 g Ti ve 4 g Nb) ve homojen bir yapı elde etmek için şekil 3.4'te gösterildiği şekilde bir bağlayıcı olarak etilen kullanılarak 15 dakika karıştırılmıştır. Ardından karışım şekil 3.5'te gösterildiği üzere 15 mm çapında boş silindir grafit kalıba alınarak 1 saat süre ile 600, 650 ve 800°C sıcaklıklarında 50MPa basınç altında preslenmiştir.

3.2.2. Yüksek sıcaklıkta sinterleme

Numuneler zımparalandıktan sonra ultrasonik temizleyici ile 10 dakika temizlenerek olası kalıntılardan arındırılmış ve kurumaya bırakılmıştır. Ardından arzu edilen β fazını elde etmek ve Nb'nin Ti içinde tam çözünmesini sağlamak için numuneler alümina (Al_2O_3) krozelere alınarak dikey tüp fırında $1200\text{ }^\circ C$ 'de (Protherm PTF 14/50/450) ve argon gazı akışı altında 1, 2, 3 ve 4 saat süre ile sinterlenmiştir. Sinterleme sıcaklığı tüm numuneler için sabit tutulmuştur. Kullanılan fırın ve sinterleme süreçleri için uygulanan deneysel düzenek şekil 3.9'da sunulmuştur. Sinterleme tamamlanınca numuneler fırın içinde soğumaya bırakılmış ve $200\text{ }^\circ C$ 'de fırından alınmıştır. Sinterleme için ısınma hızı dakikada $8\text{ }^\circ C$ olup, bu değer sıcak presleme değerine göre daha düşüktür. Isıtma, sinterleme ve soğuma eğrileri şekil 3.10'da verilmiştir. Sıcak preslemenin sıcaklık-zaman eğrisi de kıyaslama açısından bu şekle eklenmiştir. Eğrilerdeki ilk lineer kısım ısıtma değerlerinin sıcak presleme ve sinterleme için sabit tutulduğu (10 ve $8\text{ }^\circ C/dakika$) ısıtma kısmını göstermektedir. İkinci ve yatay kısım sıcak presleme ve sinterleme süreçlerini ifade ederken, eğrilerin düzenli olmadığı üçüncü kısım ise soğuma süreçlerini göstermektedir. Bu durum soğuma esnasında soğuma hızının sabit olmadığını, sinterlemenin tamamlanmasının hemen ardından azami hızda olduğunu ve zaman içinde soğuma hızının azaldığını göstermektedir.

Oksitlenmeyi önlemek veya asgariye indirmek için Ti sünger parçacıkları şekil 3.13'de gösterildiği üzere oksijen gazı alıcıları olarak kullanılmıştır. Şekil 3.14 Ti gaz alıcıları kullanılarak 2 saat sabit sinterleme sıcaklığında tutulmuş numuneyi göstermektedir. Aynı şartlar altında Ti gaz alıcıları kullanılmayan numunelere göre daha az oksitlenme gözlenmiştir. Bu numunede meydana gelen yüzey oksitlenmesi, gaz alıcı kullanılmadan 1 saat sinterlenen numuneninkine denktir. Sonuç olarak, Ti gaz alıcılarının 2 saat ve üzeri süren sinterleme işlemlerinde kullanılması gerektiği kanısına varılmıştır. Ti gaz alıcıları sinterlenen numunelerin hemen üzerine yerleştirilmiştir. Sinterleme ve soğutma esnasında bu gaz alıcıları bir nevi feda malzemesi olarak kullanılarak, numunenin oksitlenmesini azaltmak için kendilerinin oksitlenmesi sağlanmıştır (Şekil 3.15)

3.3. Metalografik Numune Hazırlanması

Şekil 3.18’de görülen numuneler, Şekil 3.17’de görülen Charmilles Robofil 290 and 310 model EDM sistemler kullanılarak 8000-12000 °C kıvılcım sıcaklıklarında 5x5x10 mm ebatlarında kesilerek mikro-yapısal ve mekanik özellikleri incelenmiştir. Kesme esnasında kıvılcımları, soğumayı ve boşaltımı sağlamak için özel bir sıvı kullanılmıştır. Sıkıştırma testlerinde numuneler kesildikleri haliyle kullanılmıştır. XRD analizleri için numunelerin yüzeyi 320 SiC zımpara kâğıtları ile zımparalanarak kesme işleminde kalan olası kalıntılar uzaklaştırılmıştır. Mikro-sertlik ve SEM araştırmaları için numuneler tam metalografik hazırlık süreçlerine tabi tutularak, 230-1200 zımparalama kâğıtları ile taşlanmış, elmas solüsyonu (3µm) ile parlatılmış ve nihayet dağlanmış. Dağlama için 15 saniye süreyle Kroll çözeltisi (3 ml HF + 6 ml HNO₃ + 100 ml H₂O) kullanılmıştır.



4. SONUÇLAR

Bu çalışmada ikili $Ti_{74}Nb_{26}$ alaşımları, sıcak presleme ve yüksek sıcaklıkta sinterleme yöntemleri ilk defa bir arada kullanılarak hazırlanmıştır. Çalışmadan elde edilen genel sonuçlar aşağıda sunulmuştur:

Yoğunluk ölçümleri (Arşimet yöntemi) Ti-Nb alaşımlarının 1 saat sinterlenmesindeki en uygun sıcaklığın $800\text{ }^{\circ}\text{C}$ olduğunu göstermektedir. Bu sıcaklıkta neredeyse tam (%99'dan büyük) yoğunluk elde edilmiştir.

XRD sonuçlarına göre, $1200\text{ }^{\circ}\text{C}$ 'de farklı sürelerle sinterlenen $Ti_{74}Nb_{26}$ alaşımlarının mikro-yapılarında düşük miktarlarda α fazı ile, yine az miktarlarda çözünmemiş saf Nb bulunduğu gözlenmiştir. Yine XRD ve SEM sonuçlarına göre sinterleme süresinin uzaması ile β fazı miktarı artmaktadır.

$1200\text{ }^{\circ}\text{C}$ 'de 4 saat sinterleme bile sadece β fazı elde edilmesine yetmemiştir. Bu nedenle α fazı ve çözünmemiş Nb içermeyen tek β fazı elde edilmesi için $1200\text{ }^{\circ}\text{C}$ 'den yüksek sıcaklıklar gerektiği değerlendirilmiştir.

Sinterleme süresinin artırılması mekanik özelliklerin gelişmesini sağlamaktadır. Elastiklik katsayısı, akma ve basma dayanımı ve mikro-sertlik dâhil olmak üzere en iyi mekanik özellikleri 4 saat sinterlenen numuneler göstermiştir. Öte yandan süneklik değeri tüm sinterleme süresindeki numuneler için neredeyse aynı kalmıştır.

Elastiklik katsayısı, güç ve süneklik açılarından, üretilen alaşımların kemik ikame protez uygulamalarında kullanıma uygun oldukları değerlendirilmiştir.

CURRICULUM VITAE

Name and Family: Nuaman Jasim Filamarz AL-ZANGANA

Gender: Male

Work Address: Sulaimani Polytechnic University / Technical College of Engineering

Occupation: Senior Chief of Engineer

Home Address: IRAQ - Sulaimani

Mobile No: | 00964(0)7702562878 |

E.mail: Nuaman.Zangana@yahoo.com - Nuaman.Zangana57@gmail.com

Education:

- 1- Bachelor/Mechanical Engineering / Technical College-Baghdad / Iraq-1980-1981
- 2- Higher Diploma /Mechanical Engineering/Technical College- Baghdad - Iraq / 2004-2005
- 3-Master in Mechanical Engineering - Van Yuzuncu Yil University-Turkey -2015-2018

Languages :

- 1- Kurdish – Native language
- 2- Arabic - speak fluently, read and write with high proficiency
- 3- English – speak, read and write with good proficiency
- 4-Turkish – speak with basic competence[